Doubly-Fed Induction Machine for use in Mini-Hydro Power Plants

Technical Assessment

Rizwan Rafique Syed

Doubly-Fed Induction Machine for use in Mini-Hydro Power Plants

Technical Assessment

Rizwan Rafique

August 2015

Doubly-Fed Induction Machine for use in Mini-Hydro Power Plants
Technical Assessment

Master of Science Thesis

For obtaining the degree of Master of Science in Electrical
Engineering at Delft University of Technology and in
Technology-Wind Energy at Norwegian University of Science and
Technology.

Rizwan Rafique

August 2015

EUROPEAN WIND ENERGY MASTER - EWEM
OF
ELECTRIC POWER SYSTEM TRACK

The undersigned hereby certify that they have read and recommend to the European Wind Energy Master - EWEM for acceptance a thesis entitled **"Doubly-Fed Induction Machine for use in Mini-Hydro Power Plants"** by **Rizwan Rafique** in partial fulfillment of the requirements for the degree of **Master of Science**.

Dated: <u>August 2015</u>

Supervisor:

<u>Dr.ir. Henk Polinder of TU Delft, Netherlands</u>

Supervisor:

<u>Trond Toftevaag of NTNU, Norway</u>

Reader:

<u>Dr.Ing. Jose L. Rueda of TU Delft, Netherlands</u>

Summary

Hydropower is the most popular and fastest growing renewable energy technology among all. Environmental and ecological concerns involved with large water reservoirs limited the usage of potentially available sites. Thus, the present trend is growing towards building small hydro power plants as the hydro power is clean and economical source for power generation.

Different site parameters (head, flow) varies throughout the year which affects the power production capability of hydropower system and makes the production inefficient, in addition, some of the sites cannot be exploited fully just because of being less economical due to these parameter variations. Variable speed operation improves the efficiency of hydro power generation system by running the system at a speed so that the optimum efficiency can be achieved at different operating points. Various configurations are available for variable speed operation and Doubly Fed Induction Generator (DFIG) is also a popular configuration in wind energy systems.

This work is a study to check the performance of DFIG in mini-hydropower system. Firstly, a brief look is taken on steady state model of DFIG which is required to understand the machine characteristics then dynamic model equations for DFIG, grid circuit and DC link are derived which is required for simulation of the system then DFIG model is validated. Optimum efficiency speed module is developed to obtain the speed reference for control system based on power demand for optimum efficiency operation. Finally, control system for DFIG is developed based on vector control.

Performance of the developed model is checked by carrying out simulation at different operating conditions. The power generation capacity is affected by variation in site conditions such as water head. Therefore, the model is simulated at different water heads with different power demands. Further the super-synchronous and sub-synchronous operation of DFIG is checked based on speed reference generated by optimum efficiency speed module. Also efficiency for both variable and fixed speed operation is plotted and it is

observed that the efficiency is higher at variable speed operation compared to fixed speed operation for same power demand.

Acknowledgements

This work would not have been done without the support of many individuals and at the first place without having opportunity to participate in such a great program (EWEM). Thanks to Erasmus Mundus for providing me opportunity to participate in such a wonderful degree program.

First of all, I would like to thank Dr.ir. Henk Polinder and Mr. Trond Toftevaag for their support and supervision of my work. Whenever I asked, they always gave me valuable suggestions. In addition, I would also like to thank my Co Supervisors Prof. Tore M. Undeland and Prof. Robert Nilssen for their support.

Special thanks to Mr. Kjell Ljkelsy for giving me his time and valueable suggestions for preparing the lab setup. I would also like to thank service lab personnel, Mr. Vladimir Klubicka, Mr. Brd Alms and specially Mr. Aksel Andreas Reitan Hanssen who was engaged with me during preparation of lab setup.

Finally, I am grateful to my mother who have always been there with me in every walk of life since my childhood, I am also grateful to my siblings for their endless love, encouragement, and moral support.

Delft, The Netherlands   Rizwan Rafique
August 2015

Contents

List of Figures

List of Tables

List of Symbols

Latin Symbols

α_x	IMC filter bandwidth
$\bar{I}_{r,act}$	actual current phasor induced in rotor[A]
$\bar{I}_r$	rotor current phasor [A]
$\bar{I}_r$	rotor induced current phasor referred stator[I]
$\bar{I}_s$	stator current phasor [A]
$\bar{V}_{r,act}$	actual voltage phasor induced in rotor[V]
$\bar{V}_r$	rotor induced voltage phasor [V]
$\bar{V}_r$	rotor induced voltage phasor referred stator[V]
$\bar{V}_s$	stator induced voltage phasor [V]
$\bar{\lambda}_r$	rotor flux linkage[elect. wb.turns]
$\bar{\lambda}_s$	stator flux linkage[elect. wb.turns]
η	turbine efficiency [dimensionless]
ω_g	angular frequency of grid waveform [elect. rad/s]
ω_m	rotor shaft angular velocity [elect. rad/s]
ω_{mech}	rotor shaft angular velocity[mech. rad/s]
ω_m	rotor shaft angular velocity [elect. rad/s]
ω_{res}	Harmonic modes of shaft between turbine and generator [rad/s]
ω_{rotor}	angular frequency of rotor waveform [mech. rad/s]
ω_r	angular frequency of rotor waveform[elect. rad/s]
ω_{stator}	angular frequency of stator waveform [mech. rad/s]
ω_s	angular frequency of stator waveform[elect. rad/s]

ϕ_m	shaft twist angle between for one mass model [rad]
ϕ_{tg}	shaft twist angle between turbine and generator [rad]
σ	total leakage factor[dimensionless]
θ_e	electrical angle of generated waveform [elect. rad]
θ_m	rotor position from reference axis [mech. rad]
$\vec{v_a}$	space vector of a-axis stator volatge [V]
$\vec{v_b}$	space vector of b-axis stator volatge [V]
$\vec{v_c}$	space vector of c-axis stator volatge [V]
$\vec{v_s}$	space vector of stator volatge [V]
a	number of turns ratio [dimensionless]
a_0	inlet guide vane opening of turbine [mm]
C_{DC}	dc bus capacitor [F]
$d(s)$	disturbance from outside of plant
D_1	hydro turbine nominal diameter [m]
D_g	generator damping constant [$kg - m^2$]
D_m	one mass model damping constant [$kg - m^2$]
D_t	turbine damping constant [$kg - m^2$]
E_s	induced emf across stator winding [V]
E_r	induced emf across rotor winding [V]
eta_e	generator efficiency [dimensionless]
F_s	space vector of mmf [A.turns]
$F_x(s)$	IMC controller with two degree of freedom configured as classical controller
f_{grid}	grid frequency [Hz]
f_{res}	Harmonic frequency of shaft between turbine and generator [rad/s]
f_{rotor}	frequency of rotor waveform [Hz]
f_{stator}	frequency of stator waveform [Hz]
G_x	plant inner feedback loop gain
H	combined turbine and generator inertia constant [$kg - m^2$]
H	turbine water head [m]
H_g	generator inertia constant [$kg - m^2$]
H_t	turbine inertia constant [$kg - m^2$]
$i_{\alpha g}, i_{\beta g}$	grid current alpha beta components [A]
i_{ag}, i_{bg}, i_{cg}	grid current space vector [A]
i_c	current through dc bus capacitor [A]
J	combined inertia of generator and turbine [$kg - m^2$]
k_r	rotor winding factor [dimensionless]
k_s	stator winding factor [dimensionless]
K_{tg}	stiffness coefficient[$N - m/rad$]

$L(s)$ IMC filter

L_f inductance of grid side filter [H]

$L_{lr,act}$ actual rotor winding leakage inductance [H]

L_{lr} rotor winding leakage inductance referred to stator [H]

L_{ls} stator winding leakage inductance [H]

L_m magnetizing inductance[H]

L_r total rotor inductance referred to stator [H]

L_s total stator inductance[H]

$M_x(s)$ plant with inner feedback loop gain

N gear ratio of coupling between turbine and generator [dimensionless]

n_1 turbine unit speed [r/min]

N_r number of turns of rotor winding [dimensionless]

N_s number of turns of stator winding [dimensionless]

n_{rpm} shaft speed of generator's rotor [RPM]

p generator poles [dimensionless]

P_1 turbine unit power [kW]

p_p Number of pole pairs [dimensionless]

p_r real power exchanged through rotor [W]

P_s^{ref} real power reference[W]

$P_x(s)$ plant

P_{gap} real power through air gap[W]

p_g real power exchange between grid and converter [W]

P_{mech} total mechanical power[W]

P_{rcu} copper losses in rotor[W]

P_r Real power exchanged through rotor[W]

P_{scu} copper losses in stator[W]

P_{slip} power transferred through rotor slip rings[W]

P_s Real power exchanged through stator[W]

P_{tot} total real power[W]

Q_1 turbine flow rate [m/s^3]

q_s reactive power exchanged through stator [VAR]

Q_s^{ref} reactive power reference[VAR]

q_g reactive power exchange between grid and converter [VAR]

Q_{Lis} reactive power consumed in stator leakage inductance[VAR]

Q_{Llr} reactive power consumed in rotor leakage inductance[VAR]

Q_{Lm} reactive power consumed in magnetizing inductance[VAR]

Q_r reactive power exchanged through rotor[VAR]

Q_s reactive power exchanged through stator[VAR]

Q_{vir} reactive power modeled for converter [VAR]

R_f resistance of grid side filter [Ω]

$R_{r,act}$ actual rotor winding resistance [Ω]

R_r rotor winding resistance referred to stator [Ω]

R_s stator winding resistance [Ω]

s slip and Laplace complex argument [dimensionless]

T_e electromagnetic torque of generator [$N-m$]

T_e electromagnetic torque of generator[N-m]

T_{load} Load torque on generator shaft [N-m]

T_m turbine mechanical torque [$N-m$]

T_{tg} torque of shaft between turbine and generator[$N-m$]

V peak value of stator volatge [V]

$v_{\alpha f}, v_{\beta f}$ grid voltage alpha beta components [V]

v_{af}, v_{bf}, v_{cf} space vector grid side converter voltages [V]

v_{ag}, v_{bg}, v_{cg} grid voltage space vector [V]

V_{bus} voltage across dc bus capacitor[V]

V_{DC} DC bus voltage [V]

$V_{LL,rms}$ three phase line to line voltage[V]

$y(s)$ output of plant

$M_x^{'}(s)$ model of plant with inner feedback loop gain

Chapter 1

Introduction

Among renewable energy technologies available today, hydro power is the most important and has huge potential of future growth. The estimated share of hydro source in total electricity production of the world is 16.6% and this share for electricity production with renewable energy is 72.8% by the end of year 2014 [1] with a fast growing trend in future [2]. There are various reasons of using hydro as a source of producing power i.e. environment friendly (apart from large reservoirs), economical, clean, and reservoirs can also serve for water storage for irrigation purpose and during the time of water supply shortage.

Although the requirement of large units with higher efficiency and lower generation cost is desirable but the regulatory requirements associated to environmental and ecological concerns has nudged to opt for small scale power plants having less issues. In addition, these power plants can be built in less time, without storage option (run of river), and provide decentralized generation with added stability to the grid system.

This work deals with the variable speed control of DFIG for use in mini-hydro power systems. DFIG has already been used successfully in wind energy system. The DFIG is actually a wound rotor induction machine (WRIM) and can work both as motor and generator. In this work its operation as generator with mini-hydro power system will be employed.

1.1 Background

The generation capacity of hydro plant depends on the location; also the flow of water is not constant throughout the year thus the available power and generation efficiency of a hydro system also varies due to various parameters such as head, flow, discharge which demands to adopt different methods to improve efficiency and run the power system at optimum efficiency point. There are many sites available having moderate flow but can

not be exploited due to large deviation in flow and head which makes them uneconomical to operate [3].

Variable or adjustable speed hydro power plants are gaining popularity due to their capability to improve efficiency of the generating system while keeping the system within economical limits. Conventional power plant controls the flow of water through inlet gate opening which responds slowly to the changes in load variation or site conditions and usually have time constant in order of seconds whereas variable speed hydro power control responds relatively very quickly because of the power electronics control and the response time of a generator control is much less than the hydro turbine control. Variable speed operation not only improves the efficiency of generation system but it also increases the power density of the generation and improves the utilization of transmission network[4]. A study [5] was also carried out by replacing the conventional induction generator with Permanent Magnet Synchronous Generator (PMSM) having variable speed control and the results show that the efficiency of the existing system was increased after replacement.

Different methods have been proposed over the past few years to achieve efficient operation of hydro power systems. Some focuses on redesigning the generator specifically for efficient operation of hydro power system while other focuses on different control algorithms to achieve efficient operation.

Low speed PMSM for small hydro power application can be made efficient by redesigning generator as was shown by [6]. He proposed the modification in electromagnetic design for low speed and high torque of PMSM by using the new tools to optimize the design which will improve efficiency further along with variable speed control system. However, the generator is coupled to the turbine with shaft or could also have gearbox. A small hydro power set was developed on experimental basis using integrated approach [7], this approach combines the generator and turbine in a single module thus eliminated the gearbox and shaft. Further, the use of variable speed control strategy made it a choice not only comparable to the existing variable speed solution but it also offers an added advantage of operation over wide range of nominal flow. However, the design is specific to the hydrological conditions and must be done accordingly to acquire these advantages. The Maximum Efficiency Point Tracking (MEPT) algorithm was implemented on a micro-hydro power plant by [8]. This algorithm tracks the optimum efficiency based on changing hydrological conditions by using Perturb & Observe (P & O) technique but it also suffer from the inherent disadvantage of local maximum. Results of implementing the Direct Power Control (DPC) which was developed after Direct Torque Control (DTC) was shown in [9] and the power output contains ripples due to inherent nature of DTC which can be reduce by increasing switching frequency. Artificial Neural Network (ANN) based solution for optimum speed module (OSM) was proposed against conventional OSM for obtaining the speed reference at optimum efficiency. Although the conventional OSM works well with simulation but it uses several for loops and thus it is inefficient and takes longer time during simulation which is reduced by adopting the ANN approach[10].

DFIG is very popular in wind energy applications and an economical choice for variable speed operation due to its reduced converter size compared to synchronous generator which uses full size converter. This work performs the technical assessment for DFIG to use in mini-hydro system by comparing the efficiency of variable speed operation against fixed speed operation. For both operations separate modules have been developed to

produce reference speed then simulation is done with the DFIG to check the various parameters (such as power, torque, currents, voltages etc.).

1.2 Objective

Although feasibility assessment of any power production system can be based on many parameters but some of the most important considerations are, it should be efficient, economical, and clean. The objective of this thesis is to carry out technical assessment of the use of DFIG in mini-hydro power systems. The basis of technical assessment adopted in this work is to compare the efficiency of variable speed DFIG hydro power operation with the fixed speed operation. This has been carried out in following manner:

1. Developing steady state DFIG model.

2. Developing dynamic DFIG model.

3. Developing the optimum efficiency speed module for hydro turbine.

4. Modeling the control system for DFIG speed and power control.

5. Simulating the developed model at different conditions to determine the efficiency under variable and fixed speed operation.

6. Demonstrating efficient operation of the model by implementing in a lab setup (If time permits).

1.3 Methodology

In chapter 2 steady state model is introduced. The steady state model is thoroughly covered in the literature so model is discussed with important concepts. The concepts are covered to gain an understanding of power flow in a DFIG in different modes of operation. Further, steady state set of equations are presented which can be used to initialize the dynamic model for a particular operating point.

Dynamic model of DFIG is presented in detail in chapter 3. Space vector and reference frame transformation concept is discussed then the dynamic equations are written in different reference frames. Power and torque equations are also derived and the block diagram representation of dynamic model is introduced for simulation purpose. The method of validating the dynamic model is also given and simulation results validate the correctness of developed model. Dynamic equations for grid circuit are also written in rotating reference frame; in addition, DC link modeling is also discussed.

In chapter 4 a model for obtaining the reference speed at different power demand for optimum efficiency operation of turbine is developed which serves the control purpose without considering the detail of hydro turbine dynamics which is not the scope of this work. The model uses Hill charts to obtain different operating points and generates speed reference for given input parameters.

Control system is developed using the most popular vector control technique for DFIG control. Grid voltage orientation is used for the reference frame transformation. Internal Model Control (IMC), which is also a form of PI control, is used due to its robustness, simplicity and the degree of freedom its provide in tuning the controllers. This is discussed in chapter 5.

Efficiency comparison of fixed and variable speed operation is shown for various operating points in chapter 6. Simulation is done for different power demand values also the variation in efficiency with water head is also simulated and comparison at fix and variable speed is presented. This comparison provides a basis for technical assessment of variable speed operation of DFIG in hydro power systems.

Finally chapter 7 presents the lab work where dSpace is used as a tool to implement the control system. Different hardware and software subsystems of lab setup are discussed.

1.4 Configurations of Hydro Power Systems

Different configurations and methods have been proposed to achieve variable speed operation over the past few years. Hydro power generation systems can be broadly categorized based on their operation as fixed speed and variable speed.

1. Fixed Speed Topology

2. Variable Speed Topology

   - Variable Speed with Full Converter
   - Variable Speed with Partial Converter

1.4.1 Fixed Speed Topology

In this topology the generator is directly connected to the grid. As the grid frequency is usually constant and the speed of generator is related to the grid frequency by:

$$n_{rpm} = \frac{120.f_{grid}}{p} \tag{1.1}$$

Where n_{rpm} is speed in rpm, f_{grid} is grid frequency and p is the number of poles of generator. The generator could be coupled with turbine through gear box or directly in case for high speed turbine or generator with large number of poles. Synchronous or three phase induction generator are usually used with this configuration. Turbine is designed for one optimum value of head, flow and discharge and any variation in one of these parameters will drive the turbine to an efficiency value less than optimum so the configuration is opted for location where the deviation from designed parameters is less and also due to economic reasons.
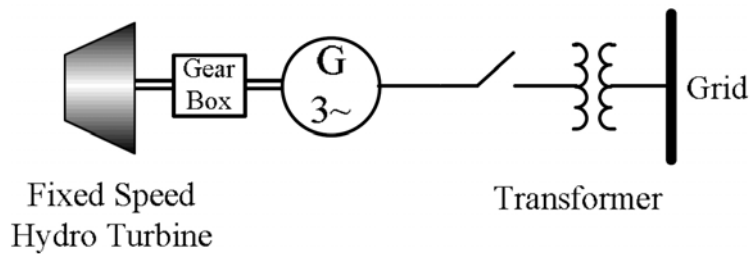
Figure 1.1: *Fixed speed configuration.*

1.4.2 Variable Speed Full Converter Topology

When it is desirable and economical to run the turbine at optimum efficiency values and the sites where there is considerable deviation from the operation point designed parameters (head, flow or discharge) of turbine then the variable speed operation is required. The full scale converter is rated almost equal to the generating unit value and serves as an interface between grid and generating unit. This offers many advantages, first the frequency of generator is independent of the grid so generator can run at any speed thus it can be directly coupled with the turbine and gear box is eliminated, which reduced installation and maintenance cost of gear box and improves system reliability. Second the converter at grid side keeps the frequency constant as per grid requirements. Third during fault condition at grid side generator is not directly connected to the grid so the fault does not transfer to the generator, further, the power factor of the system is also controlled through the converter. Squirrel cage induction generator (SCIG) and Synchronous generators can be used with this type of configuration [11, 12, 13].
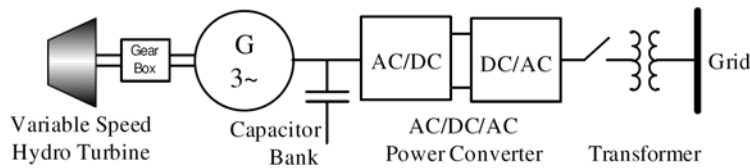
Figure 1.2: *Variable speed full rated converter connected to grid.*

1.4.3 Variable Speed Partial Converter Topology

When it is not required to have very large variation in speed then DFIG with a partial size converter can be employed. The advantage of using DFIG is that the converter only needs to be sized according to the slip power value which could be 30% of the rated speed thus the size and cost of converter is reduced. The converter at the rotor side controls the speed of DFIG and the real power flow to the grid whereas grid side converter controls the power factor and keeps the voltage of DC link capacitor, connected between both converters, constant. The control strategy depends on the connection when the generator is operated in isolated or stand alone condition the objective is to keep the stator voltage and stator frequency constant despite variations in turbine speed whereas in case of grid connected system the control of active and reactive power is desirable.
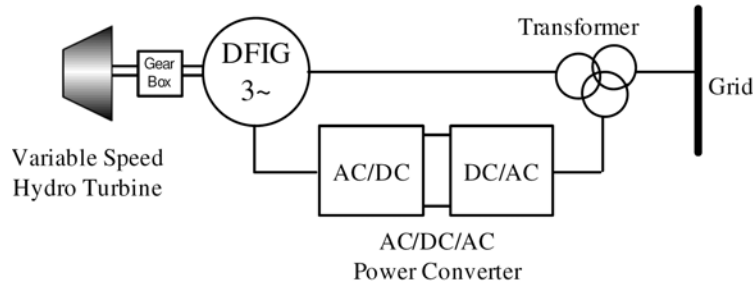
Figure 1.3: *Variable speed partial rated converter connected to grid.*

Another variation of partial converter configuration is shown in figure 1.4. The system components are turbine, gearbox, shaft, PMSM, DFIG and partially rated converter with dc link. The system can be used with weak grids where the grid does not allow the power to be drawn, such as in case of sub-synchronous speed operation (below synchronous speed) where the power needs to be injected into the rotor which comes from the dc link capacitor and the capacitor receives this power from the grid via the grid side converter but in this configuration this power is supplied by the PMSM which serves as generator while in case of super-synchronous speed the the dc link voltage rises and the PMSM consumes power so the shaft power is the sum of turbine and PMSM power.
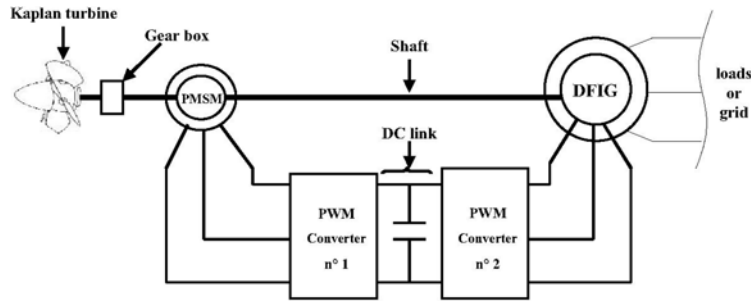
Figure 1.4: *DFIG in variable speed partial rated converter configuration with PMSM.*

1.5   DFIG Partial Converter Configuration and Power Flow

As mentioned earlier that variation in site conditions such as flow, head and discharge will alter the hydro power generation capacity. This change of parameters varies the shaft speed of turbine which in turn changes the generator speed coupled to it. The generator feeds power to the load in stand alone configuration or through grid connection, whatever the case may be, it is desirable to keep the voltage and frequency of load under specified limits. Synchronous generator field circuit produces magnetic field with direct current or through permanent magnet, therefore, the generated frequency of synchronous machine is closely related to its speed and poles (which are usually fixed see equation (1.1)), thus a change in shaft speed will bring a change in frequency of generated voltage supplied to the load. Placing full size converter between load and generator helps in controlling the fluctuation in generated voltage magnitude and frequency. If variation in turbine

speed is not very large then the size of this converter can be reduced by replacing the synchronous generator with DFIG and placing this converter between rotor circuit and grid. The relative speed between stator field and generator shaft speed determines the frequency and rotational speed of rotor induced voltage of an induction machine. Direct access to rotor circuit is not available in SCIM, while DFIG provides the flexibility to inject a voltage into the rotor circuit of required frequency and magnitude for different speeds rotor turn at. Frequency of stator side can be held at 50 or 60 HZ by controlling the voltage injected into the rotor. The power flow for both super and sub synchronous can be seen from figure 1.5.
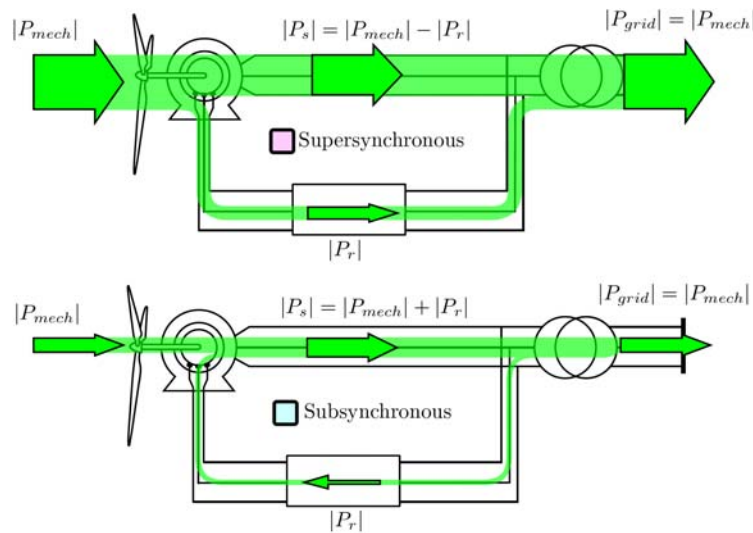
Figure 1.5: *Top: Power flow at supersynchronous speed. Bottom: Power flow at subsynchronous speed.*

The power exchange between rotor circuit and grid is called slip power and the amount of this power depends on the slip speed (relative speed between stator field and rotor), so the generator can be sized less than the rated power of turbine to an amount which is to be handled by the rotor circuit. For instance, if the generator has rated power output which could flow through stator is $2MW$ and the maximum change in rotor speed from its rated value above or below is 30% then the power converter can be sized at $600kW$ and the turbine rating will be the total power handled by both (stator and rotor) and in this case becomes $2.6MW$. At rated turbine speed, the turbine will deliver its rated power $(2.6MW)$ and this turbine speed will be the super-synchronous speed of the generator $(30\%$ above synchronous speed), stator will carry $2MW$ of power while the reset $(600kW)$ will flow to the grid through rotor circuit. Similarly below super-synchronous speed the stator will handle the power from turbine and the power injected from rotor side but this will not overload the stator circuit because the rotor will inject the power according to the slip speed and the turbine will contribute to an amount of power which is below the value at super-synchronous speed of generator since generator can handle a power of $2MW$ at super-synchronous speed which will go down below this value as the turbine speed falls below generator's super-synchronous speed.

Chapter 2

Steady State Model of DFIG

Steady state analysis of doubly-Fed induction machine is important due to two main reasons. First it provides the understanding of characteristic and operation of the machine and second it is used to calculate the values of particular operating point to initialize the machine model. Extensive literature is available on steady state circuit representation of induction machine, therefore, those concepts of machine will be discussed which are needed for this work.

2.1 DFIG Circuit Representation in Steady State

In figure 2.1 the equivalent circuit of an induction machine is shown. The rotor side of the circuit is short circuited as is the case of squirrel cage machine.
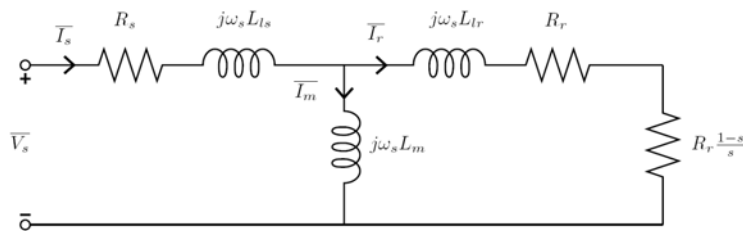
Figure 2.1: *Equivalent circuit of squirrel cage induction machine.*

The circuit contains stator and rotor resistances and leakage inductances which are referred to the stator side also notice that the frequency of rotor side is not the slip frequency rather it is synchronous and mechanical power is modeled in by the referred rotor resistance multiplied with the slip factor [14, 15, 16]. Because DFIG is fed from two sides one from stator and another from rotor so the equivalent circuit for DFIG can be represented by figure 2.2 [17, 18].
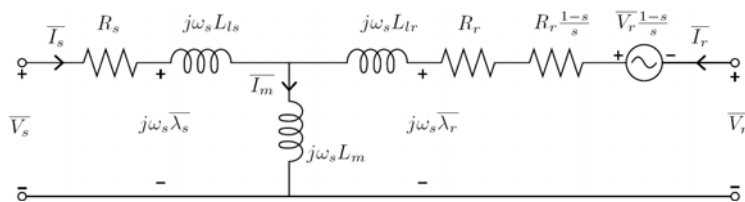
Figure 2.2: *Equivalent circuit of doubly fed induction machine.*

To understand the induction machine it is helpful to consider the multi pole pair machine as the two pole machine due to symmetry. The frequency of voltage induced in the multi pole pair machine has the relation with the actual rotation of the rotor as:
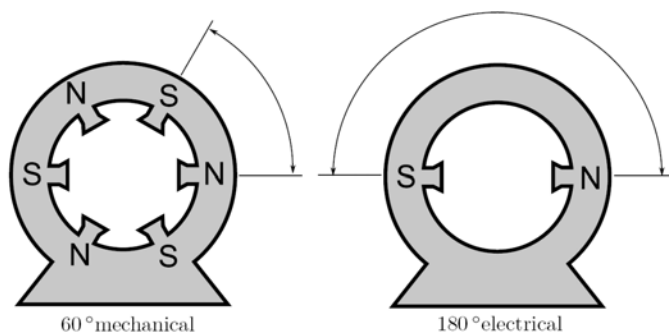
Figure 2.3: *Multi and two pole machine.*

$$\theta_e = \theta_m . p_p \tag{2.1}$$

Where θ_e is electrical angle, θ_m is mechanical angle, and p_p is number of pole pairs. The above equation implies that for instance, the angle θ_e of induced voltage in a machine having two pole pairs will be twice that of its mechanical angle thus the rotational speed ω of the generated voltage will be twice that of its mechanical speed. Further, the torque of two pole machine can be changed to the multi pole machine by just multiplying with the number of pole pairs.

2.1.1   Angular Speed and Slip Relation

The relation between frequency of induced voltage in stator, rotor are related to the machine speed as [19]:

$$\omega_{mech} = \omega_{stator} \pm \omega_{rotor} \tag{2.2}$$

Here ω_{mech} is the angular velocity of the machine, ω_{stator} is the angular frequency of the voltage induced in stator and ω_{rotor} is the angular frequency of induced voltage in rotor. The plus and minus sign depends on the phase sequence of the machine. The stator side of DFIG is energized from grid having fix frequency and stable voltage which produces revolving flux in the machine. The shaft is usually driven by a prime mover which in

this case is hydro turbine, the flow of water is controlled through governor which in turn controls shaft speed while the rotor is fed through electronic converter which supplies voltage with variable frequency and magnitude to the rotor circuit to achieve desired speed, torque or power control of the DFIG. The frequency at stator side of the machine is fixed and can be written in terms of mechanical angular speed as [14]:

$$\omega_{stator} = \frac{2.\pi.f_{grid}}{p_p} \tag{2.3}$$

Where f_{grid} is the frequency of the grid in Hz and p_p is the number of pole pairs of the machine. Knowing stator angular frequency and shaft speed, it is possible to calculate the rotor angular frequency using the following relation:

$$\omega_{rotor} = \omega_{stator} - \omega_{mech} \tag{2.4}$$

$$\omega_{rotor} = \omega_{mech} - \omega_{stator} \tag{2.5}$$

The changing of sign of stator angular frequency and mechanical angular speed in above equation can be illustrated as:
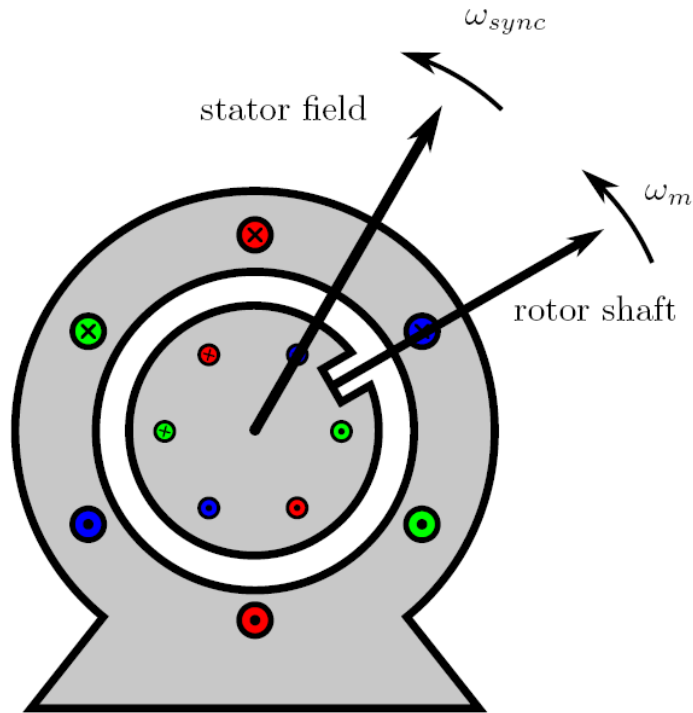
Figure 2.4: *Stator and rotor field in an induction machine.*

Imagine an observer is placed on the rotor so rotor is the reference frame and the speed of rotor appears to be constant to the observer now consider the first case when ω_{mech} is less
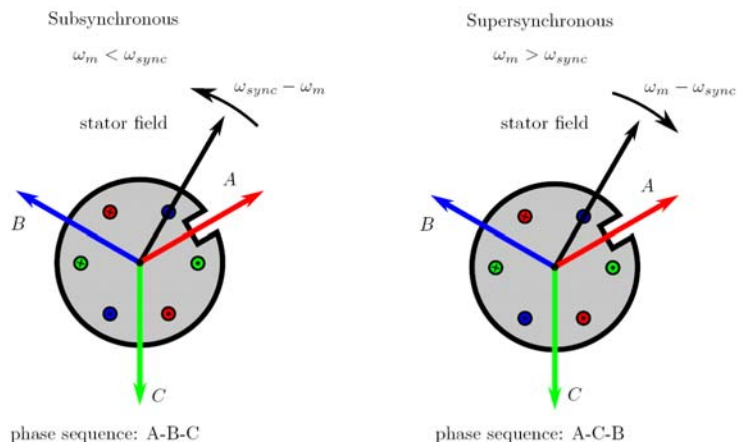
Figure 2.5: *Change in phase sequence of induction machine at super-synchronous speeds.*

than ω_{stator} and both are rotating in counter clockwise direction as shown in figure 2.5, here ω_{sync} and ω_m are the rotational speeds in electrical radians corresponding to ω_{stator} and ω_{mech} respectively. The revolving field will pass the observer with an angular velocity less than the ω_{stator} because of the relative speed between rotor shaft and stator field and the stator field will approach and pass the observer in time. Now consider the second case where ω_{mech} is higher than the stator's revolving field ω_{stator}, in this case it will be found that the revolving field is moving away from the observer. In the first case the approached magnetic field will induces voltage having phase sequence of A-B-C while in the second case its direction appears to be changed so the induced voltage will take the phase sequence A-C-B.

Stator's revolving magnetic field induces voltage in the rotor having frequency different from the grid and depends on the relative speed between revolving field and rotor. The induced frequency in rotor can be found as:

$$f_{rotor} = f_{stator} \cdot s \tag{2.6}$$

Where f_{rotor} is the frequency of voltage induced in the rotor and f_{stator} is the grid frequency while s is called slip and is given as [14]:

$$s = \frac{\omega_{stator} - \omega_{mech}}{\omega_{stator}} \tag{2.7}$$

The slip can be positive or negative depends on whether the speed of stator magnetic field is greater or less than the shaft speed respectively. The relation of equation (2.7) can be manipulated mathematically to find the mechanical speed of the shaft using equation (2.8).

$$\omega_{mech} = (1 - s)\omega_{stator} \tag{2.8}$$

2.1.2 Winding Turns Ratio Relation

Magnitude of voltage induced in the rotor is not merely depends on the slip speed. In a wound rotor machine it also depends upon the turns ratio between stator and rotor windings. The reason of referring the rotor quantities to the stator is that in a squirrel cage machine there is no access to the rotor to measure the rotor side parameters directly although this is not the case for wound rotor machine where these parameters can be measured directly from the rotor side yet in order to simplify the calculations it is handy to refer rotor parameters to stator side. The actual terminal voltage relation between stator and rotor is given as [18]:

$$\frac{E_r}{E_s} = s.\frac{k_r}{k_s}\frac{N_r}{N_s} \tag{2.9}$$

Where E_s and E_r are the stator and rotor emfs respectively, k_s and k_r are machine constants and depends on the construction of machine (i.e. pitch factor, winding factor) and is less than 1. N_s and N_r is the number of turns of stator and rotor winding. Assuming the $\frac{k_s}{k_r} \approx 1$ equation (2.9) reduces to:

$$\frac{E_r}{E_s} = \frac{s}{a} \tag{2.10}$$

Where a is the turns ratio and equal to $\frac{N_s}{N_r}$.

Using these relations, the actual parameters at the rotor side of the machine can be found from referred parameters as:

$$R_{r,act} = \frac{R_r}{(a)^2} \tag{2.11}$$

$$L_{lr,act} = \frac{L_{lr}}{(a)^2} \tag{2.12}$$

The above equations are useful to find either the actual rotor parameter referred to the stator side or to find the parameters referred to stator in case the actual values are known.

$$\bar{V}_{r,act} = \frac{\bar{V}_r}{a} \tag{2.13}$$

$$\bar{I}_{r,act} = \bar{I}_r a \tag{2.14}$$

The turns ratio is more important to find the voltage and current induced in the rotor side due to stator magnetic field and also in selecting the rotor side converter voltage level, although these parameters and turns ratios are provided by the manufacturer yet it is better to verify them before designing control as the correct estimation of parameters is the most important aspect in vector control of the machine.

2.2   Equations of DFIG in Steady State

Steady state equation can be written easily by applying the Kirchoff's voltage law to the circuit of figure 2.2, the stator and rotor voltage equations in phasor form are:

$$\bar{V}_s = R_s \bar{I}_s + j\omega_s \bar{\lambda}_s \tag{2.15}$$

$$\bar{V}_r = R_r \bar{I}_r + j\omega_r \bar{\lambda}_r \tag{2.16}$$

Where bar indicates that these quantities are in phasor form. The relation between flux linkages, machine parameters, and currents is given as:

$$\bar{\lambda}_s = L_s \bar{I}_s + L_m \bar{I}_r \tag{2.17}$$

$$\bar{\lambda}_r = L_r \bar{I}_r + L_m \bar{I}_s \tag{2.18}$$

Where $L_s = L_{ls} + L_m$ and $L_r = L_{lr} + L_m$,

These equations are complete steady state equations for the circuit of figure 2.2. They can also be written in terms of stator and rotor currents as:

$$\bar{I}_s = \frac{\begin{vmatrix} \bar{\lambda}_s & L_m \\ \bar{\lambda}_r & L_r \end{vmatrix}}{\begin{vmatrix} L_s & L_m \\ L_m & L_r \end{vmatrix}} = \frac{\bar{\lambda}_s L_r - \bar{\lambda}_r L_m}{L_s L_r - L_m^2} = \bar{\lambda}_s \frac{1}{\sigma L_s} - \bar{\lambda}_r \frac{L_m}{\sigma L_r L_s} \tag{2.19}$$

$$\bar{I}_r = \frac{\begin{vmatrix} L_s & \bar{\lambda}_s \\ L_m & \bar{\lambda}_r \end{vmatrix}}{\begin{vmatrix} L_s & L_m \\ L_m & L_r \end{vmatrix}} = \frac{\bar{\lambda}_r L_s - \bar{\lambda}_s L_m}{L_s L_r - L_m^2} = \bar{\lambda}_r \frac{1}{\sigma L_r} - \bar{\lambda}_s \frac{L_m}{\sigma L_r L_s} \tag{2.20}$$

Where σ is called the leakage factor and is equal to $1 - \frac{L_m^2}{L_s L_r}$

After writing the voltage and flux relation it is now time to look at the power relations for the circuit of figure 2.2. To keep the power relations simple, core losses, mechanical losses (i.e. windage, friction and stray losses) can be neglected. The model is still detailed enough to determine the steady state operating point of the machine [18].

2.3   Active Power

Active power can be fed from different points to the DFIG as can be seen from the figure 2.6. This DFIG circuit can receive power from three points i.e. stator terminals, rotor terminals, and mechanical shaft which depends on the operating mode the machine. Power relations can be defined in terms of motor convention whereby the current entering

the positive terminals of the source is taken as positive which implies that the current entering from stator and rotor side is the power supplied to the circuit and is positive and when the currents are out from positive terminals of stator and rotor then the power will be taken as negative.
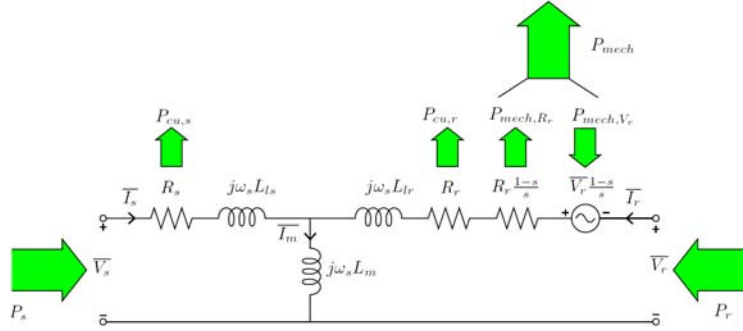
Figure 2.6: *Active power flow in a doubly fed induction machine.*

According to the motor convention mechanical power is taken as positive for motor operation and is taken as negative for generator operation. The equation for the stator power, rotor power, their losses, and mechanical power are:

$$P_s = 3Re\{\bar{V}_s\bar{I}_s^*\} \tag{2.21}$$

$$P_r = 3Re\{\bar{V}_r\bar{I}_r^*\} \tag{2.22}$$

$$P_{scu} = 3|\bar{I}_s|^2 R_s \tag{2.23}$$

$$P_{rcu} = 3|\bar{I}_r|^2 R_r \tag{2.24}$$

$$P_{mech} = P_{mech,R_r} + P_{mech,V_r} \tag{2.25}$$

$$P_{mech} = 3|\bar{I}_r|^2 R_r \frac{(1-s)}{s} - 3\frac{(1-s)}{s}Re\{\bar{V}_r\bar{I}_r^*\} \tag{2.26}$$

Note that the mechanical power contains two terms one is rotor resistance with slip factor and another is voltage fed to rotor having slip factor. The reason for the -*ve* sign of the rotor voltage term is to match the rotor voltage polarity V_r when $\frac{V_r}{s}$ is separated into two terms V_r and $\frac{V_r(1-s)}{s}$. Thus the complete power equation is:

$$P_{tot} = P_s + P_r = P_{mech} + P_{scu} + P_{rcu} \tag{2.27}$$

Further, slip and mechanical power can be expressed in terms of gap power P_{gap} and slip power P_{slip} as [20].

$$P_{mech} = (1-s)P_{gap} = \frac{(1-s)}{s}P_{slip} \tag{2.28}$$

2.4   Reactive Power

Reactive power is also essential to magnetize the machine as the electromagnetic torque in the machine is produced due to the interaction of magnetic fluxes from stator and rotor. The magnetizing inductance L_m and leakage reactance of stator and rotor side consumes reactive power and this power is supplied through quadrature component of power fed form stator and rotor side therefore reactive power relations for the machine are as follows[21].
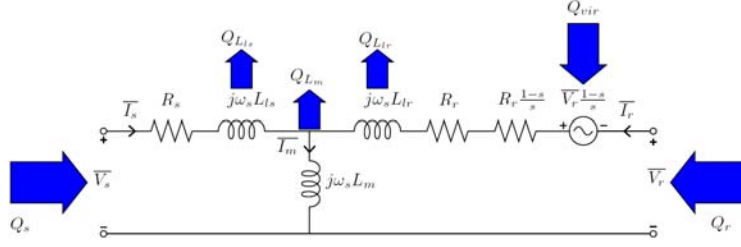
Figure 2.7: *Reactive power flow in a doubly fed induction machine.*

$$Q_{Lls} + Q_{Llr} + Q_{Lm} = Q_{vir} + Q_s + Q_r \tag{2.29}$$

Where,

$$Q_s = 3Im\{\bar{V}_s\bar{I}_s^{\,*}\} \tag{2.30}$$

$$Q_r = 3Im\{\bar{V}_r\bar{I}_r^{\,*}\} \tag{2.31}$$

$$Q_{Lls} = 3|\bar{I}_s|^2\omega_sL_{ls} \tag{2.32}$$

$$Q_{Llr} = 3|\bar{I}_r|^2\omega_sL_{lr} \tag{2.33}$$

$$Q_{Lm} = 3|\bar{I}_s + \bar{I}_r|^2\omega_sL_m \tag{2.34}$$

$$Q_{vir} = 3Im\left\{\frac{(1-s)}{s}\bar{V}_r\bar{I}_r^{\,*}\right\} \tag{2.35}$$

Note that all the terms except Q_{vir} has physical meaning, this term is a virtual effect and is introduced into the circuit to model the effect of reactive power from converter connected to the rotor [22].

2.5 Electromagnetic Torque

The torque relation in rotating machines is the link between electrical and mechanical part of the system and this mechanical torque at the shaft can be written as:

$$T_e = \frac{P_{mech}}{\omega_{mech}} \tag{2.36}$$

Also the electromagnetic torque T_e can be expressed in terms of fluxes and currents or combination of both [18].

$$T_e = 3p_p L_m Im\{\bar{I}_s \bar{I}_r^*\} \tag{2.37}$$

$$T_e = 3p_p \frac{L_m}{\sigma L_r L_s} Im\{\bar{\lambda}_s \bar{\lambda}_r^*\} \tag{2.38}$$

2.6 Modes of Operation

The Doubly-Fed Induction Machine can be run in four operating modes as can be seen from the torque and angular speed diagram in figure 2.8. In four quadrant operation of DFIG direction of angular speed is always same and this speed could be super synchronous i.e. higher than the rotating magnetic field or sub synchronous i.e. lower than the rotating magnetic field, but the direction of electromagnetic torque can change. This is slightly different from the general four quadrant operation of a motor where torque as well as angular speed both changes direction to change the operating mode, motor or generator. [18].
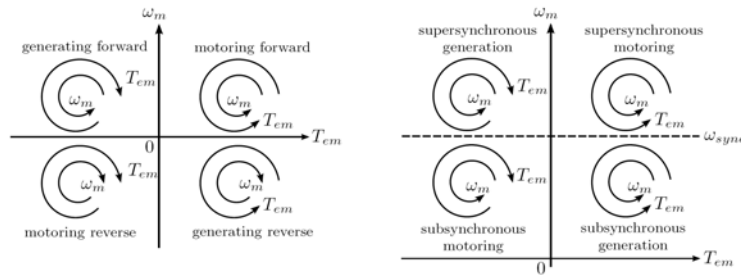
Figure 2.8: *Left: General four quadrant operation, Right: Four quadrant operation in one direction [18].*

Power flow in DFIG for all the four quadrant operation will be discussed here briefly with the help of machine flow diagrams. The power flow under discussion is only real power, in addition, power losses in stator and rotor windings are also implicitly the dissipated power and thus are not shown in diagrams.

Subsynchronous Motoring

In this mode of operation the shaft speed is less than the synchronous speed thus the slip is positive and power transferred across air gap from stator is delivered to the shaft and rotor terminals.
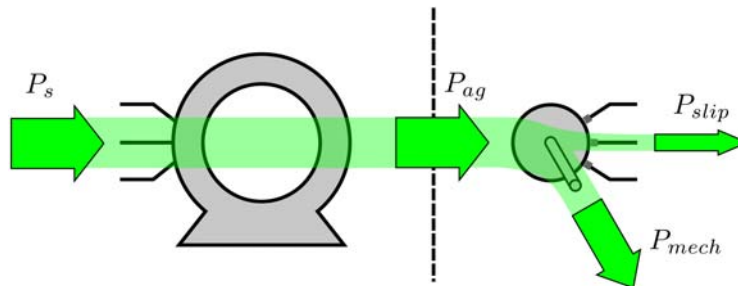
Figure 2.9: *DFIG power flow in subsynchronous motoring mode.*

Supersynchronous Motoring

In this mode of operation the shaft turns at speed greater than the synchronous speed thus the slip is negative and power delivered to the shaft comes form stator via air gap and also injected from rotor terminals.
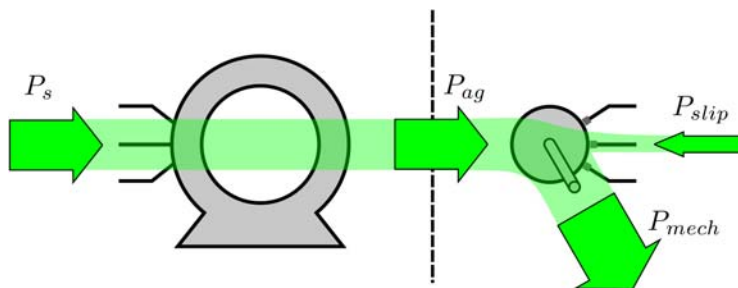
Figure 2.10: *DFIG power flow in supersynchronous motoring mode.*

Supersynchronous Generating

In this mode of operation the shaft turns at speed greater than the synchronous speed thus slip is negative and the power is supplied by mechanical shaft to stator and also to the rotor circuit.
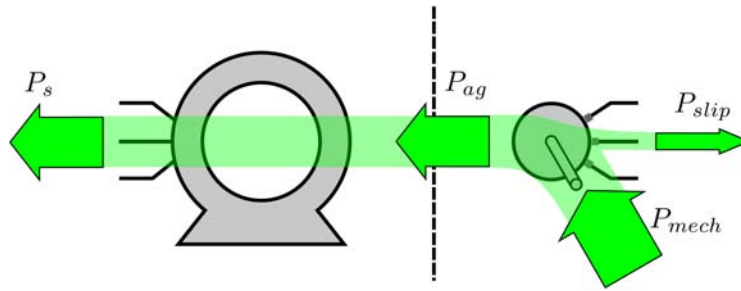
Figure 2.11: *DFIG power flow in supersynchronous generating mode.*

Subsynchronous Generating

In this mode of operation the shaft turns at speed less than the synchronous speed thus slip is positive and total power delivered to the machine stator comes from both mechanical shaft and also from rotor side.
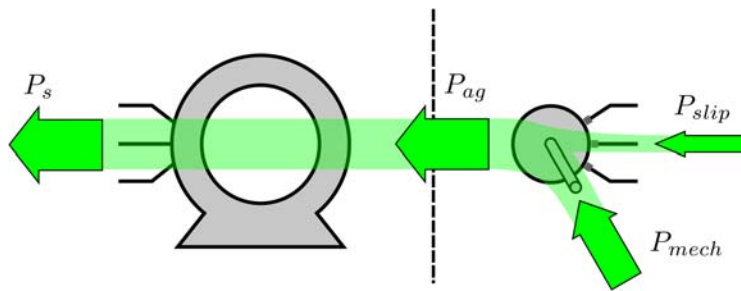
Figure 2.12: *DFIG power flow in subsynchronous generating mode.*

2.7 Steady State Solution

DFIG is fed from two sources one from stator and another from rotor, the voltage from the stator side is fixed with almost constant frequency but the rotor side voltage amplitude and frequency can be varied through converter which generates V_r based on the control set points and input parameters of the machine. Assuming the parameters of the machine are accurately known, set points or reference values are also required to achieve control. In hydro system under study this set point values are real and reactive power references for both rotor side and grid side converters, for machine side converter real power or desired speed of the turbine is set. Speed reference can be calculated from turbine model based on the change in power set point or power demand while the reactive power is based on requirement of power factor. Therefore, it is a good starting point to take the stable stator side voltage and desired reference power to find the initial values for the model. The steady state solution can be found by using equation (2.39) to equation (2.45) in the given order [18].

$$\bar{V}_s = \frac{V_{LL,rms}}{\sqrt{3}} \angle 0^o \tag{2.39}$$

$$P_s^{ref} + jQ_s^{ref} = 3\bar{V}_s\bar{I}_s^* \tag{2.40}$$

$$\bar{I}_s = \frac{P_s^{ref} - jQ_s^{ref}}{\bar{V}_s^*} \tag{2.41}$$

$$\bar{\lambda}_s = \frac{\bar{V}_s - \bar{I}_sR_s}{j\omega_s} \tag{2.42}$$

$$\bar{I}_r = \frac{\bar{\lambda}_s - \bar{I}_sL_s}{L_m} \tag{2.43}$$

$$\bar{\lambda}_r = \bar{I}_rL_r + \bar{I}_sL_m \tag{2.44}$$

$$\bar{V}_r = \bar{I}_rR_r + j\omega_r\bar{\lambda}_r \tag{2.45}$$

Chapter 3

Dynamic Model of DFIG

Dynamic model of induction machine will be derived based on space vector and rotation transformation. The set of four differential equations which relates the interaction between electrical variables along with the dynamic torque's fifth equation which links the electrical quantities to the mechanical ones. First the assumptions taken for machines model for simplification of control [23, 24, 25] will be described then space vector concept and reference frame transformation will be visited and the equations in rotating frame will be derived to simulate the DFIG and grid model finally the dynamic model block diagram for DFIG is presented and model is validated.

The objective in defining the machine model and taking assumptions is to find an adequate and accurate enough model for which a suitable and simple control system could be developed. Therefore, below assumption are being defined for the model.

- There are no iron losses in the machine and iron core has infinite permeability.

- Flux in machine air gap is radial and its wingdings are sinusoidally distributed.

- The machine is perfectly symmetrical along its entire axis.

- Thus generated or induced voltage has sinusoidal waveform and are also balanced.

3.0.1 The Space Vector

Space vectors are used to simplify the machine model and three phase quantities can be represented in a compact form. To understand it, consider a two pole machine single

phase AC machine in which the flux distribution in the entire gap is sinusoidal. If we see the cross section of the machine in figure 3.1 then winding in upper slot carrying current are outward from the page whereas the downward coils are carrying current into the page this is represented through arrow notation. The direction of flux or maximum flux density lies along the axis of the coils and can be found using the grip rule. Note in figure 3.2 that the magnitude of flux varies with current, however, the direction of flux lies perpendicular to the machine axis.
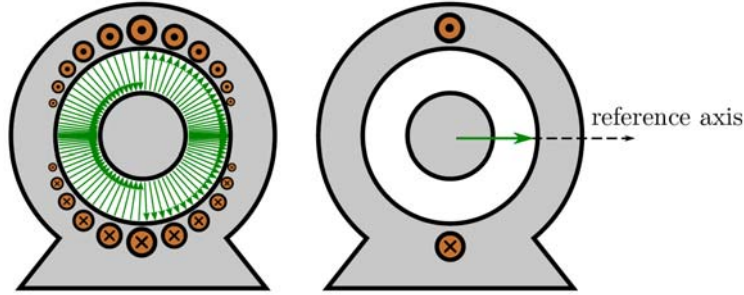
Figure 3.1: *Physical meaning of space vector in single phase machine.*
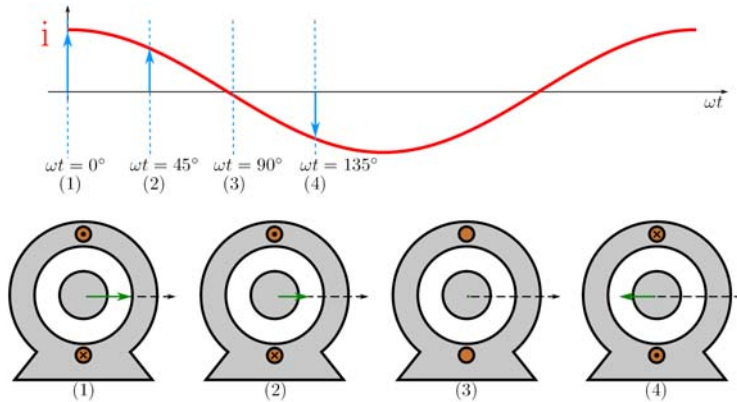
Figure 3.2: *Flux variation in a single phase machine with current at different instants.*

Because the machine to be controlled has three phase winding both on stator and rotor thus by applying the space vector concept to the machine in figure 3.3, it can be seen that the mmf space vector for each of the three phase windings can be represented by a vector of appropriate length, and direction of the this vector lies along the magnetic axis of coil.

All three sinusoidally distributed phase mmf vectors can be added together and represented by a single space vector with a constant magnitude and changes its direction based on instantaneous value of phase mmf vectors. Mathematically this can be written as:

$$\vec{F_s}^a = \vec{F_a}^a(t) + \vec{F_b}^a(t) + \vec{F_c}^a(t) \tag{3.1}$$

where F represent mmf subscript s represent resultant stator quantities and superscript a denotes that space vector is a complex number. This explanation reveals that the space
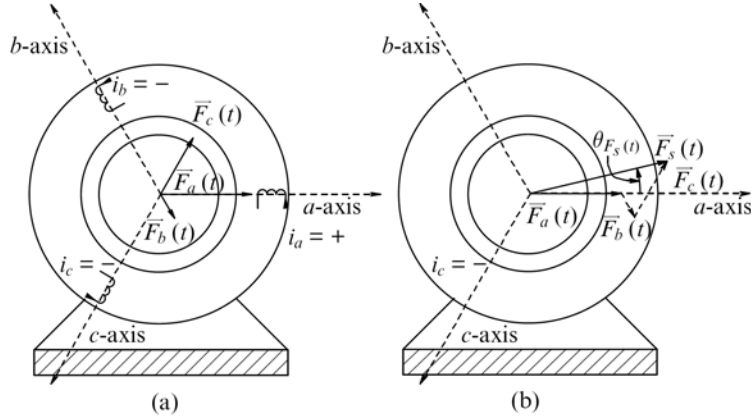
Figure 3.3: *MMF space vector in three phase machine.*

vectors can also be applied for dynamic analysis [23]. Although current, voltage, and flux linkage do not have physical meaning whereas mmf and flux is sinusoidally distributed in space and have physical meaning. Yet the current, voltage and flux linkages can be represented by space vector.
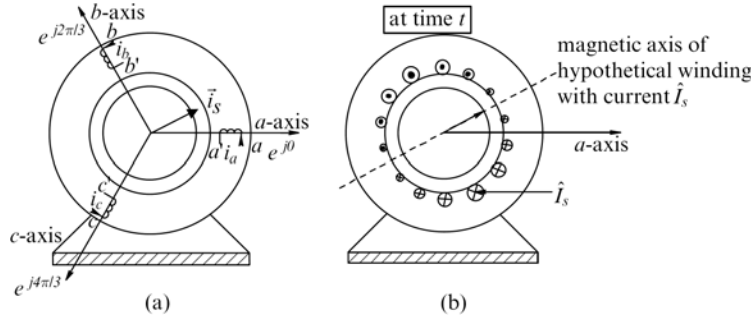
Figure 3.4: *Current space vector representation in a three phase machine.*

The current is responsible for producing the mmf in air gap and this mmf varies sinusoidally as current varies thus all three mmfs are reflection of stator current similarly the vector sum of current space vector at any instant can also be represented by a single sinusoidally distributed hypothetical winding whose magnitude and direction of mmf changes in accordance with current see figure 3.4. Thus all the three phase currents, voltages, and flux linkages can be summed up and represented in space vector form as:

$$\vec{i_s}^{\,a} = i_a(t)e^{j0} + i_b(t)e^{j\frac{2\pi}{3}} + i_c(t)e^{j\frac{4\pi}{3}} = \hat{I}_s(t)e^{j\theta_{is}(t)} \tag{3.2}$$

$$\vec{v_s}^{\,a} = v_a(t)e^{j0} + v_b(t)e^{j\frac{2\pi}{3}} + v_c(t)e^{j\frac{4\pi}{3}} = \hat{V}_s(t)e^{j\theta_{vs}(t)} \tag{3.3}$$

$$\vec{\lambda_s}^{\,a} = \lambda_a(t)e^{j0} + \lambda_b(t)e^{j\frac{2\pi}{3}} + \lambda_c(t)e^{j\frac{4\pi}{3}} = \hat{\lambda}_s(t)e^{j\theta_{vs}(t)} \tag{3.4}$$

Where symbol $\hat{}$ denotes the peak value of space vector quantities and $e^{j\theta}$ represents the position of vector and as three phases are 120^0 apart so different phase factor $(e^{j\theta})$ is multiplied with each phase. Further mathematical insight regarding the relation of space vector with phase quantities can be seen by working out the expression for voltage space vector:

$$\vec{v_a}^s = v_a(t)\angle 0^o = v_a(t)e^{j0} \tag{3.5a}$$

$$\vec{v_b}^s = v_b(t)\angle 120^o = v_b(t)e^{j\frac{2\pi}{3}} \tag{3.5b}$$

$$\vec{v_c}^s = v_c(t)\angle 240^o = v_c(t)e^{j\frac{4\pi}{3}} \tag{3.5c}$$

Where,

$$v_a(t) = \hat{V}\cos(\omega t + \phi) \tag{3.6a}$$

$$v_b(t) = \hat{V}\cos(\omega t + \phi - \frac{2\pi}{3}) \tag{3.6b}$$

$$v_a(t) = \hat{V}\cos(\omega t + \phi - \frac{4\pi}{3}) \tag{3.6c}$$

The $v_a(t)$ is time varying voltage of phase a and the superscript of space vector denotes the reference frame for space vector. Now by putting the values of all three phase voltages in above equation and adding, result in:

$$\vec{v_s}^s = \vec{v_a}^s + \vec{v_b}^s + \vec{v_c}^s \tag{3.7}$$

$$\vec{v_s}^s = \frac{3}{2}\hat{V}e^{j(\omega t + \phi)} \tag{3.8}$$

This shows that by adding three phase sinusoidal voltages the resultant voltage space vector will be having a magnitude equal to $\frac{3}{2}$ times the peak value of phase voltage and rotates with an angular speed of ω in space with time, this is same as explained previously for the flux and can be seen from figure 3.5 for voltage vector. Dynamic equation for stator and rotor voltages can be written in space vector form as:

$$\vec{v_s}^a(t) = R_s\vec{i_s}^a(t) + \frac{d\vec{\lambda_s}^a(t)}{dt} \tag{3.9}$$

$$\vec{v_r}^A(t) = R_r\vec{i_r}^A(t) + \frac{d\vec{\lambda_r}^A(t)}{dt} \tag{3.10}$$

Where superscripts a and A denotes the reference axis for stator and rotor respectively.
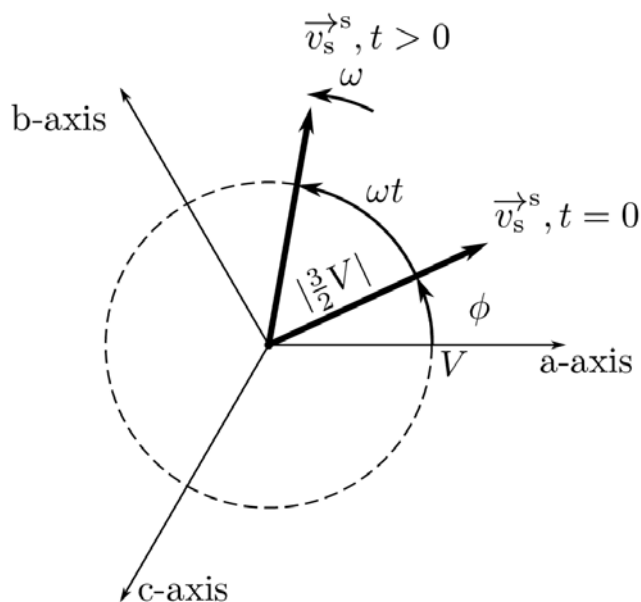
Figure 3.5: *Graphical representation of space vector rotation with time.*

3.0.2   Reference Frame Transformation

As can be seen from the previous discussion that space vector representation is a compact representation of the three phase quantities. This space vector can be decomposed into two components and a three phase machine can be represented through space vector into two axis model.

The DFIG to be controlled has two circuit one is stator and another is rotor. These stator and rotor circuits are in relative motion to each other and linked through the air gap flux. As the rotor changes its position with time the machine inductances also varies and to control the machine in real time the value of these parameters must be known and the calculation of inductances and their derivatives needs to be carried out in each time step. This makes the calculation very tedious, however, with today's powerful processing technology these computations can be performed but the transformation of both stator and rotor quantities to a common reference frame rotating at the proper speed (usually synchronous speed) can make these time varying inductances constant thus makes it useful to apply simple control techniques[23, 24, 25, 26, 27].

The time varying voltages, currents, and flux linkages can be transformed to different reference frames. Such as Clark's transformation [28, 29] which is a two axis transformation and is used in electrical system to convert the stator and rotor quantities to their respective reference frames that is a stationary frame. The x-axis is usually called alpha axis and y-axis is called the beta axis and both are orthogonal to each other. The transformation matrix and transformed quantities of Clarks transformation for three phase

quantities are given in equation (3.11).

$$
\begin{bmatrix} x_\alpha \\ x_\beta \\ x_0 \end{bmatrix} = c \begin{bmatrix} 1 & -\frac{1}{2} & -\frac{1}{2} \\ 0 & \frac{\sqrt{3}}{2} & -\frac{\sqrt{3}}{2} \\ \frac{1}{2} & \frac{1}{2} & \frac{1}{2} \end{bmatrix} \begin{bmatrix} x_a \\ x_b \\ x_c \end{bmatrix} = T_{\alpha\beta,abc}\vec{x_{abc}}
\tag{3.11}
$$

Where x is a general variable and $T_{\alpha\beta,abc}$ is called transformation matrix and c is a factor which is usually chosen to translate the magnitude of the three phase quantities equal to alpha beta. This is important so that when alpha beta quantities are converted back to the three phase again then magnitude of the three phase quantities remains same.

Here value of c is $\frac{2}{3}$ for voltage and current quantities but then the power and torque do not have same magnitude as in three phases and needs to be multiplied by a factor of $\frac{3}{2}$, this derivation can be referred in B.1.

The graphical representation in figure 3.6 shows the different reference frames, the $\alpha\beta$ frame is attached to the stator and not moving similarly the xy frame is attached to the rotor while the dq frame is rotating at a speed of ω_k. The stator voltage equation can be written in stator or $\alpha\beta$ reference frame by using Clark transformation as:
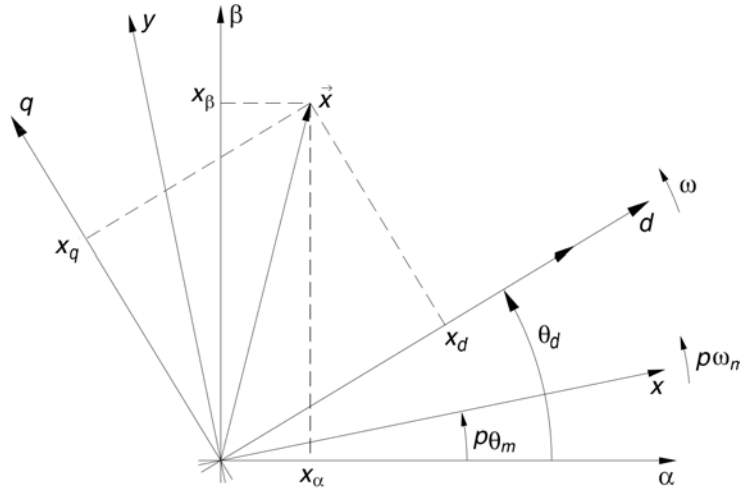
Figure 3.6: *Graphical representation of space vector rotation with time.*

$$
\vec{v_{s_{\alpha\beta}}}^\alpha = R_s \vec{i_{s_{\alpha\beta}}}^\alpha + \frac{d\vec{\lambda_{s_{\alpha\beta}}}^\alpha}{dt}
\tag{3.12}
$$

And after decomposition into alpha beta:

$$
v_{s_\alpha} = R_s i_{s_\alpha} + \frac{d\lambda_{s\alpha}}{dt}
\tag{3.13}
$$

$$v_{s_\beta} = R_s i_{s_\beta} + \frac{d\lambda_{s\beta}}{dt} \tag{3.14}$$

where $\vec{v_{s_{\alpha\beta}}}^{\alpha} = v_{s_\alpha} + jv_{s_\beta}$

Clark transformation matrix has constant values because stator coils are fixed to the stator thus has a fix phase angle difference but when the position of the coil changes with time such as the motion between stator and rotor frames then the transformation matrix does not contain the constant values so the transformation matrix for dq reference frame rotating at a speed of ω_k in figure 3.6 is given as:

$$e^{j\theta} = \begin{bmatrix} \cos\theta & -\sin\theta \\ \sin\theta & \cos\theta \end{bmatrix} = T_{rot}(\theta) \tag{3.15}$$

This transformation matrix contains cosine and sine terms which needs angle of the rotating frame relative to other frame, having quantity which is to be transformed continuously. This rotating transformation is also called Park transformation and is used to convert the quantities into a rotating frame. Now using the above transformation matrix and looking at figure 3.6 voltage equation for stator is given as:

$$\vec{v_{s,\alpha\beta}}^{\alpha} = \vec{v_{s,dq}} . e^{j\theta_k} \tag{3.16a}$$

$$\vec{i_{s,\alpha\beta}}^{\alpha} = \vec{i_{s,dq}} . e^{j\theta_k} \tag{3.16b}$$

$$\vec{\lambda_{s,\alpha\beta}}^{\alpha} = \vec{\lambda_{s,dq}} . e^{j\theta_k} \tag{3.16c}$$

where $\vec{v_{s,dq}} = v_{sd} + jv_{sq}$

Now substituting in equation (3.12), we get:

$$\vec{v_{s,dq}} . e^{j\theta_k} = R_s \vec{i_{s,dq}} . e^{j\theta_k} + \frac{d}{dt}(\vec{\lambda_{s,dq}} . e^{j\theta_k}) \tag{3.17}$$

Or

$$\vec{v_{s,dq}} . e^{j\theta_k} = R_s \vec{i_{s,dq}} . e^{j\theta_k} + \frac{d\vec{\lambda_{s,dq}}}{dt}(.e^{j\theta_k}) + j\frac{d\theta_k}{dt}(\vec{\lambda_{s,dq}} . e^{j\theta_k}) \tag{3.18}$$

where $\frac{d}{dt}\theta_k = \omega_k$

Decomposing stator voltage equation (3.18) after simplification into dq components, yields.

$$v_{sd} = R_s i_{sd} + \frac{d}{dt}\lambda_{sd} - \omega_k \lambda_{sq} \tag{3.19}$$

$$v_{sq} = R_s i_{sq} + \frac{d}{dt}\lambda_{sq} + \omega_k \lambda_{sd} \tag{3.20}$$

Or in matrix form

$$
\begin{bmatrix} v_{sd} \\ v_{sq} \end{bmatrix} = R_s \begin{bmatrix} i_{sd} \\ i_{sq} \end{bmatrix} + \frac{d}{dt} \begin{bmatrix} \lambda_{sd} \\ \lambda_{sq} \end{bmatrix} + \omega_k \begin{bmatrix} 0 & -1 \\ 1 & 0 \end{bmatrix} \begin{bmatrix} \lambda_{sd} \\ \lambda_{sq} \end{bmatrix} \tag{3.21}
$$

Following the same lines we can also write the equation for rotor in dq as:

$$
\vec{v_{r,dq}}.e^{j(\theta_k - \theta_m)} = R_r \vec{i_{r,dq}}.e^{j(\theta_k - \theta_m)} + \frac{d\vec{\lambda_{r,dq}}}{dt}(.e^{j(\theta_k - \theta_m)}) + j\frac{d(\theta_k - \theta_m)}{dt}(\vec{\lambda_{r,dq}}.e^{j(\theta_k - \theta_m)}) \tag{3.22}
$$

where $\frac{d}{dt}(\theta_k - \theta_m) = \omega_k - \omega_m$ and $\omega_m = \frac{p}{2}.\omega_{mech}$

Decomposing the rotor voltage equation (3.22) into dq components yield:

$$
v_{rd} = R_r i_{rd} + \frac{d}{dt}\lambda_{rd} - (\omega_k - \omega_m)\lambda_{rq} \tag{3.23}
$$

$$
v_{rq} = R_r i_{rq} + \frac{d}{dt}\lambda_{rq} + (\omega_k - \omega_m)\lambda_{rd} \tag{3.24}
$$

in matrix form,

$$
\begin{bmatrix} v_{rd} \\ v_{rq} \end{bmatrix} = R_r \begin{bmatrix} i_{rd} \\ i_{rq} \end{bmatrix} + \frac{d}{dt} \begin{bmatrix} \lambda_{rd} \\ \lambda_{rq} \end{bmatrix} + (\omega_k - \omega_m) \begin{bmatrix} 0 & -1 \\ 1 & 0 \end{bmatrix} \begin{bmatrix} \lambda_{rd} \\ \lambda_{rq} \end{bmatrix} \tag{3.25}
$$

Notice that a new term is introduced in voltage equations of stator and rotor after differentiation. This speed voltage term is introduced due to rotating frame transformation. As the relative speed between stator and rotating frame is ω_k so the term contains the ω_k factor whereas the relative motion between rotating frame and rotor in the difference of speed between the two frames. After writing voltage equations in a common rotating reference frame it is important to choose the state variables for simulation. Examining above equations and knowing flux and current relations it can be said that either flux or current can be chosen as the state variable, however, the flux changes slowly as compared to the currents so the simulation can be done with a larger time step so it will be a good choice to take flux as state variable for simulation. These equations can be written in terms of flux linkages to obtain state space form by rearranging the terms.

$$
\frac{d}{dt}\begin{bmatrix} \lambda_{sd} \\ \lambda_{sq} \end{bmatrix} = \begin{bmatrix} v_{sd} \\ v_{sq} \end{bmatrix} - R_s \begin{bmatrix} i_{sd} \\ i_{sq} \end{bmatrix} - \omega_k \begin{bmatrix} 0 & -1 \\ 1 & 0 \end{bmatrix} \begin{bmatrix} \lambda_{sd} \\ \lambda_{sq} \end{bmatrix} \tag{3.26}
$$

$$
\frac{d}{dt}\begin{bmatrix} \lambda_{rd} \\ \lambda_{rq} \end{bmatrix} = \begin{bmatrix} v_{rd} \\ v_{rq} \end{bmatrix} - R_r \begin{bmatrix} i_{rd} \\ i_{rq} \end{bmatrix} - (\omega_k - \omega_m) \begin{bmatrix} 0 & -1 \\ 1 & 0 \end{bmatrix} \begin{bmatrix} \lambda_{rd} \\ \lambda_{rq} \end{bmatrix} \tag{3.27}
$$

Or in vector form as,

$$
\frac{d\vec{\lambda_{s,dq}}}{dt} = \vec{v_{s,dq}} - R_s\vec{i_{s,dq}} - \omega_k \begin{bmatrix} 0 & -1 \\ 1 & 0 \end{bmatrix} \vec{\lambda_{s,dq}} \tag{3.28}
$$

$$\frac{d\vec{\lambda}_{r,dq}}{dt} = \vec{v_{r,dq}} - R_r\vec{i_{r,dq}} - (\omega_k - \omega_m)\begin{bmatrix} 0 & -1 \\ 1 & 0 \end{bmatrix}\vec{\lambda}_{r,dq} \tag{3.29}$$

To make the simulation model workable in these state space equations of flux linkages, currents need to be computed, which can be obtained by using the following current and flux linkage relations:

$$\lambda_{sd} = L_s i_{sd} + L_m i_{rd} \tag{3.30}$$

$$\lambda_{sq} = L_s i_{sq} + L_m i_{rq} \tag{3.31}$$

$$\lambda_{rd} = L_r i_{rd} + L_m i_{sd} \tag{3.32}$$

$$\lambda_{rq} = L_r i_{rq} + L_m i_{sq} \tag{3.33}$$

Writing in matrix form,

$$\begin{bmatrix} \lambda_{sd} \\ \lambda_{sq} \\ \lambda_{rd} \\ \lambda_{rq} \end{bmatrix} = \begin{bmatrix} L_s & 0 & L_m & 0 \\ 0 & L_s & 0 & L_m \\ L_m & 0 & L_r & 0 \\ 0 & L_m & 0 & L_r \end{bmatrix}\begin{bmatrix} i_{sd} \\ i_{sq} \\ i_{rd} \\ i_{rq} \end{bmatrix} \tag{3.34}$$

Solving for currents result in:

$$\begin{bmatrix} i_{sd} \\ i_{sq} \\ i_{rd} \\ i_{rq} \end{bmatrix} = inv\left(\begin{bmatrix} L_s & 0 & L_m & 0 \\ 0 & L_s & 0 & L_m \\ L_m & 0 & L_r & 0 \\ 0 & L_m & 0 & L_r \end{bmatrix}\right)\begin{bmatrix} \lambda_{sd} \\ \lambda_{sq} \\ \lambda_{rd} \\ \lambda_{rq} \end{bmatrix} \tag{3.35}$$

Currents can be computed by using the flux linkage state variables with the inverse of inductance matrix. These dynamic equations can be used to write the stator power in the chosen reference frame using the relation:

$$p_s = \vec{v_{s,abc}}^T \vec{i_{s,abc}} \tag{3.36}$$

$$p_s = (T_{\alpha\beta,abc}^{-1}\vec{v_{s,\alpha\beta}})^T(T_{\alpha\beta,abc}^{-1}\vec{i_{s,\alpha\beta}}) \tag{3.37}$$

$$p_s = \vec{v_{s,\alpha\beta}}^T(T_{\alpha\beta,abc}^{-1})^T T_{\alpha\beta,abc}^{-1}\vec{i_{s,\alpha\beta}} \tag{3.38}$$

$$p_s = \vec{v_{s,\alpha\beta}}^T\begin{bmatrix} \frac{3}{2} & 0 & 0 \\ 0 & \frac{3}{2} & 0 \\ 0 & 0 & 3 \end{bmatrix}\vec{i_{s,\alpha\beta}} \tag{3.39}$$

$$p_s = \frac{3}{2}(v_{s\alpha}^s i_{s\alpha}^s + v_{s\beta}^s i_{s\beta}^s + 2v_{s0}^s i_{s0}^s) \tag{3.40}$$

Where zero component does not contribute to flux because the system is assumed to be balance so,

$$p_s = \frac{3}{2}(v_{s\alpha}^s i_{s\alpha}^s + v_{s\beta}^s i_{s\beta}^s) \tag{3.41}$$

Or

$$p_s = \frac{3}{2}(\vec{i}_s^{\,s,T} \vec{v}_s^{\,s}) \tag{3.42}$$

Recall that voltage equations in stator or alpha and beta frame are:

$$\vec{v}_s^{\,s} = R_s \vec{i}_s^{\,s} + \frac{d\vec{\lambda}_s^{\,s}}{dt} \tag{3.43}$$

Stator flux linkage comprises of leakage and mutual flux terms so equation (3.43) can be rewritten as:

$$\vec{v}_s^{\,s} = R_s \vec{i}_s^{\,s} + \frac{d\vec{\lambda}_{ls}^{\,s}}{dt} + \frac{d\vec{\lambda}_m^{\,s}}{dt} = R_s \vec{i}_s^{\,s} + L_{ls}\frac{d\vec{i}_s^{\,s}}{dt} + \frac{d\vec{\lambda}_m^{\,s}}{dt} \tag{3.44}$$

The differential of stator current in alpha beta frame is:

$$\frac{d}{dt}\begin{bmatrix} i_{s\alpha}^s \\ i_{s\beta}^s \end{bmatrix} = \begin{bmatrix} -i_{s\beta}^s \\ i_{s\alpha}^s \end{bmatrix} p_p \frac{d\theta}{dt} = \begin{bmatrix} 0 & -1 \\ 1 & 0 \end{bmatrix}\begin{bmatrix} i_{s\alpha}^s \\ i_{s\beta}^s \end{bmatrix} p_p \frac{d\theta}{dt} \tag{3.45}$$

Where θ is mechanical angle in radians by which the rotor changes its position. Putting this in voltage equation (3.44) yields:

$$\vec{v}_s^{\,s} = R_s \vec{i}_s^{\,s} + L_{ls}\begin{bmatrix} 0 & -1 \\ 1 & 0 \end{bmatrix}\begin{bmatrix} i_{s\alpha}^s \\ i_{s\beta}^s \end{bmatrix} p_p \frac{d\theta}{dt} + \begin{bmatrix} 0 & -1 \\ 1 & 0 \end{bmatrix}\vec{\lambda}_m^{\,s} p_p \frac{d\theta}{dt} \tag{3.46}$$

Now substituting this voltage equation in power equation (3.42).

$$p_s = \frac{3}{2}\left(R_s\vec{i}_s^{\,s}\vec{i}_s^{\,s,T} + L_{ls}\vec{i}_s^{\,s,T}\begin{bmatrix} 0 & -1 \\ 1 & 0 \end{bmatrix}\begin{bmatrix} i_{s\alpha}^s \\ i_{s\beta}^s \end{bmatrix} p_p \frac{d\theta}{dt} + \vec{i}_s^{\,s,T}\begin{bmatrix} 0 & -1 \\ 1 & 0 \end{bmatrix}\vec{\lambda}_m^{\,s} p_p \frac{d\theta}{dt}\right) \tag{3.47}$$

Note that mutual flux term in power equation can be replaced using the current flux linkage relation of equation (3.48).

$$\vec{\lambda}_s^{\,s} = L_s\vec{i}_s^{\,s} + L_m\vec{i}_r^{\,s} \tag{3.48}$$

Replacing $\vec{\lambda}_m^{\,s} = L_m \vec{i}_r^{\,s}$ in equation (3.46) results in:

$$p_s = \frac{3}{2}\left(R_s \vec{i}_s^{\,s} \vec{i}_s^{\,s,T} + L_{ls} \vec{i}_s^{\,s,T} \begin{bmatrix} 0 & -1 \\ 1 & 0 \end{bmatrix} \begin{bmatrix} i_{s\alpha}^s \\ i_{s\beta}^s \end{bmatrix} p_p \frac{d\theta}{dt} + L_m \vec{i}_s^{\,s,T} \begin{bmatrix} 0 & -1 \\ 1 & 0 \end{bmatrix} \vec{i}_r^{\,s} p_p \frac{d\theta}{dt} \right) \quad (3.49)$$

The electromagnetic torque links electrical and mechanical systems. In rotating machines torque is produced due to the interaction of stator and rotor fluxes, these fluxes are the result of current flow through machine winding. Torque is a cross product of two fluxes [11]. In power equation (3.49), the first term shows the power dissipation, second term corresponding to the leakage flux is zero, and third term gives the mechanical power, this term also shows the link between power, speed and torque that is:

$$p_m = T_e \frac{d\theta}{dt} \quad (3.50)$$

Relating equation (3.50) with mechanical power term in equation (3.49). Torque can be written as:

$$T_e = \frac{3}{2}.p_p L_m \vec{i}_s^{\,s,T} \begin{bmatrix} 0 & -1 \\ 1 & 0 \end{bmatrix} \vec{i}_r^{\,s} \quad (3.51)$$

Or

$$T_e = \frac{3}{2} p_p L_m (i_{s\beta}^s i_{r\alpha}^s - i_{s\alpha}^s i_{r\beta}^s) \quad (3.52)$$

This equation can also be written in dq or Park transformation as

$$T_e = \frac{3}{2} p_p L_m (i_{sq}^k i_{rd}^k - i_{sd}^k i_{rq}^k) \quad (3.53)$$

Or using the flux current relation:

$$T_e = \frac{3}{2} p_p (i_{sq}^k \lambda_{sd}^k - i_{sd}^k \lambda_{sq}^k) \quad (3.54)$$

In DFIG power generation system, speed of the shaft depends on torque applied to the shaft. Normally the generator is driven by prime mover which in this case is hydro turbine which applies the mechanical torque on the shaft whereas electromagnetic torque is produced in the machine due to interaction of fluxes and counters the mechanical torque. The difference of these two causes the machine to accelerate or decelerate. The machine speed can be determined through the well known speed torque dynamic equation[25].

$$T_e - T_{load} = J \frac{d}{dt} \omega_{mech} \quad (3.55)$$

Where T_e is the electromagnetic torque and T_{load} is the mechanical torque applied by the prime mover to the shaft. The choice of the sign of torque depends on the direction of the torque which is usually taken as positive for motor convention and negative for generator, however, the prime mover always spins in the same direction. Let's assume this direction is positive for counter clockwise then the direction of T_e is negative if it is in the clock wise direction and thus generating whereas it will be in motoring mode when T_e is positive i.e. in the same direction as ω_m.

$$\frac{d}{dt}\omega_m = \frac{p_p}{J}(T_e - T_{load}) \tag{3.56}$$

This dynamic equation (3.56) shows the torque speed relation and can be used to obtain rotor speed.

3.1 Dynamic Model of DFIG for Simulation

Using the equations from previous section a model for simulation of DFIG can be built in Matlab/Simulink. Block diagram of the model is shown in figure 3.7.
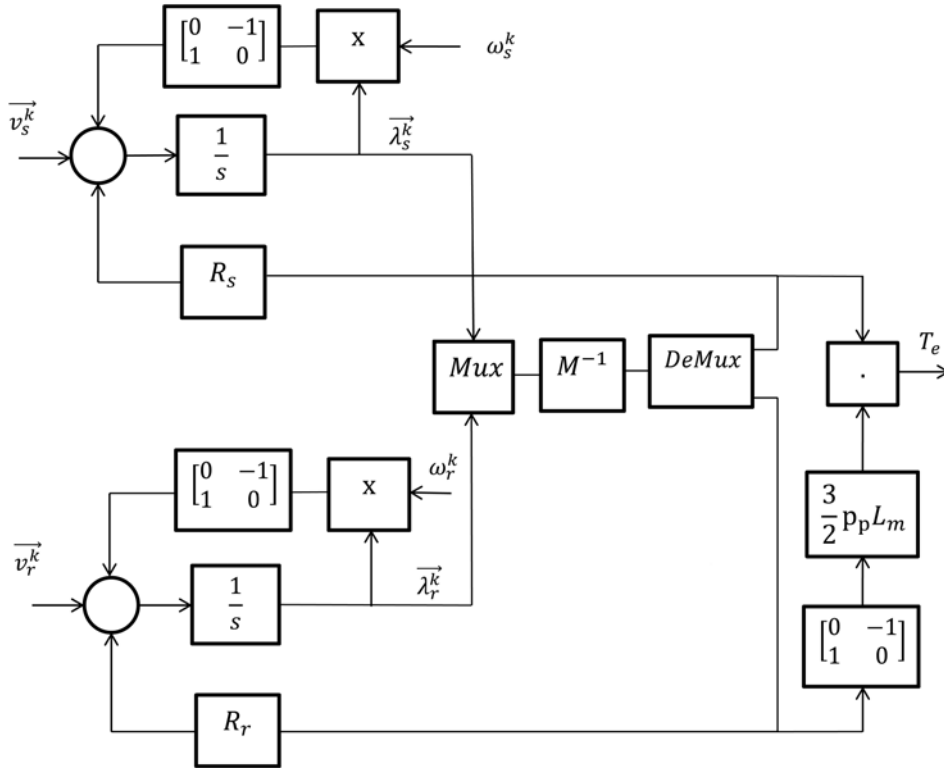
Figure 3.7: *Dynamic Model of DFIG for simulation.*

3.2   Dynamic Model of Grid

Grid side modeling can be done in a similar way as the machine modeling is done. Steady state and dynamic model of the grid side will be defined then the relation of power in terms of grid side voltage and currents with their parameters will be introduced.

At the rotor side converter, speed reference can be defined based on power demand of the system. Thus the real power control is done through speed and torque whereas at the grid side the main objective is to control the dc link voltage and reactive power can be control based on the requirements, usually the reactive power reference is set to achieve the unity power factor or the reference is set to zero.

Further the grid side converter voltages are controlled using vector control technique thus the grid voltages are transformed to the d-q component using the angle obtained through Phase Lock Loop (PLL). The figure 3.8 is a representation of grid side converter, filter, and grid itself.
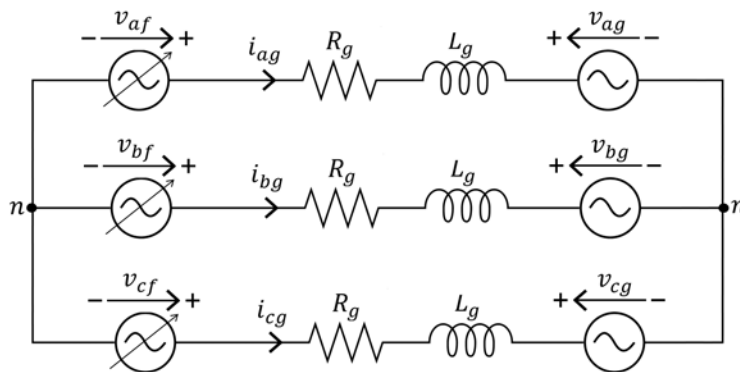
Figure 3.8: *Grid side converter and grid schematic representation.*

The voltages v_{ag}, v_{bg}, and v_{cg} are grid voltages. R_f and L_f is resistance and inductance of the filter which connects the output of the grid side converter to the grid and v_{af}, v_{bf}, and v_{cf} are output phase voltages of the grid side converter [18]. Note that the line through the symbol of the converter shows that these voltages are variable which is obvious as they varies based on the variation of the reference value of dc link voltage and reactive power.

Single phase circuit representation of figure 3.8 is given in figure 3.9, voltage equations can be written by applying the Kirchhoff's voltage law on figure 3.9 circuit:

$$Max(v_{af})_1 = \frac{V_{bus}}{\sqrt{3}} \tag{3.57}$$

$$v_{ag} = v_{af} + (R_f + jL_{fs})i_{ag} \tag{3.58}$$

The active and reactive power for the above circuit can be written in the phasor form using:
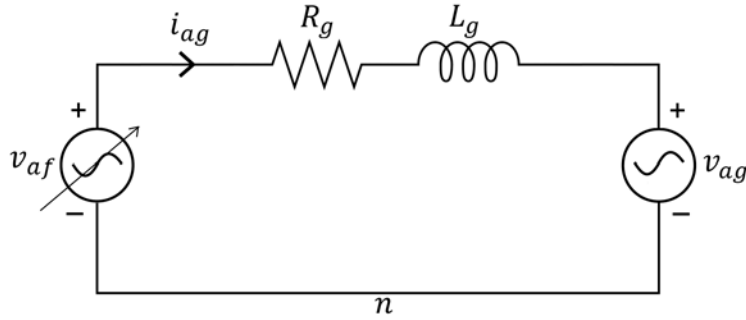
Figure 3.9: *Single phase representation GSC and grid.*

$$p_g = |v_{ag}|.|i_{ag}|.\cos\phi \tag{3.59}$$

$$q_g = |v_{ag}|.|i_{ag}|.\sin\phi \tag{3.60}$$

It is important to note that flow of real power to the grid depends on the dc link voltage when the voltage of the dc link rises above reference value then the access power is delivered to the grid $p_g > 0$ and this is taken as positive while in case the dc link voltage drops below reference then the power is drawn from the grid so $p_g < 0$ and taken as negative. Dynamic equations for three phases can be written as:

$$v_{ag} = R_f i_{ag} + L_f \frac{d}{dt} i_{ag} + v_{af} \tag{3.61}$$

$$v_{bg} = R_f i_{bg} + L_f \frac{d}{dt} i_{bg} + v_{bf} \tag{3.62}$$

$$v_{cg} = R_f i_{cg} + L_f \frac{d}{dt} i_{cg} + v_{cf} \tag{3.63}$$

This set of dynamic equations can now be represented in Clark and Park reference frames.

3.2.1   Dynamic Model of Grid in alpha beta

The transformation from abc to alpha beta is repeated here:

$$\vec{x_{\alpha\beta0}} = T_{\alpha\beta,abc}.\vec{x_{abc}} \tag{3.64}$$

Applying alpha beta transformation for set of equation (3.61) to equation (3.63), yields:

$$\vec{v_{g,\alpha\beta}}^{s} = R_f \vec{i_{g,\alpha\beta}}^{s} + L_f \frac{d\vec{i_{g,\alpha\beta}}^{s}}{dt} + \vec{v_{f,\alpha\beta}}^{s} \qquad (3.65)$$

Decomposing the equation (3.65) in to alpha and beta components results in:

$$v_{g\alpha} = R_f i_{g\alpha} + L_f \frac{di_{g\alpha}}{dt} + v_{f\alpha} \qquad (3.66)$$

$$v_{g\beta} = R_f i_{g\beta} + L_f \frac{di_{g\beta}}{dt} + v_{f\beta} \qquad (3.67)$$

The α β circuit representation of these equations is given in figure 3.10 and figure 3.11:
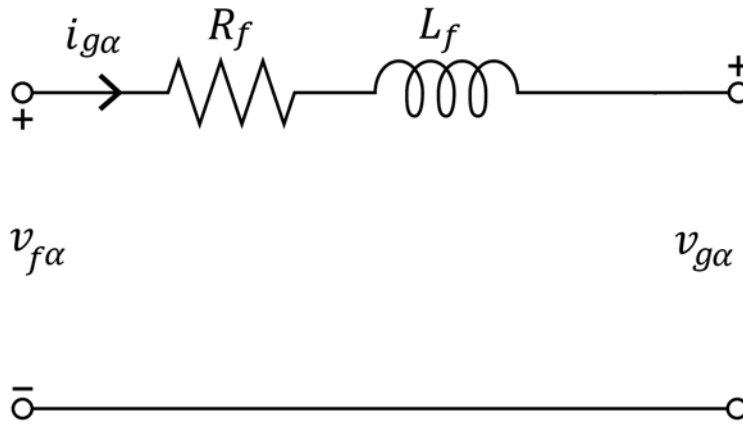
Figure 3.10: *alpha circuit representation.*
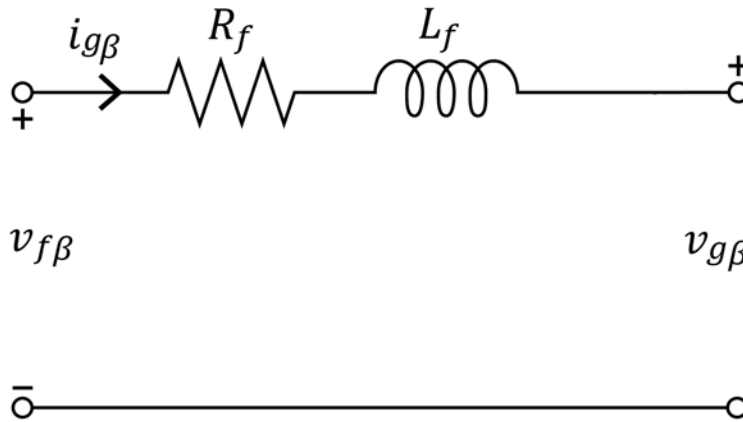
Figure 3.11: *beta circuit representation.*

3.2.2   Dynamic Model of Grid in dq

The set of dynamic model of the grid in equation (3.61) to equation (3.63) can now be written in terms of rotating reference frame by multiplying with the operator $e^{j\theta}$ [18].

$$\vec{v_g}^s e^{j\theta_k} = R_f \vec{i_g}^s e^{j\theta_k} + L_f \frac{d}{dt} \vec{i_g}^s e^{j\theta_k} + \vec{v_f}^s e^{j\theta_k} \tag{3.68}$$

Now separating d and q components in equation (3.68), we get:

$$v_{gd} = R_f i_{gd} + L_f \frac{di_{gd}}{dt} - \omega_k L_f i_{gq} + v_{fd} \tag{3.69}$$

$$v_{gq} = R_f i_{gq} + L_f \frac{di_{gq}}{dt} + \omega_k L_f i_{gd} + v_{fq} \tag{3.70}$$

Equivalent circuit representation based on dq equations is shown in figure 3.12 and figure 3.13.
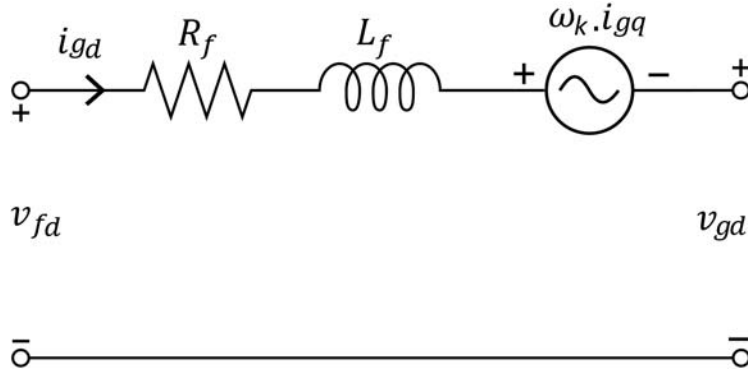
Figure 3.12: *direct axis circuit representation.*
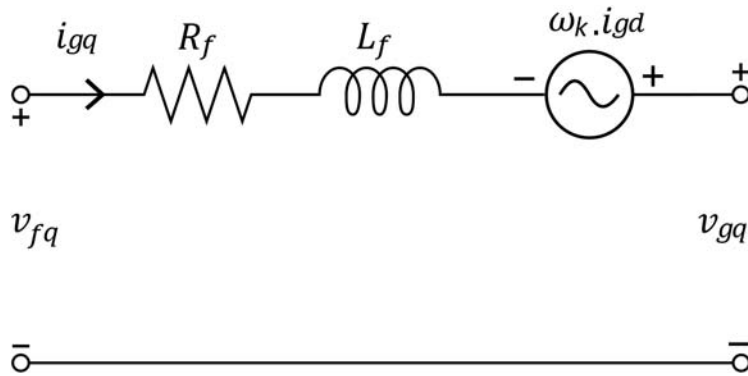
Figure 3.13: *quadrature axis circuit representation.*

3.3   Dynamic Model of DC Link

The capacitor between back to back converters is called DC link as shown in figure 3.14. This capacitor provides input voltage to the rotor side converter and if voltage across this capacitor is not kept within specified limits then it will affect the operation of rotor side converter. This capacitor could supply and receive power from both the converters, as steady state operating point of the system changes. Therefore, it is important to control the voltage across capacitor for proper operation of the rotor side converter.
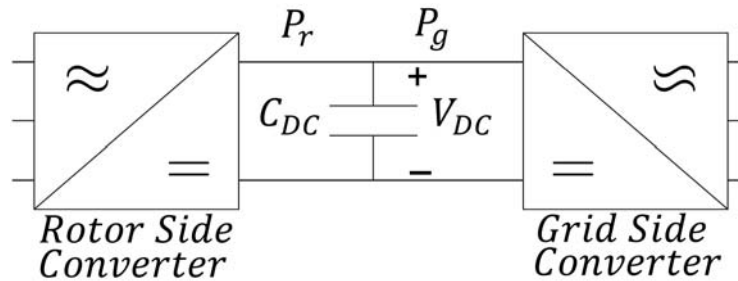
Figure 3.14: *DIFG back-to-back converter with DC-link.*

To write current equation for dc link capacitor, consider the circuit of figure 3.15 current flow through capacitor is algebraic sum of d-axis currents from rotor side (i_{rd}) and current from grid side (i_{gd}), current balance can be written by applying the KCL at DC link node:

$$i_c = i_{gd} - i_{rd} \tag{3.71}$$

Then V_{DC} across capacitor will be:

$$i_c = C_{DC} \cdot \frac{d}{dt} V_{DC} \tag{3.72}$$

$$V_{DC} = \frac{1}{C_{DC}} \int i_c dt \tag{3.73}$$

The dc link voltage can also be modeled using power balance from RSC and GSC. The difference of energy from both converters will be stored in the capacitor or supplied by the capacitor. This energy or power balance can be written in dynamic equation form as [30]:

$$\frac{d}{dt} W_{DC} = \frac{1}{2} C_{DC} \frac{d}{dt} V_{DC}^2 = P_g - P_r \tag{3.74}$$
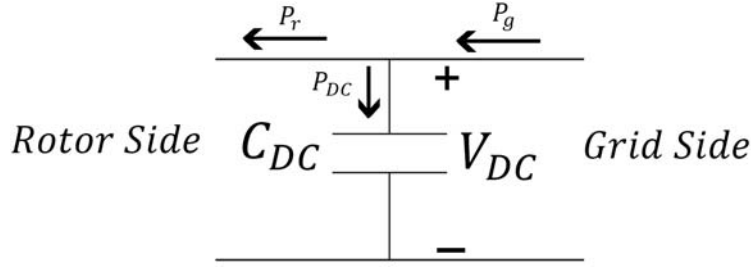
Figure 3.15: *Current flow through DC-link capacitor.*

3.4   DFIG Model Validation

Until this point, we have looked at mathematical modeling of DFIG, grid, and DC link. Before putting this system into work (for simulation and subsequently implementation) to obtain results, it is important to test or validate all the components of system individually to ensure that the components are modeled properly. Once this test is done and the individual component response is satisfactory then all these components will be put together and whole system will be subjected to different operating conditions to get the results. In this section, validation test will be performed on DFIG dynamic model.

DFIG is actually a wound rotor induction machine where electrical inputs can be applied from stator side and also from rotor side whereas mechanical input to the model is shaft torque. The machine model does not have provision to set speed reference directly. However, the indirect way to set speed reference is through the control system of the machine.

In PC Krause book, Analysis of Electric Machinery and Drive Systems, a model for squirrel cage induction machine is developed [25]. Although, the machine used in this work is wound rotor induction machine but setting the rotor side voltage to zero, in developed model, has the same effect as short circuiting the slip ring terminals of wound rotor machine which will turn the WRIM model into SQIM model. The squirrel cage model in PC Krause book is subjected to free acceleration test to observe characteristics of the machine and graph of speed vs torque is given so in order to validate DFIG model. That test can be taken as reference by setting the parameters i.e. resistances, inductances etc. given in the book in our DFIG model and comparing the resulting response after simulation with the one given in the book. The parameters of Krause machine are:

Initial condition of torque and flux loaded in state space model are:

$$\omega_m(0) = \lambda_{sd}(0), \lambda_{sq}(0), \lambda_{rd}(0), \lambda_{rq}(0) = 0$$

Voltage applied at the stator and rotor terminals are:

$$v_{as} = \sqrt{\tfrac{2}{3}} V_{LLrms} \cos(2\pi f_s t), \qquad v_{ar} = 0$$

$$v_{bs} = \sqrt{\tfrac{2}{3}} V_{LLrms} \cos(2\pi f_s t - \tfrac{2\pi}{3}), \qquad v_{br} = 0$$

$$v_{cs} = \sqrt{\tfrac{2}{3}} V_{LLrms} \cos(2\pi f_s t + \tfrac{2\pi}{3}), \qquad v_{cr} = 0$$

Parameter	Symbol	Value	Unit
rated power	P_{rat}	2250	hp
rated stator frequency	f_s	60	Hz
rated stator voltage	V_s	2300	V
number of pole pairs	p_p	2	−
stator resistance	R_s	29	$m\Omega$
stator leakage inductance	L_s	0.6	mH
referred rotor resistance	R_r	22	$m\Omega$
referred rotor leakage inductance	L_r	0.6	mH
magnetizing inductance	L_m	34.6	mH
inertia	J	63.87	$Kg.m^2$

Table 3.1: *Krause's machine parameters [25].*
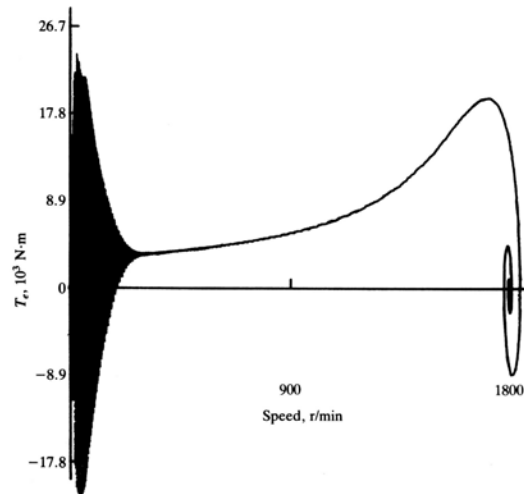
Figure 3.16: *Krause's model Torque vs Speed graph [25].*
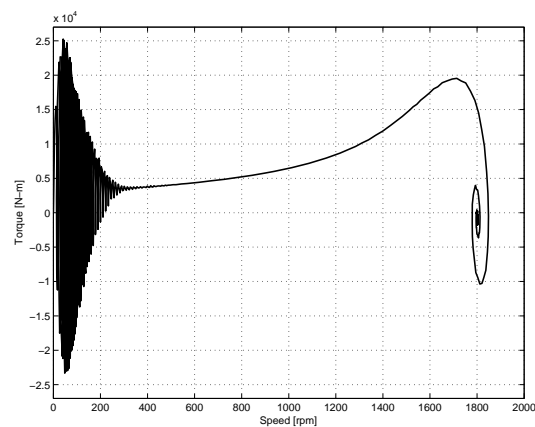
Figure 3.17: *Torque vs Speed graph of model under test.*

It can be seen from figure 3.16 and figure 3.17 that the graph obtained, after simulating the DFIG model, between torque and speed resembles the one given in Krause book thus this test validates the correctness of the developed DFIG model.

Chapter 4

Optimum Efficiency Operation of Hydro Turbine

This chapter deals with hydro turbine modeling. As objective of this work is to control the generator speed to achieve optimum efficiency for a particular operating point. Hill charts for a given turbine can be used to find the speed corresponding to optimum efficiency for a specific power value. Therefore, optimum efficiency speed module is presented along with shaft model which incorporates the mechanical dynamics of the turbine and generator for a change in speed this is sufficient to check the DFIG response as hydro turbine dynamic response is slower than DFIG's dynamic response.

4.1 Hydro Turbines

The turbine is basically used to convert hydro energy into mechanical energy that that is finally converted into electrical energy. Depending upon the principle of operation, hydro turbines can be classified into two groups:

1. Impulse turbine

2. Reaction turbine

4.1.1 Impulse Turbine

Impulse turbine uses the velocity of flowing water, a fast moving flow of water through nozzle hits the turbine blades which after hitting could change its angle or comes back. The blades of impulse turbine are bucket shaped, this helps them to catch the fluid so that energy of flowing water could be transferred to the turbine efficiently. They are used where the flow rate is slow and water head is high [31]. A Pelton wheel turbine in figure 4.1 is an example of impulse turbine which has one or more free jets of discharging

water impinged on turbine. Pelton wheel turbine does not use draft tube because the runner is located above tail-water and works at atmospheric pressure.
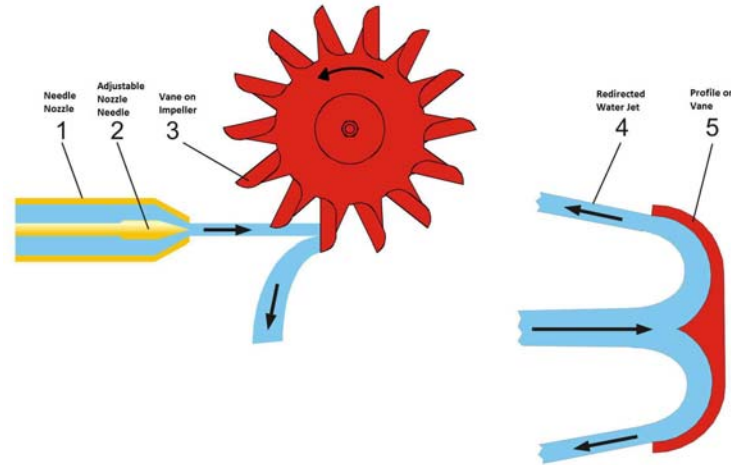
Figure 4.1: Pelton wheel Turbine.

4.1.2 Reaction Turbine

Reaction turbine is used for low head and high speed flow of water as opposed to the impulse turbine. Because the runner is placed directly in the water flow rather than striking each blade as in case of impulse turbine. The pressure of water at discharge is low because pressure drops as water flows through the vanes of turbine and velocity at discharge increases [31, 32, 33]. Reaction turbine can be of various types but can be broadly classified based on direction of flow as radial or axial flow turbines. Axial flow turbines are low head and fast flow rate whereas the radial flow turbines are medium head and medium flow rate.

Francis turbines are the most popular and widely used turbines and they are called mixed flow turbines because flow enters the turbine radially and leaves it axially. This work uses Francis turbine data for simulation, therefore, further discussion will be based on Francis turbine.

4.1.3 Francis Turbine

Francis turbines are used for water head ranges from 40m to 600m. The overall efficiency of turbine is very high, about 90% to 95% [34]. In figure 4.2 main parts of a Francis turbine are shown, flow enters the turbine from outer perimeter of spiral casing and moves along the casing before it hits the runner blade (Impeller) radially after passing through guide vanes.
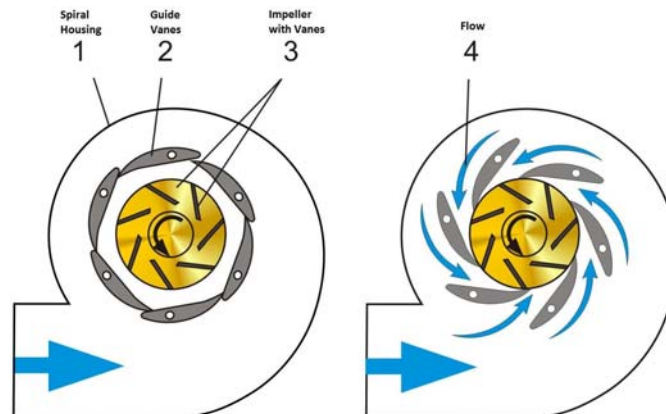
Figure 4.2: Flow of water in Francis Turbine

The area along spiral casing is reduced as water moves form outer perimeter to inner perimeter. This is because the flow rate is reduced along the spiral casing so in order to ensure that water enters the runner at uniform velocity, area of spiral casing reduces along its length. Water passes through guide vanes before entering to the runner, guide vanes serves two purposes. First it controls the flow rate of water entering into the runner blade thus power available at the shaft can be changed which means during load variation of generator, coupled to the turbine, power can be controlled by adjusting the guide vanes. Second it ensures that the inlet water flow angle to the runner blade is optimum this in turn ensure the maximum power extraction from fluid. The blade of Francis turbine are like thin foil shape so when water flows across the foil it produces low and high pressure across the foil thus a resultant force on foil drives the turbine.

Mathematical modeling of Francis turbine is available in the literature [34], however, the objective of present work is to find an operating point (i.e. speed, torque and efficiency) from the turbine model for a given power demand. These parameters or the required operating point can be obtained by using Hill Charts.

4.2   Hill Charts

Efficiency of a Francis turbine varies with speed and gate opening. Hill Charts characterizes variable speed operation of the turbine at different speeds, flow rates, and gate openings. To draw a Hill Chart, gate opening is kept constant and speed is varied, with this variation of speed corresponding points of flow rate or power are obtained now for each combination of constant gate opening, speed, and flow rate the efficiency is calculated. This process can be repeated for different gate openings then graph obtained by plotting these points is called Hill Chart. As can be seen from figure 4.3 that speed n_1 is ordinate and flow Q_1 is abscissa on the graph while gate opening is the third parameter. The figure 4.3 gives a realization of a hill with peak and different slopes. The machine can be made to operate at the highest available efficiency corresponds to a specific power

or flow rate and at a specific gate opening.
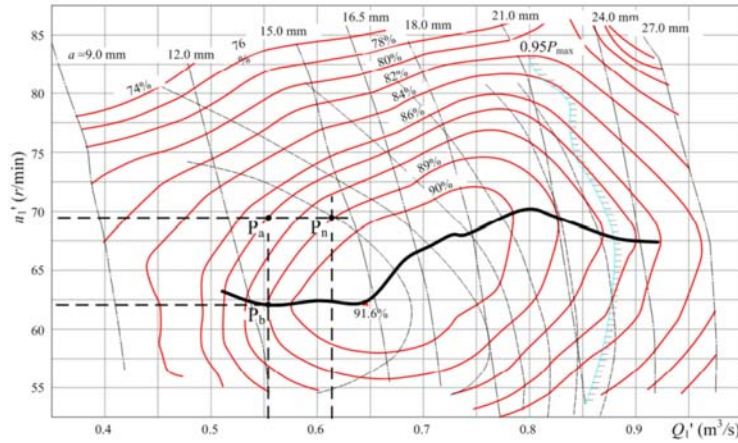
Figure 4.3: Hill Chart of Francis Turbine.

4.3 Finding Speed for Optimum Efficiency Operation

Speed at optimum efficiency can be found out for a given power demand using the Hill Chart in figure 4.3. Method to find out the optimum speed operation is outlined here. The calculation model is as follows.

1. Each point on Hill Chart represents four quantities i.e. unit speed, unit flow, efficiency, and guide vane opening. All these quantities for different operating points can be extracted from the Hill Chart.

2. Find out the unit power by multiplying the extracted unit flow Q_1 and efficiency η points.

3. Based on the calculated unit power points in step 2 find the polynomial expression of 4 or 5 degree (relating the unit power with unit speed n_1, efficiency η, unit flow Q_1, and guide vane opening) using the interpolation tool (cftool) from Matlab.

4. Use the expression from step 3 and compute the unit speed n_1, efficiency η, unit flow Q_1, and guide vane opening a_0 for different power demand with required accuracy.

5. Now these set of points computed in step 4 can now be used in lookup tables to build the simulation model in Matlab to generate the speed for optimum efficiency operation.

Once points for optimum efficiency with required accuracy are obtained using steps 1 to 5. Now these points obtained are unit specific quantities thus to find the speed and efficiency for any power demand the model needs inputs in turbine specific parameters

i.e. unit speed, unit flow, unit power etc.

Power demand input to the model is first converted to the hydraulic turbine specific parameters. Then unit power of hydraulic turbine can be computed using:

$$P_1 = \frac{P}{\eta_e \sqrt{H^3} D_1^2} \tag{4.1}$$

Where P_1 is unit power, P is power demand, D_1 is the nominal diameter of turbine in meters, η_e is the efficiency of generator, and H is the water head.

This calculated unit power input is compared with the lookup table unit power points, obtained from Hill Chart for optimum efficiency and corresponding operating point (unit speed, unit flow, and efficiency) can be determined. Finally the unit speed can be converted to the actual speed values using the equation (4.2) to generate speed reference for the controller.

$$n = \frac{n_1 \sqrt{H}}{D_1} \tag{4.2}$$

Where n_1 is the specific or unit speed and n is the actual speed both in rpm.

Block diagram of model for calculating speed and efficiency for variable speed optimum efficiency operation is shown in figure 4.4.
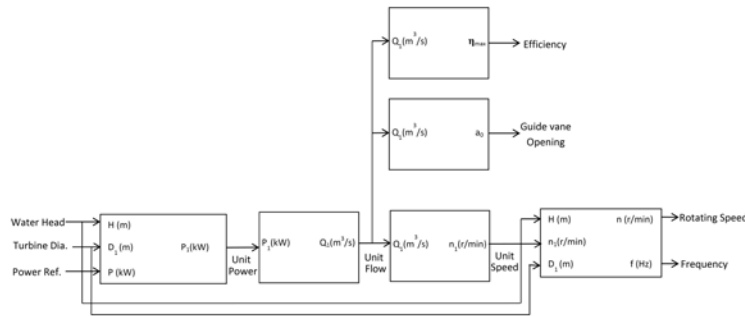
Figure 4.4: *Block diagram of efficiency and speed calculation for variable speed operation.*

4.4 Efficiency Calculation for Fixed Speed Operation

Fixed speed operating points can also be found from the Hill Chart using the same interpolation and table lookup method. But now operating points will be obtained based on constant or fixed speed rather than based on optimum efficiency values. Unit flow $Q1$ and efficiency for fixed speed operation are found using 2-D interpolation method. Fixed speed block diagram representation is shown in figure 4.5.
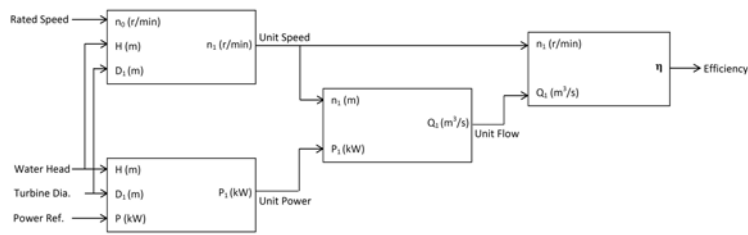
Figure 4.5: *Block diagram of efficiency calculation for fixed speed operation.*

4.5   Shaft Model

Shaft between turbine and generator is subjected to heavy mechanical load and stress. It is important to examine the forces mechanical shaft is subjected to, because if the system design does not take in to account the un-damped natural frequencies then these forces could affect the life time of equipment or even damage the system. In this section we will look at the turbine generator shaft mechanical model.

4.5.1   Drive Train

All rotating parts such as turbine propeller, shaft, gear box, mechanical coupling, and generator rotor are included in the drive train of the system. They can be divided into two basic categories.

- Geared drive train.

- Direct drive train.

Geared Drive Train

This type of drive train is used where generator speed is high compared to the turbine although the situation could be opposite. The gear system translates the speed of turbine from one level to another depending on gear ratio while the torque also varies i.e. the torque is high at low speed side while low at high speed side. This provides advantage that a high speed generator has better cooling so weight and size of the generator is reduced. But with this advantage, gear box has some disadvantages as well; they need additional investment, regular maintenance, noise, reduced reliability, power losses [35].

Direct Drive Train

The relation between induction machine speed, frequency and number of pole pairs allows the generator to be designed at low speed with high number of poles which can generate same frequency at low speed. Another advantage is that there is no capital and

maintenance cost for gear box, besides efficiency and reliability of the system increases. However, main disadvantage is that size and weight of the machine will increase and further if the turbine which generator is coupled to does not has constant speed then a full rated converter is required to interface it to the grid.

4.5.2 Drive Train Model

Modeling of mechanical drive train depends upon the purpose of study to be carried out and if available the nature of actual system to be known. Mechanical drive train can be modeled in different ways and different models are available such as lumped three mass model, two mass model, and one mass model. This study employs two mass model which is enough for practical purposes [36].

$$2H_g \frac{d\omega_g}{dt} = -T_e + T_{tg} \tag{4.3}$$

$$2H_t \frac{d\omega_t}{dt} = -T_{tg} + T_m \tag{4.4}$$

$$\frac{d\phi_{tg}}{dt} = \omega_t - \omega_g \tag{4.5}$$

$$T_{tg} = K_{tg}\phi_{tg} + D_{tg}(\omega_t - \omega_g) \tag{4.6}$$

Where H_t, H_g are inertia, ω_t, ω_g are rotational speed respectively. D_{tg} is damping coefficients of shaft between turbine and generator. K_{tg} is the stiffness constant which can be taken as zero if the shaft is to be modeled as rigid body. ϕ_{tg} is the angle of twist of shaft between turbine and generator. T_m is the mechanical torque from turbine, T_e is the electromagnetic torque developed in the generator and T_{tg} is the shaft torque due to damping and stiffness of shaft. The torque convention is usually taken as positive for motoring and negative for generator.

In two mass model the shaft between generator and turbine is not rigid and have some stiffness and damping coefficients, however, if we consider a rigid shaft then we can neglect stiffness and damping of the shaft thus we can represent the entire mechanical mass from turbine to generator as a single rotating mass as shown in figure 4.7 which will result in [36]:

$$2H \frac{d\omega_m}{dt} = -T_e + T_m + D_m\omega_m \tag{4.7}$$

$$\frac{d\phi_m}{dt} = \omega_m \tag{4.8}$$
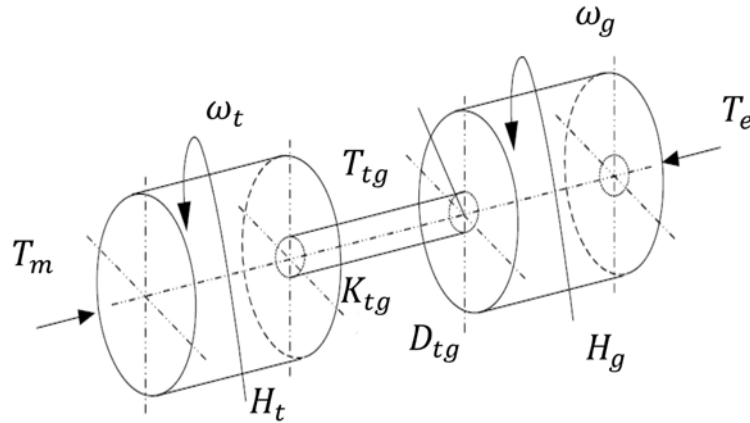
***Figure 4.6:** Two mass model diagram of drive train.*

Where T_m and T_e are the mechanical and electromagnetic torque from turbine and generator respectively. D_m is the damping coefficient and H is the inertia constant of the mechanical drive train.

In hydro turbine where the propeller, mechanical shaft and generator are directly coupled also the shaft is considered as rigid body then inertia can be represented as lumped one mass model [37].
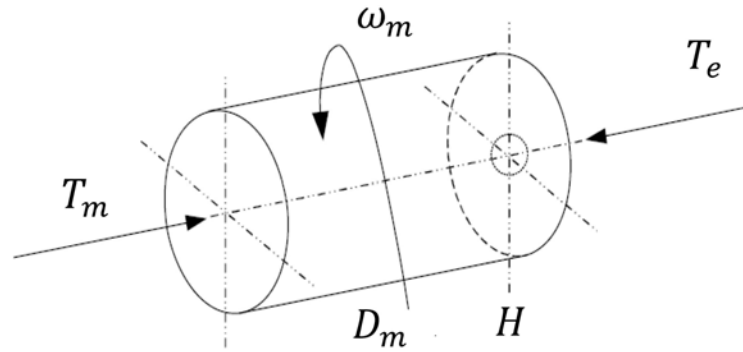
***Figure 4.7:** One mass model diagram of drive train.*

Two-mass lumped shaft model with gear ratio is given in literature [38] and can be written as.

$$2H_g\frac{d\omega_g}{dt} = -T_e + \frac{1}{N}T_{tg} \tag{4.9}$$

$$2H_t\frac{d\omega_t}{dt} = -T_{tg} + T_m \tag{4.10}$$

$$T_{tg} = K_{tg}\phi_{tg} + D_{tg}(\omega_t - \omega_g) \tag{4.11}$$

$$\frac{d\phi_{tg}}{dt} = \frac{d(\phi_t - \phi_g)}{dt} = \omega_t - \frac{1}{N}\omega_g \tag{4.12}$$

Where N is the gear ratio.

$$M_H\ddot{\phi}_s + D\dot{\phi}_s + K\phi_s = T \tag{4.13}$$

The equation (4.13) can be written in matrix form as [39]:

$$M_H = \begin{bmatrix} H_t & 0 \\ 0 & H_g \end{bmatrix}, K = \begin{bmatrix} \frac{K_{tg}}{N^2} & \frac{-K_{tg}}{N} \\ \frac{K_{tg}}{N} & -K_{tg} \end{bmatrix}, D = \begin{bmatrix} \frac{D_{tg}}{N^2} & \frac{-D_{tg}}{N} \\ \frac{D_{tg}}{N} & -D_{tg} \end{bmatrix}, \phi_s = \begin{bmatrix} \phi_t \\ \phi_g \end{bmatrix}, T = \begin{bmatrix} T_m \\ T_e \end{bmatrix} \tag{4.14}$$

Where M_H is called mass matrix and contains the turbine and generator inertia constants, K is shaft stiffness matrix, and D is damping matrix, note that stiffness and damping is increased or decreased according to the gear ratio. Further ϕ_s is angle and T is the torque matrix.

These equations can be used to find the speed of shaft, because in two mass model due to shaft stiffness the turbine and generator both could have different position at an instant which is found based on their inertia, damping and stiffness constants and the shaft speed is based on difference of their torques. The block diagram of mathematical model can be seen in figure 4.8.

Drive Train Resonance

The dynamic equation (4.13) for determining speed links electrical and mechanical system. There are other operating conditions that need to be taken into account when designing a system. Resonance is an important situation which can be very severe and cause system damaged if the system is not properly damped and operated in the range of natural frequency [39]. Therefore, it is important to calculate these frequencies so that the operation within the range of these frequencies could be avoided.

Harmonic Modes

Setting damping and torque equal to zero in equation (4.13), then undamped harmonic modes for mechanical system are:

$$M_H.\ddot{\phi}_s + K\phi_s = 0 \tag{4.15}$$
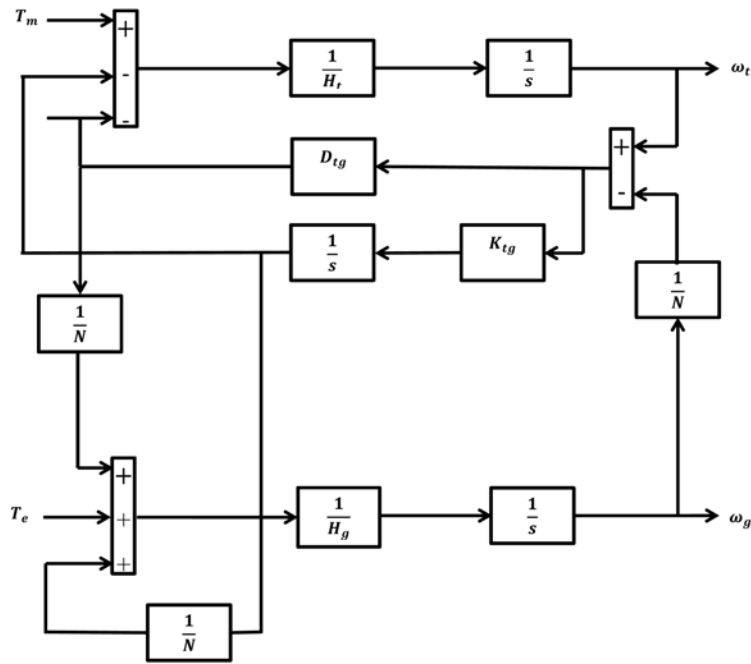
Figure 4.8: *Mechanical shaft model.*

Assuming free vibration solution:

$$\ddot{\phi}_s = -\omega_{res}^2.\phi_s \tag{4.16}$$

equation (4.16) can also be written as:

$$M_H^{-1}.K\phi_s = -\omega_{res}^2.\phi_s = \aleph.\phi_s \tag{4.17}$$

where $\omega_{res} = M_H^{-1}.K$.
Eigen values and eigen vectors can be found using the above relation then using eigen values of $M_H^{-1}.K$, It is possible to find undamped modes:

$$\omega_{res,n} = \sqrt{\aleph_n} \tag{4.18}$$

Where n is the range of matrix. Once the undamped modes are known then frequencies are given as:

$$f_{res} = \frac{\omega_{res}}{2.\pi} \tag{4.19}$$

As discussed earlier that these frequencies are natural frequencies of the system, therefore, mechanical system should be avoided to operate in these range of frequencies.

Damping

To find the damping matrix D first modal damping matrix needs to be calculated as [39].

$$D_i = 2.\epsilon_i.\omega_{res,i} \tag{4.20}$$

The damping factor ϵ_i in equation (4.20) lies between range of 1 to 5 percent. And its value for drive train could be 5 percent. Now damping matrix D is:

$$D = (\phi_s^T)^{-1}.D_i.\phi_s^{-1} \tag{4.21}$$

The mode shape vector or eigen vector, calculated earlier during harmonic modes analysis, could have an order of 2x2 or 3x3 which depends on the drive train model under study i.e. lumped three mass model or lumped two mass model. This eigen vector can be normalized as:

$$\phi_s^T.M_H.\phi_s = I \tag{4.22}$$

The details of this procedure has been given in referenced literature to compute the harmonic modes or oscillations in shaft which could occur during system operation. Although, computing the shaft oscillation is not the scope of present work. However, it is touched very briefly to give a realization of its importance in system operation.

Chapter 5

Vector Control of Grid Connected DFIG

The objective of vector control of the machine is to achieve fast dynamic response. To control the power of DFIG we control speed and torque[23]. In separately excited dc machine torque control is usually done through armature current control. DC machine has fast dynamic response because of the separate field and armature circuit which are decoupled with each other i.e. varying any one of the quantity will not affect the other in contrast three phase induction machine has magnetic coupling not only between phases of stator circuit itself but also with the rotor circuit so varying the voltage or frequency will affect the magnetic circuit parameters and due to coupling between circuits the response is nonlinear with slower dynamics.

The idea of vector control is to transform the actual three phase induction machine into a hypothetical machine having two circuits d and q like dc machine which are decoupled with each other. This decoupling allows induction machine to behave like a dc machine with linear and faster dynamic response. The control of d and q axis voltage magnitude and phase angle allows the independent control of torque and machine flux[24].

5.1   Vector Control

Three phase quantities of induction machine such as voltage, current, and fluxes can be represented by space vectors. Vector control principle is the idea to control these quantities by controlling the magnitude and phase angle of their space vectors. Torque is produced due to interaction of stator and rotor fluxes and by controlling torque, real power flow of the machine can be controlled.

In squirrel cage induction machine access to only stator side is available whereas in DFIG, both stator and rotor circuits are available. DFIG stator is usually tied with grid having fixed voltage and frequency and produces a constantly rotating field flux. Rotor circuit is

connected to grid through back to back converter thus control is performed at the rotor side by injecting a voltage or current of desired magnitude and frequency.

As discussed earlier that inherently induction machine has various magnetic couplings between its rotor and stator circuits. Therefore, to achieve better dynamic performance and independent control of real and reactive power or machine torque and flux, it is important to separate the components of current which are responsible for producing torque from the one which produces flux.

The dq transformation is used to separate these components in d and q but to achieve accurate enough transformation, it is not only important to identify machine parameters but also the magnitude and position of flux at each time step. Then d axis can be aligned with either stator flux or the stator voltage. Once reference frame is chosen and aligned with d-axis then the rotor current which is controlling variable is transformed into dq components. Then one component of rotor current controls machine flux while the other component controls machine torque [23].

As evident from above discussion that control is based on transformation so it is very important to find the correct angle of stator flux or stator voltage vector. For estimation or measurement of angle, two methods (i.e. stator flux and grid voltage vector) are usually used to obtain the angle.
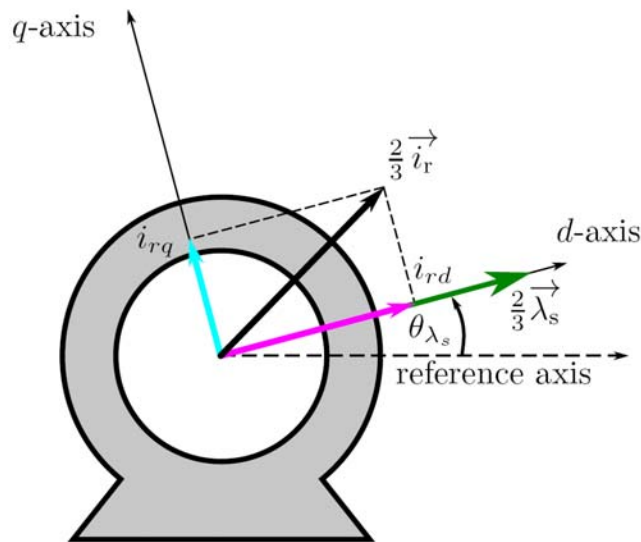
Figure 5.1: *Vector control visualization in a a machine.*

5.1.1   Stator Flux Orientation

In stator flux orientation, stator flux vector is aligned with d-axis. The angle of stator flux can be obtained by using the measured stator voltage and stator current as in equation (5.1) [29].

$$\vec{\lambda_s} = \int (\vec{v_s} + R_s \vec{i_s}) dt \tag{5.1}$$
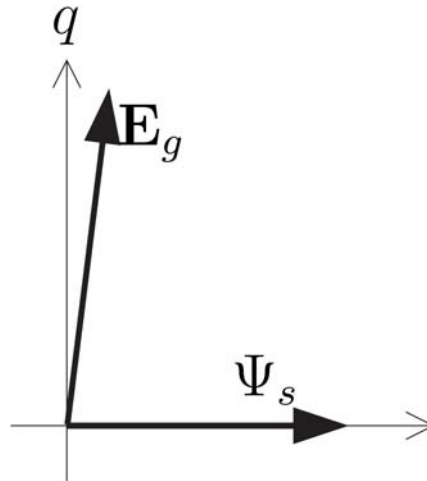
Figure 5.2: *Stator flux vector aligned with d-axis.*

5.1.2   Grid Voltage Orientation

In grid voltage orientation method, phase lock loop is used to obtain angle from the grid voltage. To synchronize grid voltage with d or q axis, using PI control, reference of the other axis is set to zero and PI control corrects the angle theta to align the stator voltage with d or q axis[18]. Grid voltage orientation is more stable as compare to stator flux method therefore is adapted in this work.
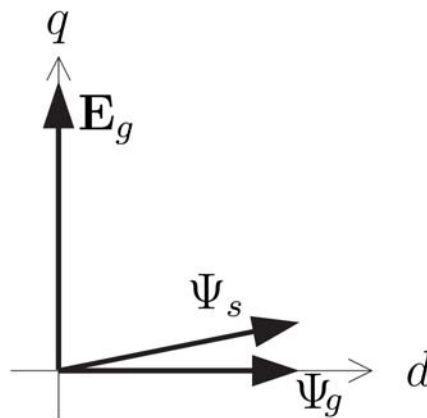
Figure 5.3: *Grid voltage vector aligned with q-axis.*

5.2   Cascaded Control

Cascade control is simple and efficient control methodology which is very commonly used
to control the machines. Real world systems are usually complex and nonlinear therefore
it is useful to make some assumption which can make control system implementation
simple and reduces complexity[27]. In cascaded control, system is broken down into sub-
systems and assumed to be linear around an operating point then simple control strategy
can be used to control the system[23, 24]. Consider the speed or power control loop shown
in figure 5.4 for DFIG control, this is a cascade control loop where outer loop controls
speed while inner current loop gets its reference value from outer speed loop based on
correction made by controller.

Outer speed loop gets its reference speed from hydro turbine model which generates ref-
erence speed based on power demand, this speed is then compared with the measured
shaft speed which produces an error, in case of not being equal, this error is sent to the
controller, controller makes correction based on error which becomes reference to the in-
ner current loop, again inner loop controller correct the current error and this signal is
applied to the plant or machine to produce the required current or speed or demanded
power. The inner loop has higher bandwidth and much faster than the outer loop so it
appears to be constant to outer loop.
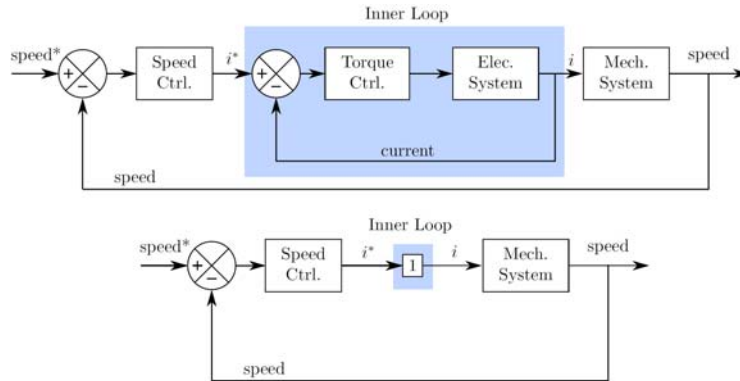
Figure 5.4: *Top: Standard representation of cascade control structure with inner current loop;*
Bottom: Inner current loop with fast dynamics behave instantaneously.

In this work IMC (Internal Model Controller) is used. IMC is also a PI controller, al-
though it includes some model of the plant to be controlled and thus results in a more
robust and efficient control.

5.2.1   Internal Model Control (IMC)

Internal Model Control is based on internal model of the process, which means that the
controller used to control the plant must include some representation of the process.

The block diagram in figure 5.5 shows structure of the IMC, if output from the controller $G(s)$ is applied to actual plant $P(s)$ and $P'(s)$, where $P'(s)$ is exact representation of actual plant $P(s)$ then difference of their output will be zero thus the system will become an open loop and if $G(s) = P'^{-1}(s)$ then output will follow the set point. But this ideal control is impossible to implement in practice because the proper model of plant need to use a differentiator which is not practical for unfiltered continuous time signals [40, 41].
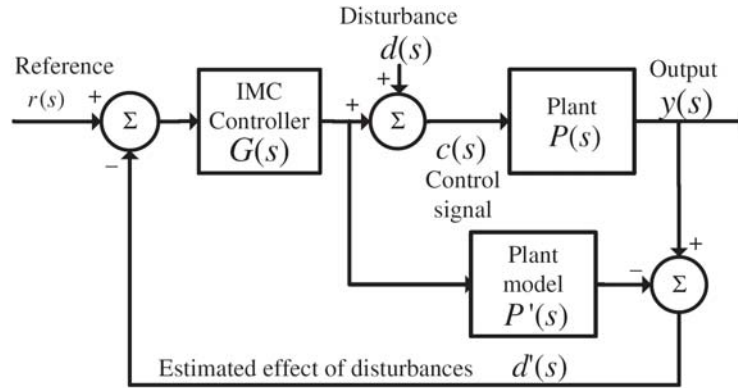
Figure 5.5: *Internal model control structure.*

Therefore, a low pass filter is added to the controller to add some poles to achieve closed loop system tracking properties.

$$L(s) = \left(\frac{\alpha}{s + \alpha}\right)^n \tag{5.2}$$

Where $L(s)$ is transfer function of low pass filter and α is the bandwidth of filter. This type of control provides a better flexibility as alpha is the only parameter to be set to achieve the desired response from control system. Although, introduction of filter in controller has an effect of detuning the parameters yet it is robust and some trade off of performance to the ideal is inherent to all systems but response is still very fast if controller includes a good representation of process.

An additional degree of freedom can be achieved in control system if an internal feedback loop is added to the system as shown in figure 5.6. This feedback loop provides better disturbance rejection and is essentially useful for poorly damped systems.

Transfer function $M(s)$ for inner feedback loop is given as:

$$M(s) = \frac{P(s)}{1 + P(s)G_a} = \frac{1}{P(s)^{-1} + G_a} \tag{5.3}$$
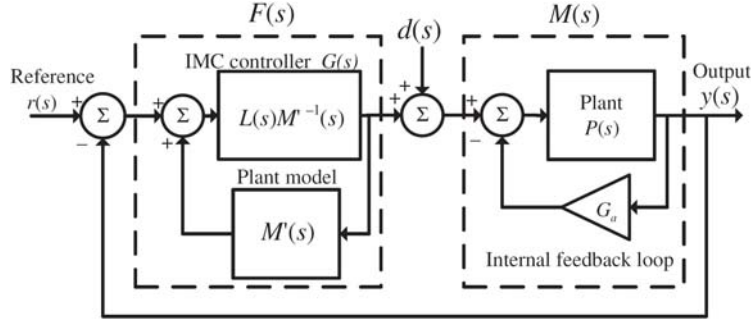
Figure 5.6: *IMC controller with two degree of freedom.*

And transfer function $F(s)$ for controller is:

$$F(s) = \frac{L(s)M'^{-1}(s)}{1 - L(s)M'^{-1}(s)M'(s)} = \frac{\alpha}{s}M'^{-1}(s) \tag{5.4}$$

The inner feedback loop is added to achieve an additional degree of freedom and value of G_a is chosen to match the poles of controller $F(s)$ from disturbance $d(s)$ to $y(s)$ output. So the transfer function from disturbance to output using inner feedback loop is:

$$\frac{y(s)}{d(s)} = \frac{M(s)}{1 + F(s)M(s)} = \left(\frac{s}{s+\alpha}\right)\frac{1}{P^{-1}(s) + G_a} \tag{5.5}$$

G_a can be chosen to reduce the equation (5.5) to equation (5.6):

$$\frac{y(s)}{d(s)} = \left[\left(\frac{s}{s+\alpha}\right)\frac{K}{s+\alpha}\right] = K\left[\frac{s}{(s+\alpha)^2}\right] \tag{5.6}$$

Where K is a constant and the value of α can be chosen to achieve the rise time t_r. Now we will look at the control system of back to back converters for DFIG.

5.3   Rotor Side Converter

The real and reactive power of stator is controlled through d and q axis rotor currents respectively. Stator voltage vector is aligned to the d-axis of rotating reference frame this makes stator voltage equal to:

$$\vec{v_s} = v_{sd} \tag{5.7}$$

$$v_{sq} = 0 \tag{5.8}$$

Further, stator flux lags the stator voltage almost at $\frac{\Pi}{2}$, resistance drop is very small and can be neglected, see equation (5.1). So after aligning the stator voltage with d-axis of rotating frame and neglecting resistance drop in flux equation (5.1) results in:

$$\vec{\lambda_s} = \lambda_{sq}(const) \rightarrow \frac{d}{dt}\lambda_{sq} \approx 0 \tag{5.9}$$

$$\lambda_{sd} = 0 \rightarrow \frac{d}{dt}\lambda_{sd} = 0 \tag{5.10}$$

5.3.1 Rotor Speed or Power Control loop

Rotor speed reference will be generated by optimum efficiency speed module based on power reference. This speed reference will be used to compute electromagnetic torque reference which will be used further to generate current reference for d-axis rotor current $i_{rd,ref}$ see figure 5.7.
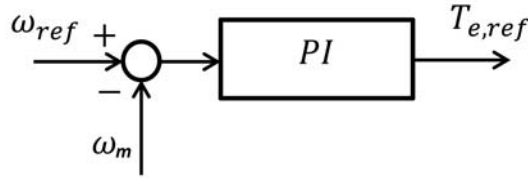
Figure 5.7: *Speed controller to produce torque reference.*

Torque is used to generate the $i_{rd,ref}$ for a given speed or power reference. Rewriting torque equation gives.

$$T_e = \frac{3}{2}p_p(i_{sq}^k\lambda_{sd}^k - i_{sd}^k\lambda_{sq}^k) \tag{5.11}$$

Substituting stator flux value for chosen d-axis aligned to the stator voltage vector. Torque equation becomes:

$$T_e = -\frac{3}{2}p_p\left(i_{sd}\lambda_{sq}\right) \tag{5.12}$$

Note that superscript k is omitted for chosen stator voltage reference frame, and this convention will be followed from this point on. Stator flux is fixed as stator is tied to the grid, then i_{sd} in equation (5.12) can be replaced with stator flux-current relation for the chosen reference frame to find the torque relation is terms of rotor current as:

$$T_e = -\frac{3}{2}p_p\left(\frac{-L_m\lambda_{sq}}{L_s}\right)i_{rd} \tag{5.13}$$

Rearranging equation (5.13) results in:

$$i_{rd} = \frac{2}{3}\frac{1}{p_p}\left(\frac{T_e L_s}{L_m \lambda_{sq}}\right) \tag{5.14}$$

This is the reference current for rotor d-axis current controller and is based on torque generated by speed controller see figure 5.8:
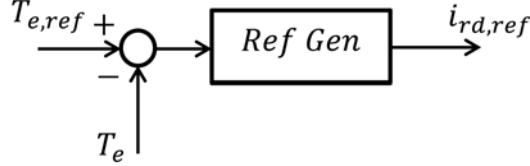
Figure 5.8: *d-axis rotor current reference generation for RSC.*

5.3.2 Rotor Voltage Dynamics

The reference rotor current $i_{rd,ref}$ will be compared with measured d-axis current and inner PI loop will generate the d-axis rotor voltage which is applied to the rotor side converter. Rotor voltage dynamics can be expressed in terms of rotor currents. Rewriting rotor voltage equations for chosen reference frame:

$$v_{rd} = R_r i_{rd} + \frac{d}{dt}\lambda_{rd} - \overbrace{(\omega_s - \omega_m)\lambda_{rq}}^{d-axis\,cross\,coupling} \tag{5.15}$$

$$v_{rq} = R_r i_{rq} + \frac{d}{dt}\lambda_{rq} + \overbrace{(\omega_s - \omega_m)\lambda_{rd}}^{q-axis\,cross\,coupling} \tag{5.16}$$

Terms $(\omega_s - \omega_m)\lambda_{rq}$ and $(\omega_s - \omega_m)\lambda_{rd}$ can be treated as disturbances and compensated as feed-forward. So by eliminating cross coupling terms in rotor voltage equations:

$$v_{rd} = R_r i_{rd} + \frac{d}{dt}\lambda_{rd} \tag{5.17}$$

$$v_{rq} = R_r i_{rq} + \frac{d}{dt}\lambda_{rq} \tag{5.18}$$

Furthermore, the control variable is rotor current so equation needs to be represented in terms of rotor currents. Stator current equations for the chosen reference frame are:

$$i_{sd} = \frac{-L_m i_{rd}}{L_s} \tag{5.19}$$

$$i_{sq} = \frac{\lambda_{sq} - L_m i_{rq}}{L_s} \tag{5.20}$$

Substituting these stator currents in rotor flux linkages equation yields:

$$\lambda_{rd} = L_r i_{rd} + L_m \left(\frac{-L_m i_{rd}}{L_s} \right) \tag{5.21}$$

$$\lambda_{rq} = L_r i_{rq} + L_m \left(\frac{\lambda_{sq} - L_m i_{rq}}{L_s} \right) \tag{5.22}$$

Putting these rotor flux equations in rotor voltage equation (5.17) and equation (5.18) results in:

$$v_{rd} = R_r i_{rd} + \left(\frac{L_r L_s - L_m^2}{L_s} \right) \frac{d}{dt} i_{rd} \tag{5.23}$$

$$v_{rq} = R_r i_{rq} + \left(\frac{L_r L_s - L_m^2}{L_s} \right) \frac{d}{dt} i_{rq} \tag{5.24}$$

equation (5.23) and equation (5.24) are linear first order equations. Cross coupling terms i.e. q-axis term in d-axis equation and vice verse can be eliminated by incorporating the feed-forward gain in the control system. As can be seen from figure 5.9, these cross coupling terms are added or subtracted after the voltage output signal from current PI controller and before applying this voltage signals to the plant.

These cross coupling contains rotor flux which in turn depends on machine parameters to calculate the feed-forward terms. Inner rotor current loop with feed-forward compensation can be seen in figure 5.9.
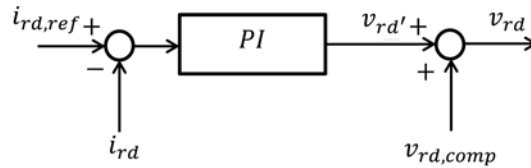
Figure 5.9: *d-axis inner current loop with compensation.*

After adding compensation terms, voltage v_{rd} is applied to the converter to generate the rotor voltage. A complete d-axis control loop is shown in figure 5.10.
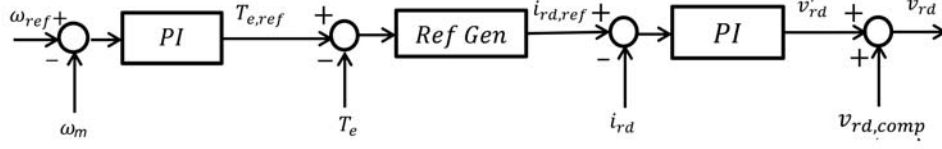
Figure 5.10: complete d-axis cascaded loop with compensation.

5.3.3   Reactive Power Control of RSC

Reactive power of stator in term of dq components can be written as:

$$q_s = \frac{3}{2}(v_{sd}i_{sq} - v_{sq}i_{sd}) \tag{5.25}$$

Using selected reference frame of stator voltage and using equation (5.7) and equation (5.8), reactive power equation reduces to:

$$q_s = \frac{3}{2}v_{sd}i_{sq} \tag{5.26}$$

As explained earlier that power at the stator is controlled through rotor side converter and RSC current controller needs reference rotor currents to produce control voltage. Rotor current is related to stator current through flux-current relation see equation (5.27). Therefore, to generate reference rotor current for reactive power (q_s) control, equation (5.26) can be rewritten using stator and rotor current relation as:

$$i_{sq} = \frac{\lambda_{sq} - L_m i_{rq}}{L_s} \tag{5.27}$$

$$q_s = \frac{3}{2}v_{sd}\left(\frac{\lambda_{sq} - L_m i_{rq}}{L_s}\right) \tag{5.28}$$

Rearranging equation (5.28),

$$i_{rq} = \left(\frac{\lambda_{sq}}{L_m} - \frac{2}{3}\frac{q_s L_s}{v_{sd}L_m}\right) \tag{5.29}$$

This equation generates the current reference i_{rq} for inner loop current controller based on reference reactive power, machine parameters, voltage v_{sd}, and λ_{sq} which can be measured or estimated, flux can not be measured directly and is estimated usually. Estimation could cause error which can be compensated using integral action. Thus equation (5.28) after adding integral action becomes:

$$K_q(s) = \frac{K_{iq}}{s}\left[\frac{\lambda_{sq}}{L_m} - \frac{2}{3}\frac{q_s L_s}{v_{sd}L_m}\right] \tag{5.30}$$

This current reference i_{rq} will be compared with measured rotor current and PI controller will generate the q-axis voltage v_{rq} based on current error. As can be seen from q-axis
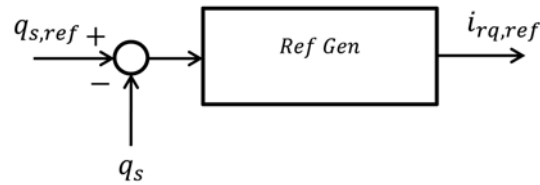
Figure 5.11: *q-axis current reference generation for reactive power of RSC.*

rotor voltage equation (5.16) that a cross coupling term also exist in q-axis. This term can be compensated by feed-forward control, finally the q-axis rotor voltage is applied to the converter see figure 5.12.
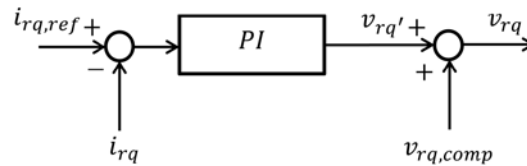
Figure 5.12: *q-axis inner current loop with compensation.*

A complete q-axis control loop with compensation is shown in figure 5.13.
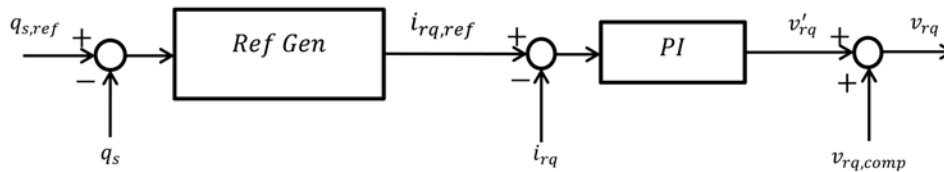
Figure 5.13: *complete q-axis loop with compensation.*

5.4 Grid Side Converter

Grid side converter maintains the voltage across DC link capacitor and can also exchange reactive power to and from grid and can work as both rectifier and inverter. As explained in DC link modeling that DC link voltage depends on power flow between RSC and GSC. When the power flows from RSC toward DC link capacitor the grid should supply excess power to the grid otherwise this excess power will raise the voltage across capacitor. Similarly when the power flows from DC link capacitor to rotor the gird must supply the power required otherwise DC link voltage will drop. Control loop of both active and reactive power for GSC will be discussed next.

5.4.1   DC Link Control Loop

Power from RSC for d-axis aligned with stator voltage vector can be written as:

$$p_r = \frac{3}{2}(v_{rd}i_{rd} + v_{rq}i_{rq}) \tag{5.31}$$

And the power for grid side converter is:

$$p_g = \frac{3}{2}(v_{gd}i_{gd} + v_{gq}i_{gq}) \tag{5.32}$$

The d-axis is rotating at synchronous speed of grid frequency, and is aligned with the grid voltage a-axis for grid side converter control so equation (5.32) becomes:

$$p_g = \frac{3}{2}v_{gd}i_{gd} \tag{5.33}$$

Then dynamic power equation in terms of voltage across DC link capacitor can be written as:

$$p_g - p_r = \frac{1}{2}C_{DC}\frac{d}{dt}V_{DC}^2 \tag{5.34}$$

To write the control equation for DC link controller in terms of grid current i_{gd}, rotor power p_r term can be considered as disturbance then equation (5.34) reduces to:

$$p_g = \frac{3}{2}v_{gd}i_{gd} = \frac{1}{2}C_{DC}\frac{d}{dt}V_{DC}^2 \tag{5.35}$$

Transfer function for equation (5.35) can be given as:

$$\frac{v_{dc}^2(s)}{i_{gd}(s)} = P_{dc}(s) = \frac{3v_{gd}}{C_{DC}s} \tag{5.36}$$

This transfer function inherently contains pole at the origin which makes it very sensitive to disturbance and a large or abrupt change could lead to oscillation of process variables if the controller is tuned to track the set point, which is required. Addition of an inner loop into DC link model adds an artificial pole to the plant and thus adds disturbance rejection property to the system. The transfer function for DC plant model after adding inner feedback loop is:

$$M_{dc}(s) = \frac{P_{dc}(s)}{1 + P_{dc}(s)G_{dc}} = \frac{3v_d}{Cs + 3v_dG_{dc}} \tag{5.37}$$

Where G_{dc} is the gain of inner loop added to the plant model.
PI controller for DC link voltage generates d-axis current reference $i_{gd,ref}$ for inner loop of GSC controller see figure 5.14.
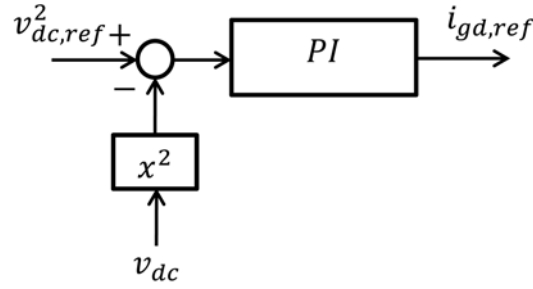
Figure 5.14: *reference generation for d-axis current loop of GSC.*

5.4.2 Grid Voltage Dynamics

Grid voltage equations have already been written for dq grid model. Those equations can be rewritten after omitting the superscript k for the selected grid voltage reference frame as:

$$v_{gd} = R_f i_{gd} + L_f \frac{d}{dt} i_{gd} + v_{fd} - \omega_g L_f i_{gq} \tag{5.38}$$

$$v_{gq} = R_f i_{gq} + L_f \frac{d}{dt} i_{gq} + v_{fq} + \omega_g L_f i_{gd} \tag{5.39}$$

Where ω_g is grid frequency. Writing equation (5.38) and equation (5.39) in terms of grid converter voltage yields:

$$v_{fd} = \overbrace{-R_f i_{gd} - L_f \frac{d}{dt} i_{gd}}^{d-axisdynamics} + \overbrace{v_{gd} + \omega_g L_f i_{gq}}^{d-axiscrosscoupling} \tag{5.40}$$

$$v_{fq} = \overbrace{-R_f i_{gq} - L_f \frac{d}{dt} i_{gq}}^{q-axisdynamics} + \overbrace{v_{gq} - \omega_g L_f i_{gd}}^{q-axiscrosscoupling} \tag{5.41}$$

As can be seen from equation (5.40) and equation (5.41) that they contain corresponding d and q axis voltage drops as well as cross coupling terms which involves d-axis current in q-axis equation and vice verse, grid voltage for corresponding axis can also be compensated through feed-forward gain.

For control purposes these cross coupling terms can be treated as disturbances and added as feed-forward compensation as shown in figure 5.15

After adding compensation to the DC link control loop the d-axis complete control loop can be seen in figure 5.16.
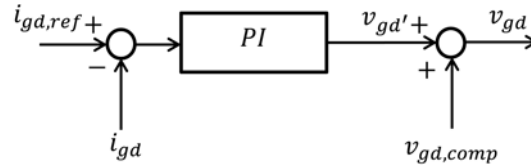
Figure 5.15: *d-axis inner current loop of GSC with compensation.*
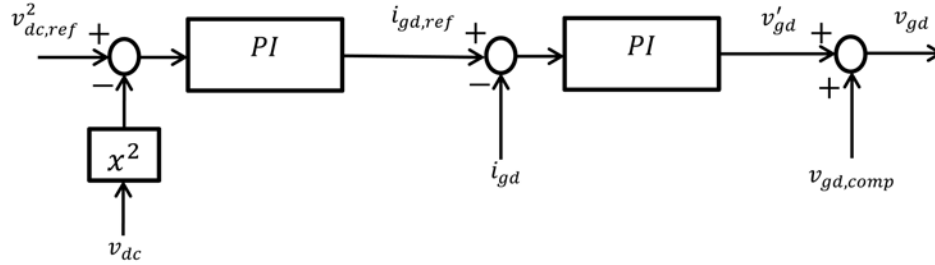
Figure 5.16: *complete d-axis loop of GSC with compensation.*

5.4.3   Reactive Power Control of GSC

Reactive power exchange at grid side in terms of dq components can be written as:

$$q_g = \frac{3}{2}(v_{gd}i_{gq} - v_{gq}i_{gd}) \tag{5.42}$$

Grid voltage is aligned to the d-axis of reference frame rotating at grid frequency ω_g.

$$\vec{v_g} = v_{gd} \tag{5.43}$$

$$v_{gq} = 0 \tag{5.44}$$

Thus reactive power (q_g) equation (5.42) reduces to:

$$q_g = -\frac{3}{2}v_{gd}i_{gq} \tag{5.45}$$

This equation (5.45) can be rearranged to produce reference current signal $i_{gq,ref}$ for inner loop of grid converter controller as:

$$i_{gq} = -\frac{2}{3}\frac{q_g}{v_{gd}} \tag{5.46}$$

The current reference i_{gq} for inner loop current controller depends on reference reactive power and voltage v_{ds} which can be measured.
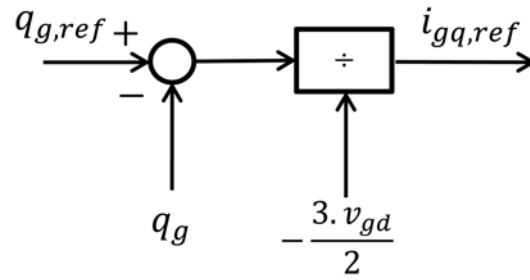
Figure 5.17: *reference current generation for q-axis of GSC.*

This current reference i_{gq} will be compared with measured grid current and PI controller will generate the q-axis voltage $v_{gq,ref}$ based on current error.
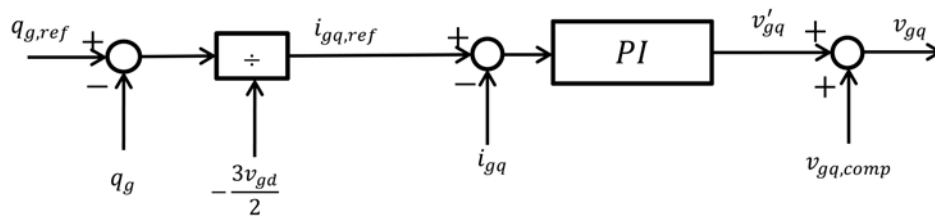
Figure 5.18: *complete q-axis current loop with compensation.*

Cross coupling terms also exist in q-axis as can be seen from grid voltage equation (5.41) and can be compensated by feed-forward gain. Finally, q-axis grid voltages are applied to the grid converter. A complete q-axis loop control with compensation can be seen from figure 5.18.
A complete control scheme of DFIG is shown in figure 5.19.
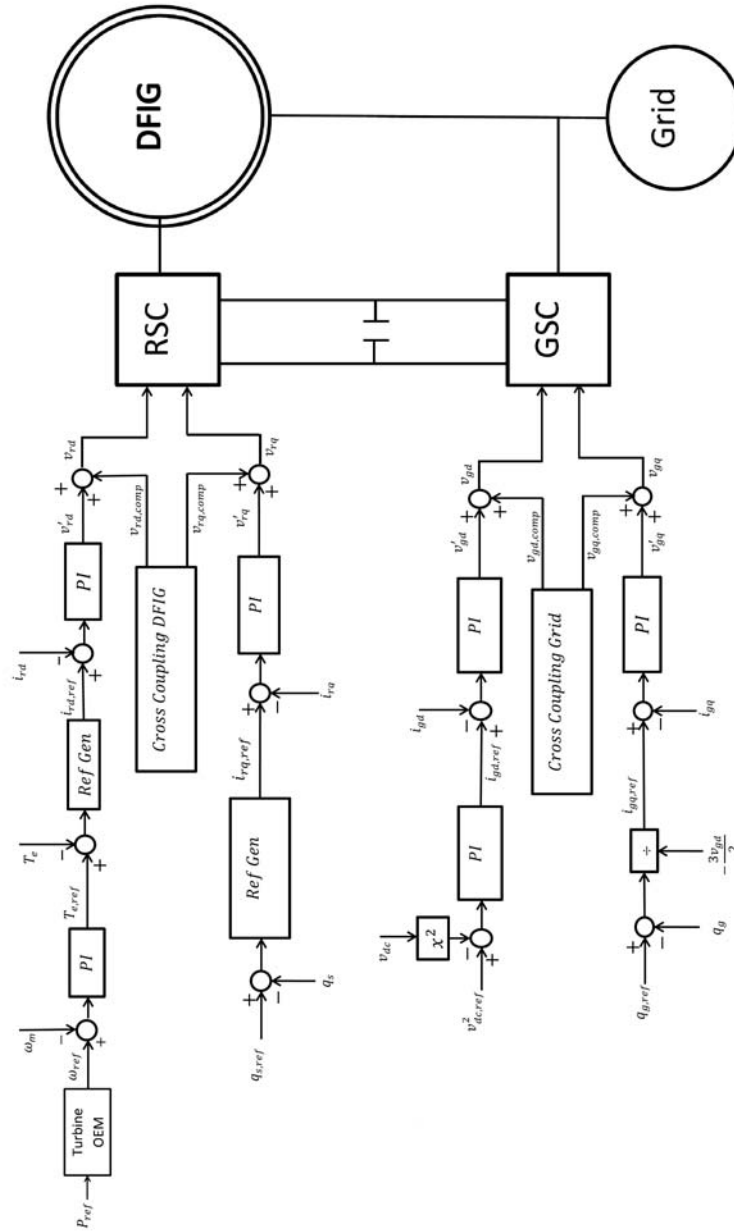
Figure 5.19: *A complete control scheme for DFIG.*

Chapter 6

Variable and Fixed Speed Operation of DFIG

This chapter deals with simulation of Variable Speed Operation (VSO)and Fixed Speed Operation (FSO) of hydro turbine power generation system model developed in previous chapters under different scenarios. Response of system is shown for different operation scenarios under VSO and FSO. The model is simulated at following scenarios:

- Response of system for a step change in power demand from 50% to 20%.

- Response of system for a step change in power demand from 50% to 90%.

- Response of system for a gradual change in power demand from 20% to 90% over time.

- Power production under different head conditions i.e. for head variation of 25%, 50%, 75% and 100%.

Finally, efficiency comparison for variable and fixed speed operation will be presented through the graph obtained for various operating points. DFIG data used for simulation is given in C.1.

6.1 Response of System for a Step Change in Power Demand from 50% to 20%.

The figure 6.1 and figure 6.2 shows the response of DFIG at (VSO) and (FSO) when power demand changes in step from 50% to 20% at 15sec. Stator power for both VSO and FSO follows the change in power demand, a very small amount of power was carried by rotor which depends on value of slip. The response of speed for VSO shows that the speed increases as the power demand decreases to attain optimum efficiency for a given

power demand or the flow rate as shown in Hill Chart. This speed reference was generated by the optimum efficiency speed module to move the operating point at a value to obtain optimum efficiency during VSO whereas in case of FSO, the speed was decreased for some time but again came back at fixed speed reference value. Torque and d-axis current also follows the power demand which shows the vector control performance as well.
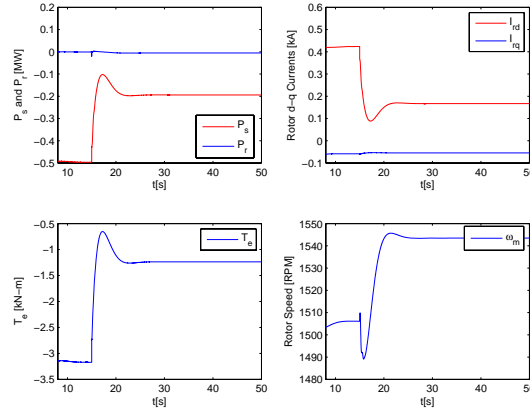
Figure 6.1: *VSO response for a change in power demand from* 50% *to* 20%.
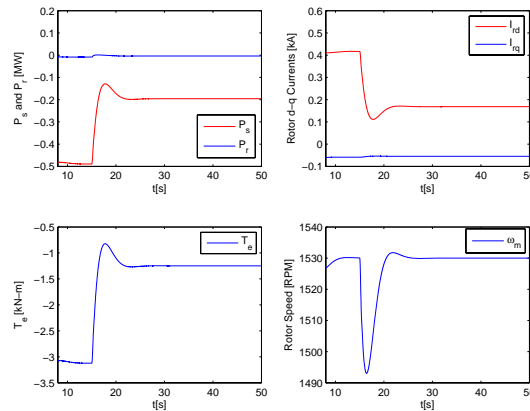
Figure 6.2: *FSO response for a change in power demand from* 50% *to* 20%.

6.2   Response of System for a Step Change in Power Demand from 50% to 90%.

Response of DFIG for a 40% step change in power from 50% to 90% is shown in figure 6.3 and figure 6.4. Speed reference generated by speed module for VSO operation to attain optimum efficiency causes the speed to decrease from super-synchronous value, approximately 5rpm above synchronous speed 1500rpm, to 1465rpm. Stator power, torque, and current follows the same response for both VSO and FSO while speed reference is fixed for FSO and comes back to its set point after slight disturbance for brief period of time

due to response of mechanical system. Recall that the power convention was defined positive for motor operation and negative for generator operation. Following the same convention note that the rotor power for VSO is changed from negative to positive as the speed changed from super-synchronous to sub-synchronous speed because of change in slip from negative to positive as discussed in the operation modes of DFIG. However, rotor power during FSO remained negative because the speed is super-synchronous and slip is negative although disturbance occurs for a brief period due to speed response.
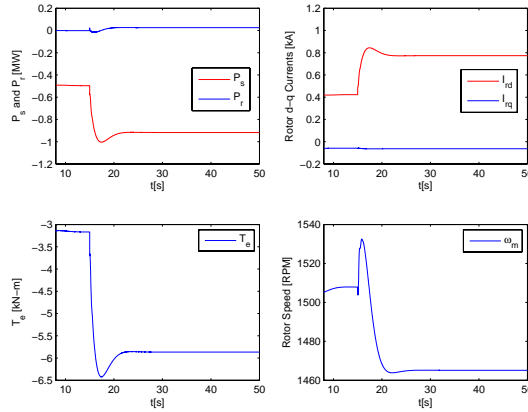
Figure 6.3: *VSO response for a change in power demand from* 50% *to* 90%.
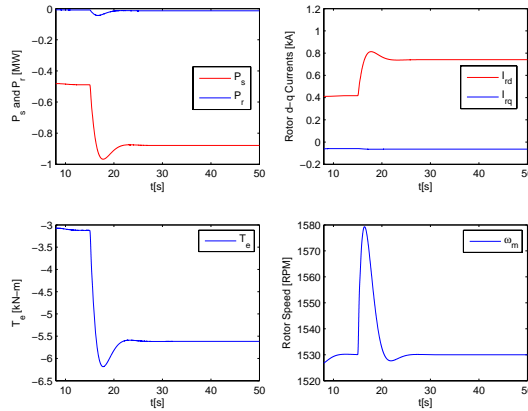
Figure 6.4: *FSO response for a change in power demand from* 50% *to* 90%.

6.3 Response of System for a Gradual Change in Power Demand from 20% to 90%.

Response of DFIG for transition from super-synchronous generation to sub-synchronous generation mode for VSO and at fixed speed reference for FSO can be seen from figure 6.5 and figure 6.6 respectively. Stator power, torque, and corresponding d-axis current changes as the power demand varies in a ramp fashion from 20% at $t = 15sec$ and reaches

to 90% at $t = 40sec$. Note the direction of rotor power flow changes from negative to positive as the DFIG speed changes its speed from super-synchronous to sub-synchronous speed during VSO while during FSO rotor power never changes its direction because the speed of DFIG during this operation never reaches at or goes down below synchronous speed. Speed error in FSO is increased as the power ramps up and so the rotor slip increases but controller finally restores the constant speed reference once the ramping period is over and the rotor supplies power according to the slip and rest of power flows through stator side. Speed response is not a straight line during VSO because the speed reference is generated by optimum efficiency speed module, which is obtained from Hill Chart, that is nonlinear function of flow.
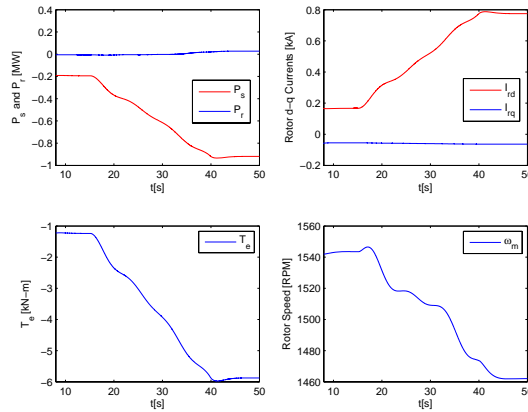
Figure 6.5: *VSO response for a ramp change in power demand from* 20% *to* 90%.
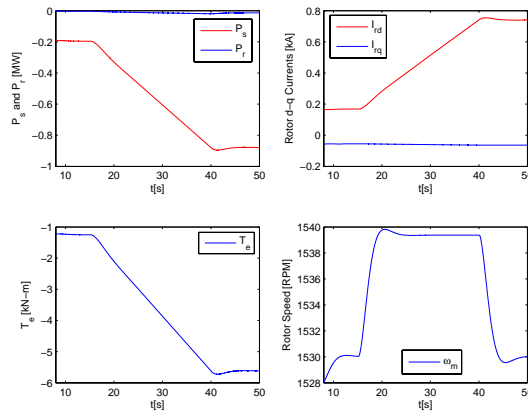
Figure 6.6: *FSO response for a ramp change in power demand from* 20% *to* 90%.

6.4   Power Generation Under Different Head Conditions i.e. for Head Variation of 25%, 50%, 75% and 100%.

As mentioned before that hydro turbine is designed to deliver its rated or maximum efficiency at rated parameters. However, some of the rated conditions (head, flow etc)

are not constant throughout the year and thus deviation from these conditions results in turbine operation below its rated or reduced efficiency. In this section operation of DFIG under different head conditions will be looked at i.e. at head values of 25%, 50%, 75% and 100%. Available hydro power depends on the head as:

$$P_h = q.H.g \tag{6.1}$$

Where P_h is the available hydro power, q is the flow, H is water head, and g is acceleration due to gravity. As can be seen from equation (6.1) that available hydro power varies directly with the variation in water head.

6.4.1   Power Generation at 25% Head

When the head reduces to 25% of its rated value then the maximum power available reduces too. The figure 6.7 and figure 6.8 shows the operational parameters of VSO and FSO respectively under 25% head level. It can be seen from figure 6.7 that a step change in power from 20% to 100% at $t = 10sec$ changes the stator power, torque, and d-axis current as expected and discussed in previous sections. Note that stator power is more than 25% of total power i.e. $1MW$. This is because of speed which is sub-synchronous and rotor power which is positive.
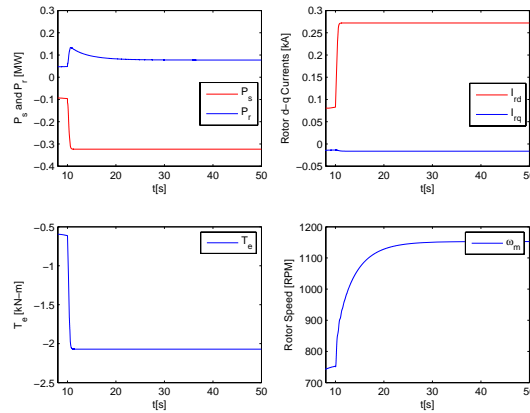
Figure 6.7: *VSO response for a change in power demand from* 20% *to* 100% *at* 25% *head.*

As discussed in chapter 2(operation modes), that in sub-synchronous generation mode slip is positive and stator carries power fed from shaft and rotor. However, only power fed from shaft is delivered to the grid while rotor power flows back to sustain the sub-synchronous generation mode, therefore, the stator power is negative whereas rotor power is positive. This can also be confirmed from FSO where stator power, torque and d-axis follows the change in power demand but the generator speed reference is above synchronous speed thus slip is negative and rotor power is also negative, see figure 6.8.
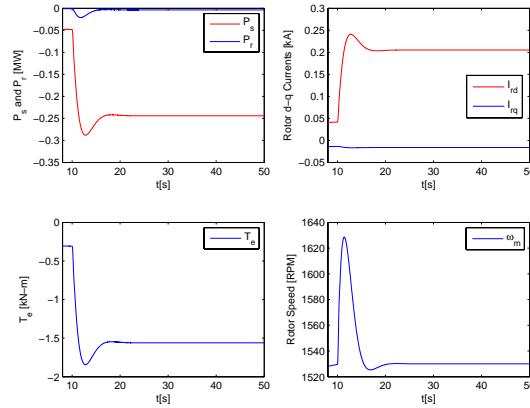
Figure 6.8: *FSO response for a change in power demand from* 20% *to* 100% *at* 25% *head.*

6.4.2   Power Generation at 50% Head

The same trend in stator power, torque, speed, and d-axis current can be seen from figure 6.9 and figure 6.10 for a head level of 50%. Speed for VSO operation is generated by optimum efficiency speed module according to the power demand whereas for FSO it is fixed at slightly above synchronous speed.
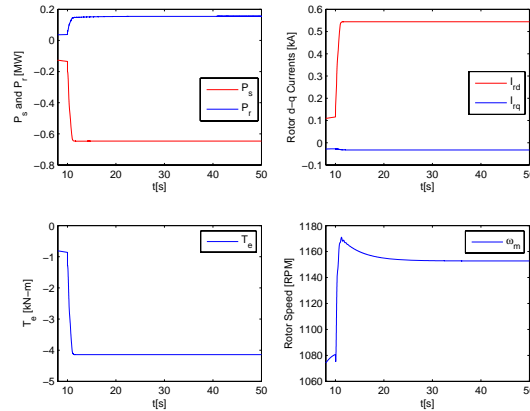
Figure 6.9: *VSO response for a change in power demand from* 20% *to* 100% *at* 50% *head.*

6.4.3   Power Generation at 75% Head

The figure 6.11 and figure 6.12 shows the same trend in stator power, torque, speed, and d-axis current for a head level of 75%, as in case of 25% and 50%. An important observation regarding speed values can be made for 25%, 50%, and 75% head level that amount of rotor power in DFIG is carried according to the value of slip. But this is not the case here as the rotor power is different from the percentage slip value in all three conditions. First it is due to the actual speed of turbine which depends on water head
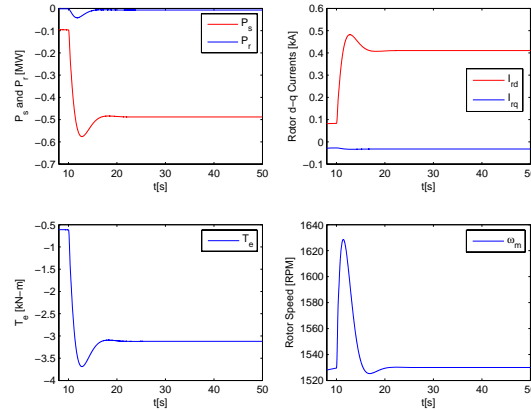
Figure 6.10: *FSO response for a change in power demand from* 20% *to* 100% *at* 50% *head.*

level, turbine diameter and turbine unit speed, recalling from chapter 4.

$$n = \frac{n_1 \sqrt{H}}{D_1} \qquad (6.2)$$

As can be seen from equation (6.2) that the actual speed of turbine depends on head value so it varies as the head level varies. Therefore, speed is used to control power, and speed reference is generated from optimum efficiency speed module based on turbine operating conditions.
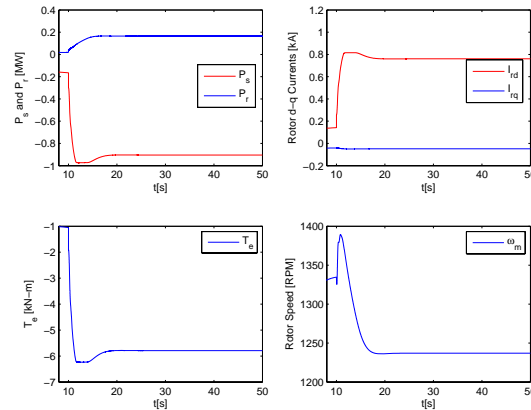
Figure 6.11: *VSO response for a change in power demand from* 20% *to* 100% *at* 75% *head.*

6.4.4   Power Generation at 100% Head

Response of the system at 100% head level is shown in figure 6.13 and figure 6.14, discussion from previous sections is also valid here. Although, in this case, an important
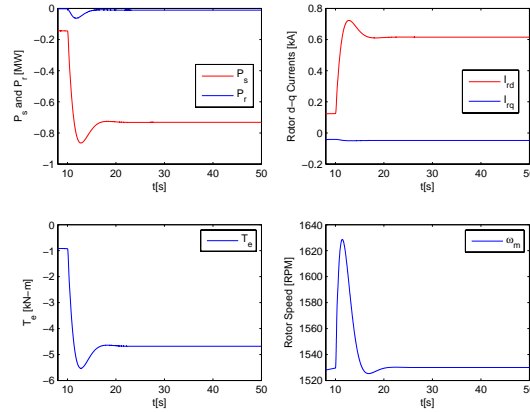
Figure 6.12: *FSO response for a change in power demand from* 20% *to* 100% *at* 75% *head.*

thing needs to be mentioned regarding stator power for VSO. As can be seen from fig-
ure 6.13 that the power which is carried by stator at 100% head level is increased slightly
above rated power i.e. $1MW$. The reason is as mentioned before that it is due to the
sub-synchronous generation mode. Although the rotor power recovers back and only the
turbine power is delivered to the grid. This is not the problem with FSO where speed
is super-synchronous so total power coming from the turbine is divided between stator
and rotor, thus stator carries power within its rated value and a part of that power flows
through the rotor and finally to the grid. The problem of high stator power in VSO can
be handled in two ways. First, as VSO during this condition runs at higher efficiency
compared to FSO, therefore, either the generator can be sized slightly overrated if the
gain in efficiency outweighs the extra investment in generator rating. Second option could
be incorporated in control strategy by switching the operation from VSO to FSO as the
power in stator crosses the certain limit but this will cause the sacrifice of extra efficiency
which could have been gained in case of VSO.
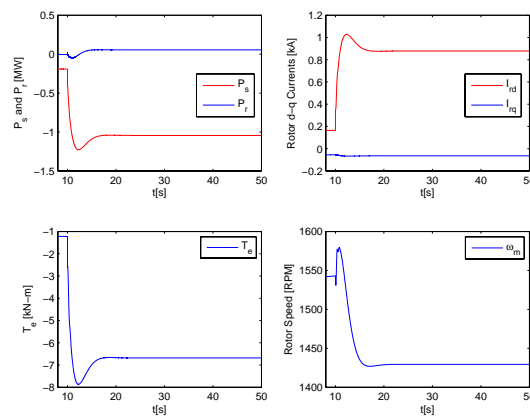
Figure 6.13: *VSO response for a change in power demand from* 20% *to* 100% *at* 90% *head.*
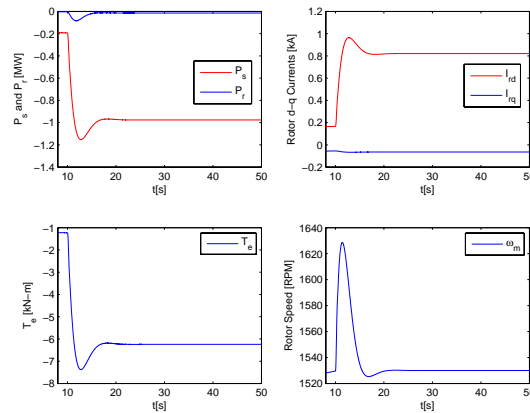
Figure 6.14: FSO response for a change in power demand from 20% *to* 100% *at* 90% *head.*

6.5   Comparison of Efficiency of VSO and FSO.

Response of the system under different operational conditions have been investigated in the previous sections. The graph of turbine efficiency for variation in generated power is shown in figure 6.15. This graph is plotted at 100% head condition by varying the power or flow rate. It is quite evident from the graph that efficiency under VSO is always higher than FSO as for each operating point or required power, optimum efficiency speed module generates the speed reference which moves the operating point up hill or sets the speed reference to a value where efficiency is the highest. This is not the case for FSO where speed is fixed. However, efficiency of FSO approaches close to VSO as the system power point moves close to the rated value of turbine which was expected because the unit is usually designed to deliver power at highest efficiency at or around its rated power.
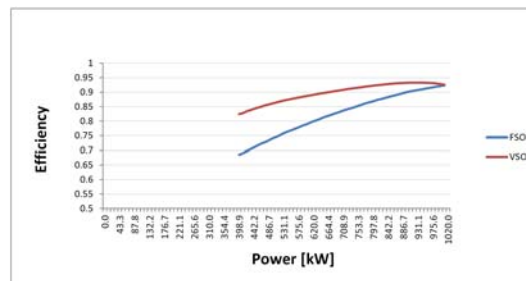
Figure 6.15: Efficiency plot of hydro-turbine during VSO and FSO.

Chapter 7

Implementation in Lab

Modeling and simulation of system under study have been done until this point. Simulation results obtained in chapter 6 can be validated by implementing the system in a lab setup this is important to observe the real world behavior of system. In this chapter first a brief introduction of subsystems (both hardware and software) will be discussed and then real time operation of close and open loop motor control, developed to test these subsystem, will be presented. Motor and generator set data is given in C.2.

7.1 System Components

Different hardware and software are required to emulate the system behavior in lab. In this chapter first a brief look is taken at different subsystem of the setup and then machine operation will be presented.

7.1.1 Motor Generator Set

A squirrel cage induction motor coupled with a DFIG is available for the experimental setup, see figure 7.1. For a power generation system setup SQIM is supposed to work as prime mover, to make it work as prime mover. Shaft torque produced by SQIM will drive the DFIG.
Signal conditioning for voltage and current signals and interfaces to the control system have been designed. Firstly, a motor control system has been designed and implemented to test the dSpace kit, sensors, measurement, driver circuit, and software.

7.1.2 dSpace Kit 1104

Controller used to implement the control is dSpace kit 1104. It is an efficient controller which is used for rapid prototype design building, as the control system models built in

Figure 7.1: *Motor Generator set.*

Matlab/Simulink can be directly (after slight modification) used to generate the code for Control Desk (software used with dSpace), this greatly reduces implementation time and effort and is the main advantage of using dSpace systems. A view of dSpace interface board is shown in figure 7.2.

Figure 7.2: *dSpace interface board.*

7.1.3   Rotary Encoder

Rotary encoder is a sensor which converts position or speed of rotating shaft into electrical signals. Encoder used for this project is quadrature incremental encoder (QIE). This QIE have two channels each of which provides equally spaced pulses per revolution and phase difference between generated pulses from both channels is 90° degrees. Because of the dual channel its resolution is high and direction of rotation can also be detected by detecting the relative phase difference (lead or lag) between channels, see figure 7.3.

During each revolution it produces a marker signal which can be used as an indication
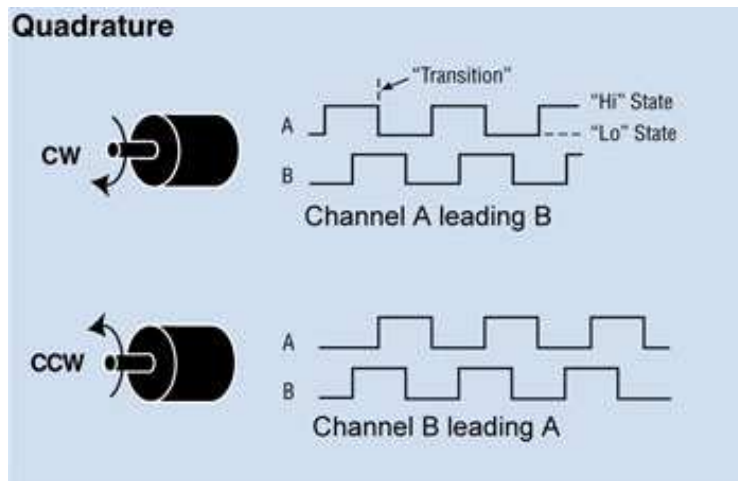
Figure 7.3: *Pulses generated by quadrature encoder for CW and CCW rotation.*

for one complete revolution or can be used as reference for position, figure 7.4 shows the encoder mounted on shaft.

7.1.4 Voltage and Current Measurements

Three phase voltages to the rectifier, dc link voltage and three phase currents were measured using the LEM transducers. LEM transducers are very popular and have following advantages as mentioned in the data sheet, see D.2.

- Precise accuracy and linearity in measuring range.

- Low temperature drift.

- High frequency bandwidth and no insertion losses.

- Immunity to external interface

- Optimized response time

- Capacity of current overload

Voltage Measurement

Three phase voltages to the rectifier and dc link voltage are measured using $LV25 - 800$ transducer as shown in figure 7.5. This voltage transducer can measure upto $800V$. The current rating at high voltage side should be kept within specified limits of $\pm14mA$ or $\pm10mA$, and it can work with $\pm15V$ or $\pm12V$ supply voltage.

Resistance value to limit the current at input of transducer can be found using:

$$R_{lim} = \frac{V_{LLrms}}{I_p} \tag{7.1}$$
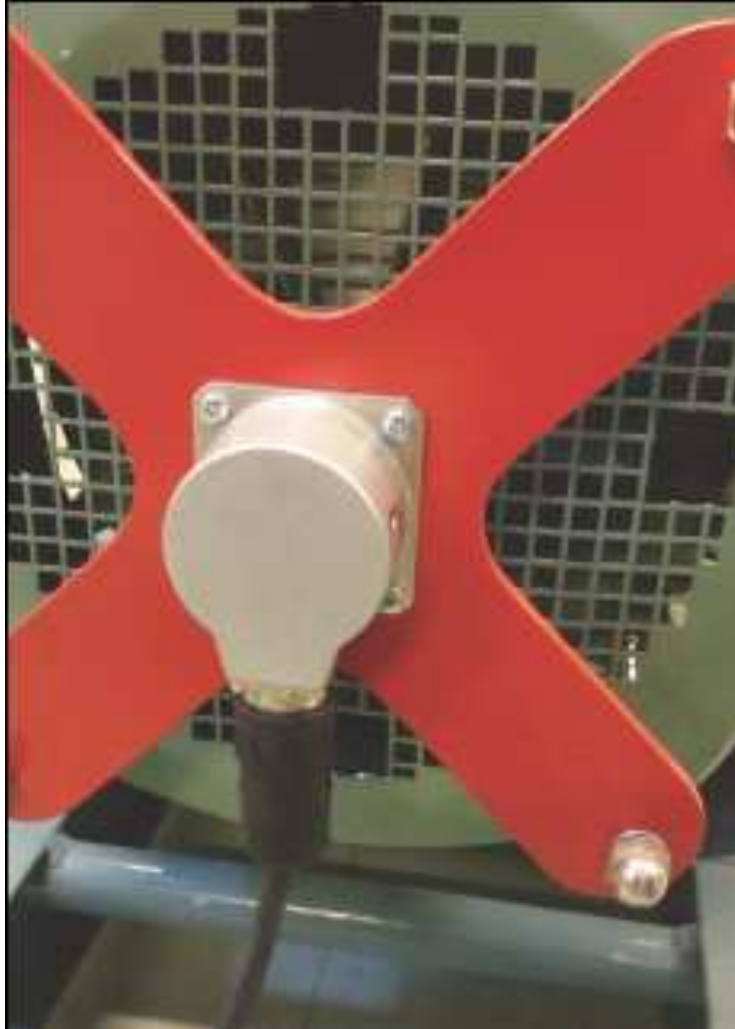
Figure 7.4: *quadrature encoder mounted on shaft.*
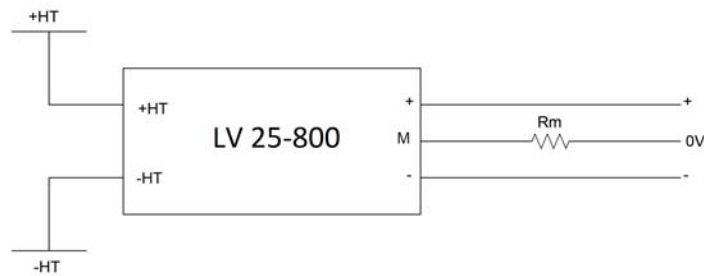
Figure 7.5: *LEM voltage transducer connection block diagram.*

Where R_{lim} is the value of resistance to limit current at primary side, V_{LLrms} is input voltage and I_p is the current at primary side of transducer.

Then current at output or secondary side can be calculated using the transformation ratio between primary and secondary as:

$$I_m = n.I_p \qquad (7.2)$$

Where I_m is the measured current at secondary side and n is the transformation ratio. This I_m can be converted to voltage using the resistance value as:

$$R_m = \frac{V_m}{I_m} \qquad (7.3)$$

R_m is the called measuring resistance which must lie within the range specified in data sheet, see D.2.

Line to Line Voltage Measurement

Line to Line rms voltage measured at the input side of rectifier is $380V$. By adding a safety margin of 20% arbitrarily, to rated voltage to avoid saturation of transducer, voltage becomes $456V$. Resistance value can be calculated for this voltage while further calibration can be done in software by adjusting the multiplication factor.

DC Link Voltage Measurement

DC link voltages also measured using the LEM transducer which can work upto $800Vdc$. DC link voltage is around 546 but the maximum value it can with stand is $756V$. Thus this value is selected for calculating resistance value, in this case, safety margin has already been taken into account by choosing the maximum voltage value because the rated dc link voltage is already much less than the maximum value, see figure 7.6 for five channels voltage transducer box.
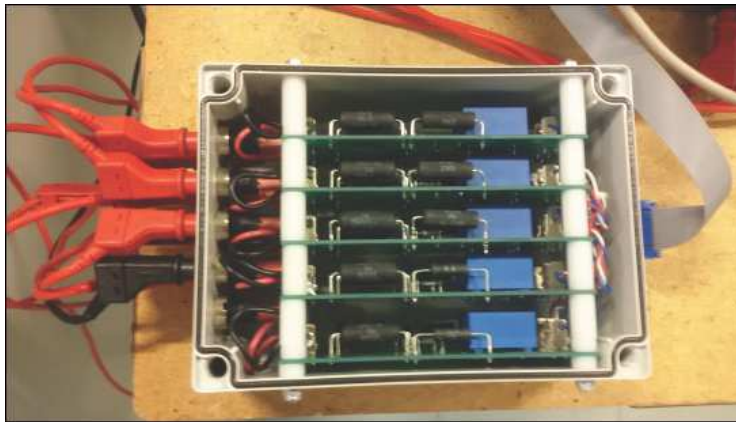
Figure 7.6: *LEM transducer box.*

Current Measurement

Current measurement was done at three phases between converter and machine power supply terminals. LEM transducer $LA205 - S$ translates current at the primary side by a specified ratio to the secondary side, given in the data sheet, see D.2.

$$I_s = n.I_p \tag{7.4}$$

Where I_p is primary current, n is the current transformation ratio and I_s is the current at secondary side of transducer.

Figure 7.7: *LEM current transducer connection block diagram.*

Secondary side current I_s can be converted to voltage by selecting the measuring resistance from a range of values specified in data sheet, see D.2.

$$R_m = \frac{V_m}{I_s} \tag{7.5}$$

Where V_m is the chosen voltage,

The important consideration in selecting the measuring resistance R_m value both for voltage and current measurements is that the voltage V_m obtained by multiplying the maximum possible current at secondary side of the transducer with measuring resistance must not exceed the input ADC channel limit of $\pm 10V$ of dSpace kit otherwise it could damage the input channel.

7.1.5 Signal conditioning board

Although, it is possible to connect signals from the output of voltage and current transducers directly. But this signal contains some high frequency noise so in order to improve the quality of that signal or to filter/reject noise, signal conditioning board is used. A parallel RC filter is connected across each voltage channel port as shown in figure 7.8.

Operational amplifier circuit is used for current signals conditioning, see figure 7.9 and figure 7.10. Three phase currents are sensed at the output terminals of converter while three phase voltages are measured at the incoming power supply to rectifier. .
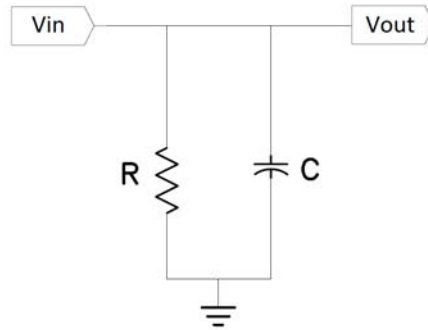
Figure 7.8: *Passive RC filter for power line voltage channels.*
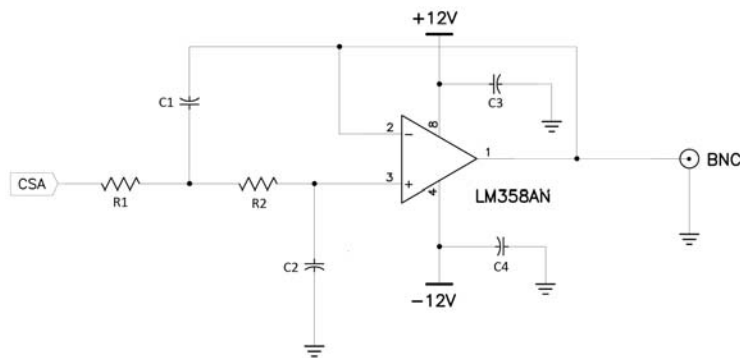
Figure 7.9: *Active op-amp filter for current channel.*
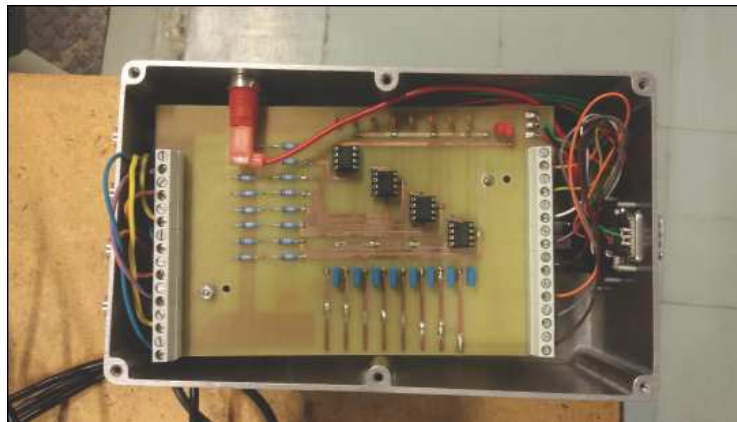
Figure 7.10: *op-amp board for current signals.*

7.1.6 Converter

Converter used to drive the machine consist of rectifier-inverter with DC link capacitor. Its bridge rectifier uses diodes and is connected to 3-phase supply, a dc link capacitor

smooths out the output from rectifier and this dc voltage is an input to the IGBT inverter. A view of this converter can be seen from the figure 7.11. Three phase output from IGBT lags is directly connected to the machine terminals.
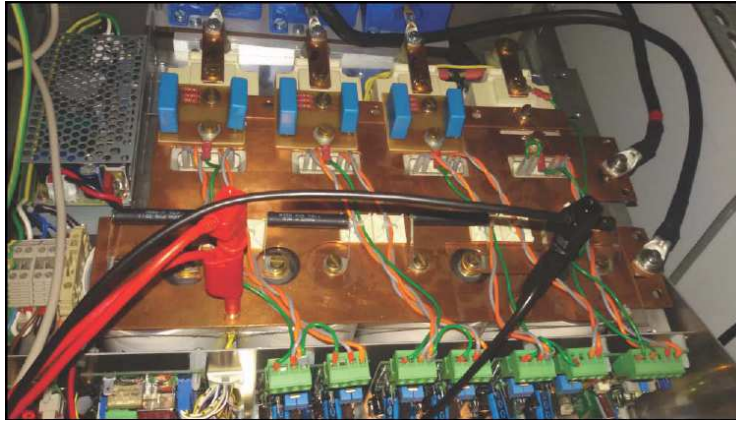
Figure 7.11: *A view of IGBT inverter.*

7.1.7   Driver Circuit

Each leg of inverter has two IGBTs which can be turned on or off through control signals applied to their gate terminals. PWM control signals are generated by dSpace which can not supply enough current to directly drive the IGBTs and thus can not be interfaced directly with dSpace. Therefore, a power driver circuit is added which is an interface between control signals generated from dSapce and IGBTs gate terminals, it draws current within safe limits from dSpace controller and supplies the required current to drive the IGBTs, see driver circuit figure 7.12. Further, the two IGBTs in each leg should not be in on state or conducting at any instant of time as it will produce the short circuit across dc link. Therefore, a time delay is required between turn on state of IGBTs of each leg. To ensure this delay between switch on, driver circuit has built in dead time for switches of each leg.

7.1.8   Matlab/Simulink

dSpace is a rapid development tool which can directly use the models built into Matlab/Simulink. After testing the motor model in Matlab/Simulink, input and output of the model are replaced with dSpace real time blocks. Then this model is compiled to generate the files which can be used by the Control Desk.

7.1.9   Control Desk

Control Desk is a software program used to design the layout of control and monitoring panels for the system. System layout is organized into monitoring, control, and protection

Figure 7.12: *Driver circuit for inverter.*

& fault diagnostic panels. This will be explained further in the next section by putting motor into operation.

7.2 Machine Operation

In this section the data recorded during motor operation and description of the control desk layout designed for the motor control will be discussed.

7.2.1 Monitoring Panel

Different real time parameters of motor can be observed on monitoring panel. A screen print of monitoring panel during close and open loop operation of motor at run time can be seen from figure 7.13 and figure 7.14. It shows three phase line to line voltages of all three phases, DC link voltage, three phase line currents, and speed in rpm. In addition, motor can be put in and out of operation by pressing start and stop buttons available on monitoring panel.

7.2.2 Control Panel

It is very important to operate the motor within its specified limits, for instance, its current must not exceed beyond certain limits also over voltage and over speed above specified limits could damage the machine, therefore, to ensure safe operation of the machine maximum limits for different operational parameters needs to be set on control panel. As shown in figure 7.15 and figure 7.16 that maximum limit for current, dc link voltage, line to line voltage, and speed can be set on panel, these numerical input boxes accept values in a predefined limit so that any value entered beyond safe limits will be discarded.
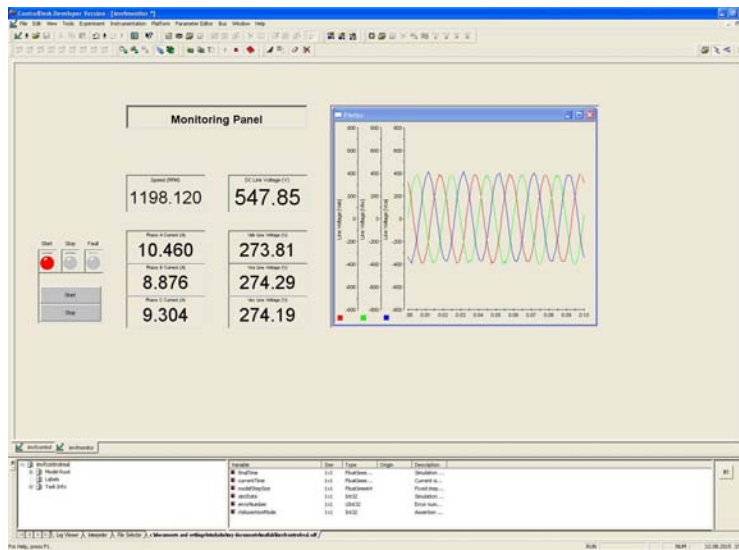
Figure 7.13: *Monitoring panel screen print during close loop operation of Motor.*
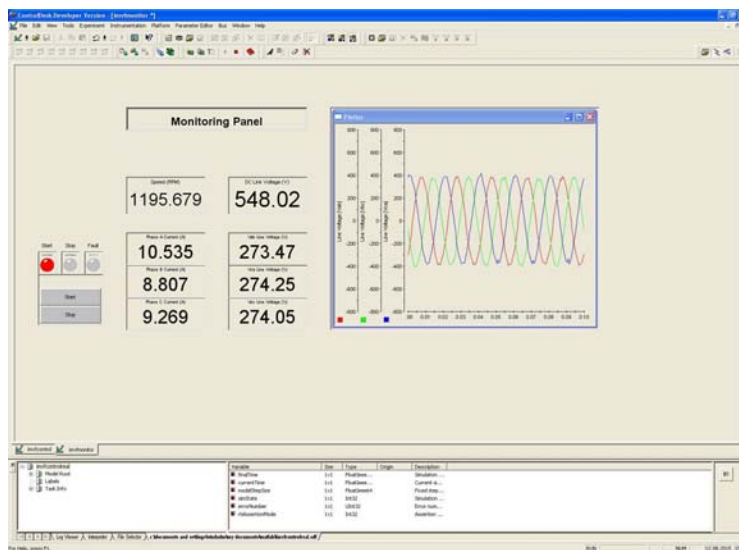
Figure 7.14: *Monitoring panel screen print during open loop operation of Motor.*

Further, control panel has start and stop control for the motor, a drop down menu to select forward or reverse direction of rotation, and selection to run the machine in open or close loop speed control mode. Selection for direction of rotation and open/close loop operation can be changed during real time operation of motor whereas the maximum limit set points will be disabled during real time motor operation. For closed loop operation, proportional and integral gains of the controller can be adjusted online by entering gain values in numerical input boxes also the reference speed value (in rpm) can be entered on control panel during run time, see screen print of control panel in figure 7.15 and figure 7.16 during close and open loop operation.
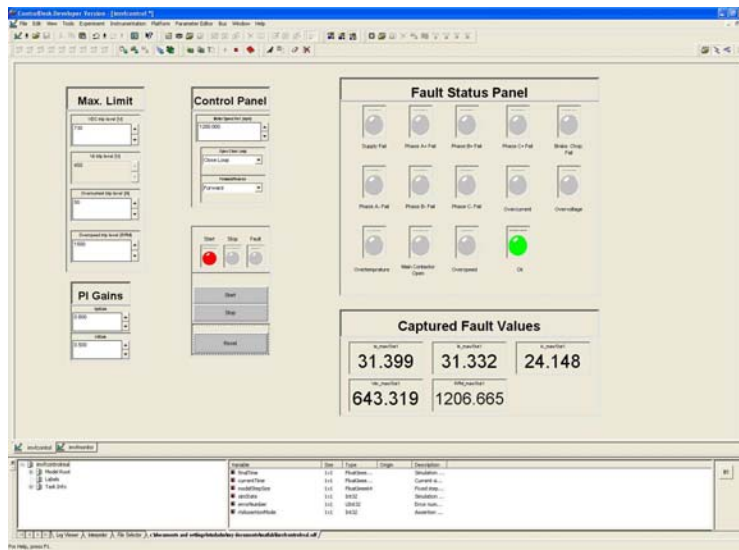
Figure 7.15: *Control panel screen print during close loop operation of Motor.*
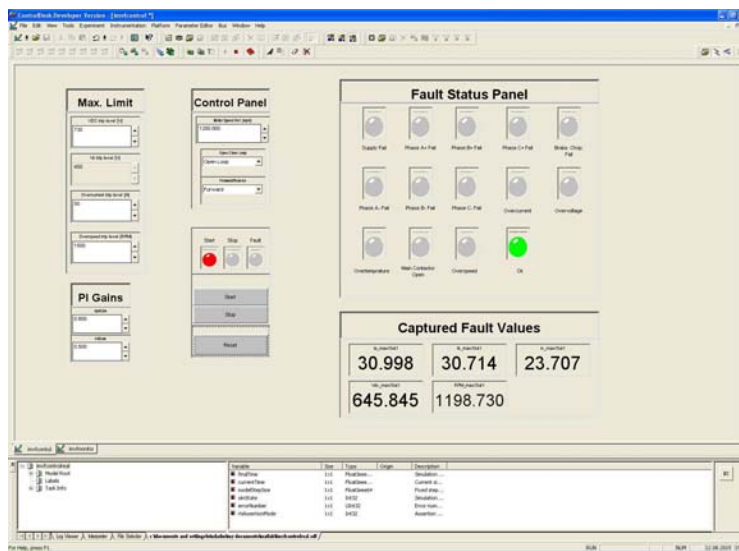
Figure 7.16: *Monitoring panel screen print during open loop operation of Motor.*

7.2.3 Protection and Diagnostic Panel

It is desirable to run the machine within safe operating limits, however, machine could go into unsafe region during its operation. Therefore, in case of any deviation from maximum set points, protection system will send the trip signal to the motor control and stop further operation to avoid damage. Moreover, diagnostic panel will also indicate the cause of protection activation by turning on an LED's color to red on fault status panel,

a screen print taken at DC link overvoltage is shown in figure 7.17.
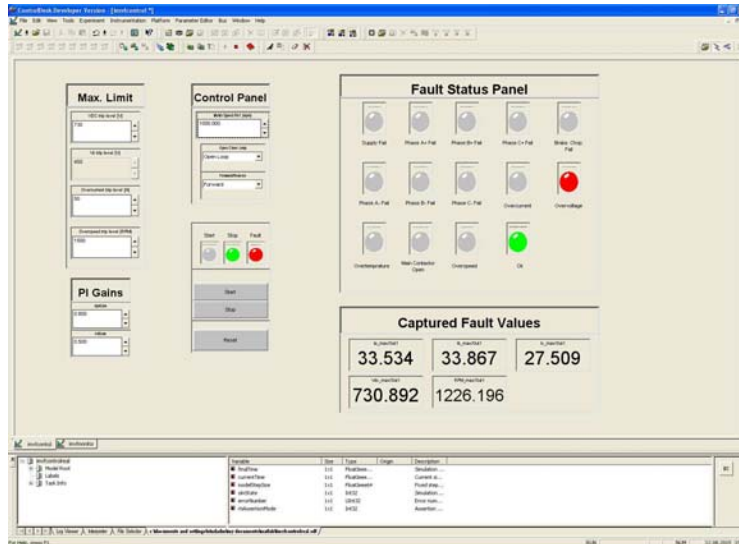
Figure 7.17: *Fault status and fault capturing panel screen print at overvolatge.*

Figure 7.18: *A view of control system setup.*

Fault captured panel will record and display the level of fault value, this captured value can be used for diagnostic purposes. System will not issue start command to the machine unless all the faults on panel are reset and come down within safe limits. A description of faults on fault status panel is given in *table*7.1.

S.No.	T3	T2	T1	T0	Unit
15	L	L	L	L	+5V supply failure /Start up
14	L	L	L	H	Failure Phase A+
13	L	L	H	L	Failure Phase B+
12	L	L	H	H	Failure Phase C+
11	L	H	L	L	Failure Brake Chopper
10	L	H	L	H	Failure Phase A-
9	L	H	H	L	Failure Phase B-
8	L	H	H	H	Failure Phase C-
7	H	L	L	L	Overcurrent
6	H	L	L	H	NC
5	H	L	H	L	Overtemperature
4	H	L	H	H	NC
3	H	H	L	L	Overvoltage
2	H	H	L	H	NC
1	H	H	H	L	Main Contactor Open
0	H	H	H	H	OK,Ready

Table 7.1: *Fault Status LEDs*

Chapter 8

Conclusion

8.1 Conclusion

The objective of this work was to carry out a technical assessment of DFIG for use in mini-hydro power systems while economic assessment was an optional task. As mentioned in chapter 1 that assessment was based on the efficiency comparison of DFIG at fixed speed and variable speed operation. Dynamic model of DFIG was developed and validated by simulating in Matlab/Simulink. Dynamic equations for DC link and grid were also written in dq reference frame moving at synchronous speed.

As explained in Hill Charts that hydro turbine efficiency for a particular power demand or load can be improved by running the turbine at a specific speed. Using this fact Hill Charts were used to develop an optimum efficiency speed module which generates the speed reference value to run the turbine at a speed where optimum efficiency can be achieved for a given power demand. As turbine speed can be controlled by controlling the DFIG speed, so a vector control system was developed to control the speed/power and reactive power of DFIG. For any real power demand of the system, optimum efficiency speed module finds the speed for optimum efficiency which is input to the DFIG speed control system and the control system runs the DFIG and hydro turbine coupled to it at that speed.

This developed model was put to simulation under different scenarios to check the variable and fixed speed operation of DFIG. Operation modes of DFIG, such as sub-synchronous and super synchronous operation, under different scenarios were also observed. It can be seen from the results of simulations that DFIG attains the speed reference well as the power demand changes. Finally comparison was made using efficiency graph for both variable and fixed speed operation for a range of power demand and it has been found that efficiency under VSO was always better than FSO, furthermore, efficiency under VSO approaches FSO as the power demand approaches near rated value of unit.

A lab setup has to be prepared to implement the control of DFIG to validate the simulation results. Signal conditioning boards and different interfaces were designed, for measured signals, i.e. voltage and currents, these boards, interfaces, and dSpace kit was

tested by developing a motor control.

8.2   Future Work

As shown through simulation that efficiency of VSO is always better than FSO for a range
of unit power. These results can be validated by implementing the simulated model on
a small scale in lab. Signal conditioning boards and different interfaces for the available
B2B converter were developed as shown in chapter 7. Furthermore, converter was also
tested by implementing a motor control and testing in open and close loop and found to
be working well but the implantation of overall control could not be carried out due to
the delays in lab work and time limitations. Following guidelines are being listed down
here which will be useful for implementation in future.

1. As mentioned before dSpace kit 1104, signal conditioning boards, and different
   interfaces have already been developed and tested with one of the converter. Since
   there are two converters and input channels of dSpace board 1104 are not enough
   to control both converters. So another dSpace kit 1103 is also available in lab which
   still needs to be tested along with second converter, although signal conditioning
   boards and corresponding interfaces for the second converter are ready and have
   already been tested.

2. Once both converters are working well with their respective dSpace boards then the
   motor can be controlled through already built motor drive which will serve as prime
   mover for the system.

3. Although, the parameters of DFIG are already known but it would be better to
   verify them again before putting DFIG in operation as performance of vector control
   depends on the accuracy of these parameters.

4. After testing/implementing the system with developed model. Dynamic model of
   hydro turbine can be further enhanced by including penstock and guide vane opening
   dynamics using real turbine data. In addition, mechanical shaft losses between
   turbine and generator can also be included.

5. Lastly economic analysis can be performed after acquiring the real time data after
   implementation and running in lab. Although better efficiency of system during
   VSO is an indicator of increased production, yet the economic analysis also depends
   on specific site conditions.

References

[1] REN21. Renewables 2015 global status report. Technical report, Renewable Energy Policy Network for the 21st Century, 2015.

[2] WEC. Charting the upsurge in global hydropower development 2015. Technical report, World Energy Council, 2015.

[3] Luis Maroto Juan I. Perez, Jose R. Wilhelmi. Adjustable speed operation of a hydropower plant associated to an irrigation reservoir. *Department of Hydraulic and Energy Engineering, Technical University of Madrid (UPM), Madrid, Spain.*

[4] Terje Gjengedal Roald Sporild, Jan Ove Gjerde. Economic and technical aspects of adjustable speed hydro (ash) machines applied for improved stability in power networks. *Power Engineering Society Summer Meeting, IEEE, Seattle, WA*, 2000.

[5] Luise F Raffin P Degano M Tessarolo, A. Traditional hydropower plant revamping based on a variable-speed surface permanent-magnet high-torque-density generator. *Clean Electrical Power (ICCEP), 2011 International Conference on, Ischia*, 2011.

[6] C. Klingler A. Dietz, A. Groeger. Efficiency improvement of small hydroelectric power stations with a permanent-magnet synchronous generator. *Electric Drives Production Conference (EDPC), 1st International*, 2011.

[7] Wegiel T. Borkowski, D. Small hydropower plant with integrated turbine-generators working at variable speed. *Energy Conversion, IEEE Transactions on*, 2013.

[8] D. Roye L. Belhadji, S. Bacha. Modeling and control of variable-speed micro-hydropower plant based on axial-flow turbine and permanent magnet synchronous generator (mhpp-pmsg). *IECON 2011 - 37th Annual Conference on IEEE Industrial Electronics Society, Melbourne, VIC*, 2011.

[9] Benot ROBYNS Stefan BREBAN, Mircea M. RADULESCU. Direct active and reactive power control of variable-speed doubly-fed induction generator on micro-hydro energy conversion system. *Electrical Machines (ICEM), XIX International Conference on, Rome*, 2010.

[10] J. Fraile-Mora J. I. Prez I. Sarasa J. Fraile-Ardanuy1, J. R. Wilhelmi. Speed control of run-of-river variable speed hydro plants. *Departamento de Ingeniera Civil: Hidrulica y Energtica E.T.S.I.C.C. y P., Universidad Politcnica de Madrid Profesor Aranguren s/n, 28040 Madrid (Espaa)*, 2006.

[11] Geyer T. Bradshaw J.B. Vilathgamuwa D.M. Madawala, U.K. Modeling and analysis of a novel variable-speed cage induction generator. *Industrial Electronics, IEEE Transactions on*, 2011.

[12] J.M. Pacasc J.L. Mrqueza, M.G. Molinab. Modeling and analysis of a novel variable-speed cage induction generator dynamic modeling, simulation and control design of an advanced micro-hydro power plant for distributed generation applications. *Industrial Electronics, IEEE Transactions onInternational Journal of Hydrogen Energy*, 2010.

[13] Albu M. Bostan V. Dumitrescu A.M. Magureanu, R. Optimal operation of francis small hydro turbines with variabiable flow. *Industrial Electronics, 2008. ISIE 2008. IEEE International Symposium on*, 2008.

[14] S. Chapman. *Electric Machinery Fundamentals, ser. Power and Energy Series.* McGraw-Hill, 2005.

[15] I. Boldea and S. Nasar. *The induction machine handbook.* CRC, 2001.

[16] C. Kingsley A. Fitzgerald and S. Umans. *Electric Machinery, 6/E, ser. McGraw-Hill series in electrical and computer engineering.* McGraw-Hill, 2002.

[17] N. Zargari B.Wu, Y. Lang and S. Kouro. *Power conversion and control of wind energy systems.* Wiley-IEEE Press, 2011.

[18] G. Iwanski et al G. Abad, L. Marroyo. *Doubly Fed Induction Machine: Modeling and Control for Wind Energy Generation.* Wiley-IEEE Press, 2011.

[19] I. Boldea. *Variable speed generators.* CRC, 2005.

[20] R. Krishnan. *Electric Motor Drives: Modeling, Analysis, and Control.* Prentice Hall Upper Saddle River, NJ, 2001.

[21] A. Tapia G. Tapia and J. Ostolaza. Two alternative modeling approaches for the evaluation of wind farm active and reactive power performances. *Energy Conversion, IEEE Transactions on*, 2006.

[22] T. Miller. Theory of the doubly-fed induction machine in the steady state. *in Electrical Machines (ICEM), 2010 XIX International Conference on*, 2010.

[23] N. Mohan. *Advanced Electric Drives: Analysis, Control and Modeling using Simulink.* Minnesota Power Electronics Research and Education (MNPERE), 2001.

[24] P. Vas. *Vector Control of AC machines.* Clarendon press Oxford, 1990.

[25] P. Krause. *Analysis of Electric Machinery.* McGraw-Hill, 1986.

[26] R. Park. Two-reaction theory of synchronous machines generalized method of analysis-part i. *American Institute of Electrical Engineers, Transactions of the*, 1929.

[27] N. Mohan. *Electric Drives: an Integrative Approach.* Minnesota Power Electronics Research and Education, 2003.

[28] M. W. Schulz W. C. Duesterhoeft and E. Clarke. Determination of instantaneous currents and voltages by means of alpha, beta, and zero components. *American Institute of Electrical Engineers, Transactions of the*, 1951.

[29] Navid Zargari Samir Kouro Bin Wu, Yongqiang Lang. *Power Conversion and Control of Wind Energy Systems.* Wiley-IEEE Press, 2011.

[30] Rolf Ottersten. *On control of back-to-back converters and sensor-less induction machine drives.* Ph.D. Thesis, Chalmers University of technology, Goteborg, Sweden, 1999.

[31] R. Rudramoorthy C.P Kothandaraman. *Fluid mechanics and machinery.* New age international publishers, 2007.

[32] Zainal Alimuddin Zoeb Husain, Zulkifly Abdullah. *Basic fluid mechanics and hydraulic machines.* BS publications, 2008.

[33] Angela Lu. Object oriented modeling and simulation of kaplan turbines. Master's thesis, KTH Electrical department, 2008.

[34] K. Subramanya. *Hydraulic Machines.* Tata McGraw Hill, 2013.

[35] Nima Madani. Design of permanent-magnet synchronous generator for vertical axiswindturbine. Master's thesis, Degree project in Electrical engineering, Master of Science, KTH, Stockholm, Sweden, 2011.

[36] Peng Wang Xiaoqing Han, Pengmin Wang. Transient stability studies of doubly-fed induction generator using different drive train models. In *Power and energy society general meeting.*

[37] Zhe Chen Qiang Gao Ren-jie Ye, Hui Li. Comparison of transient behaviors of wind turbines with dfig considering the shaft flexible models. In *Electrical machines and systems,*.

[38] Seyed Mohsen Nourbakhsh; Knudsen Torben; Kragelund Martin Nygaard; Bak Thomas Grunnet, Jacob Deleuran; Soltani. European wind energy conference and exhibition.

[39] Vesa Ruuskanen Jussi Sopanen. Dynamic torque analysis of a wind turbine drive train including a direct driven permanent-magnet generator. *IEEE Journal, Industrial electronics, IEEE transaction*, 2011.

[40] Edgar Moreno-Goytia Grain Adam Olimpo Anaya-Lara, David Campos-Gaona. *Offshore Wind Energy Generation: Control, Protection, and Integration to Electrical Systems.* Wiley, 2014.

[41] Janaka Ekanayake Phill Cartwright Olimpo Anaya-Lara, Nick Jenkins. *Wind Energy Generation: Modelling and Control.* Wiley-Blackwell, 2009.

Appendix A

Additional Graphs from Simulation

Additional graphs are being presented here for the following three scenarios simulated in chapter 6.

- Response of system for a step change in power demand from 50% to 20%.

- Response of system for a step change in power demand from 50% to 90%.

- Response of system for a gradual change in power demand from 20% to 90% over time.

These graphs include power frequency, reactive power, rotor currents, and DC link voltage for both VSO and FSO.

A.1 Step Change in Power Demand from 50% to 20%

A very small variation in frequency, reactive power, and DC link voltage is observed both in VSO and FSO and system remains stable when the power demand changes in step from 50% to 20%, see figure A.1 and figure A.2.

Figure A.1: *VSO response for a change in power demand from* 50% *to* 20%.
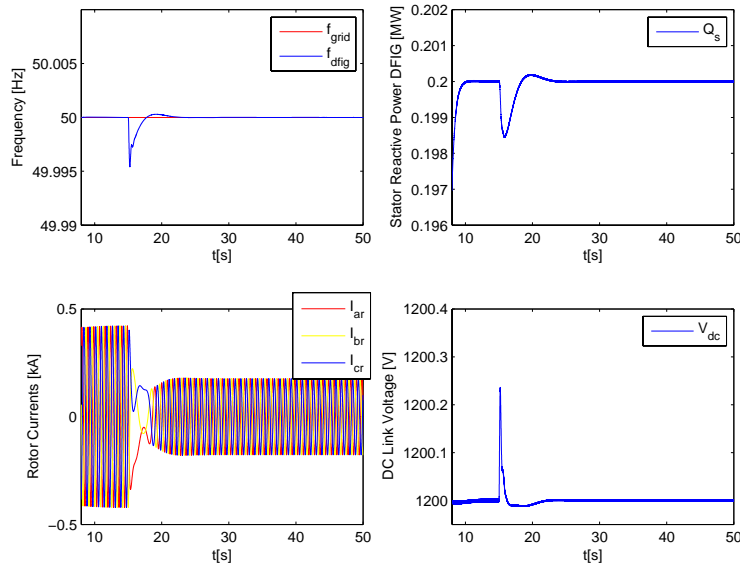
Figure A.2: *FSO response for a change in power demand from* 50% *to* 20%.

A.2   Step Change in Power Demand from 50% to 90%

Same trend can be seen from figure A.3 and figure A.4 that variation in frequency, reactive power and DC link voltage is very small when power demand changes from 50% to 90%.
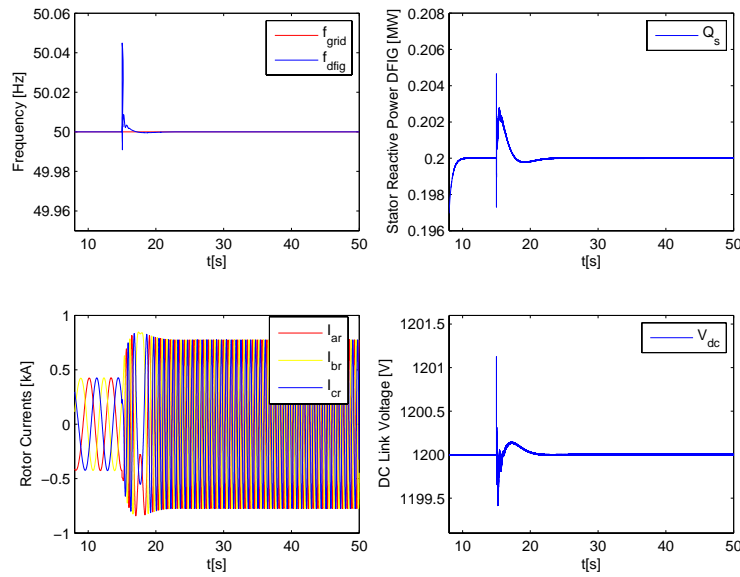
Figure A.3: *VSO response for a change in power demand from 50% to 90%.*
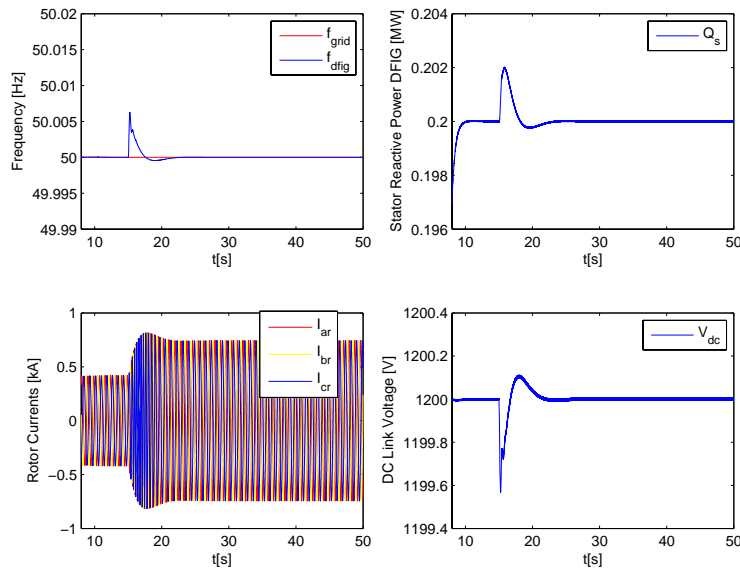
Figure A.4: *FSO response for a change in power demand from 50% to 90%.*

A.3 Gradual Change in Power Demand from 20% to 90%

Response of system for a gradual change in power demand from 20% to 90% can be seen from figure A.5 and figure A.6, note that variation in frequency, reactive power and DC link voltage is even smaller in this case compared to the case of step change.

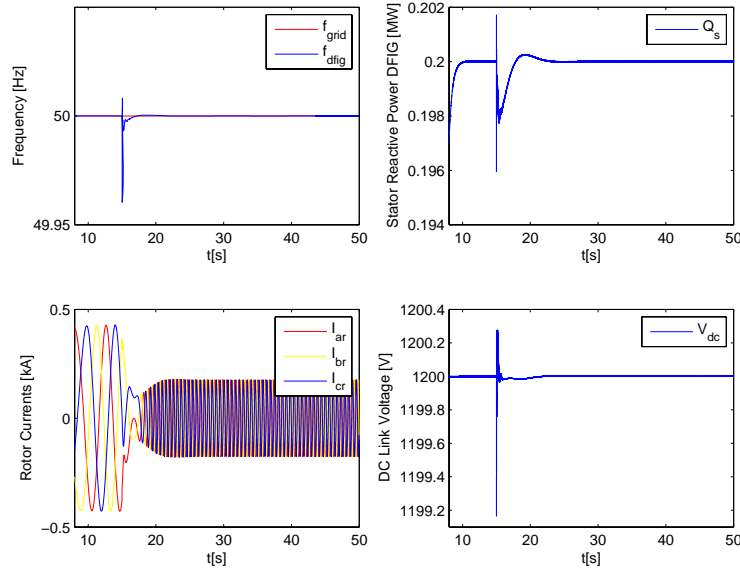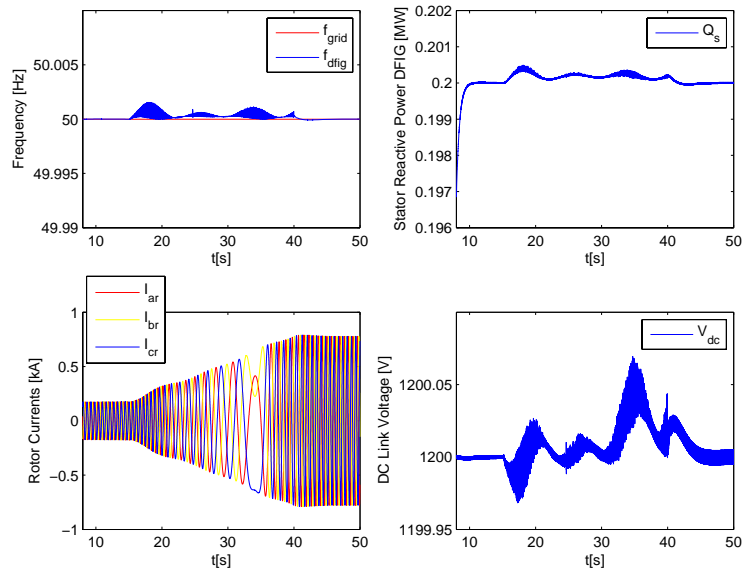**Figure A.5:** *VSO response for a change in power demand from* 20% *to* 90%.
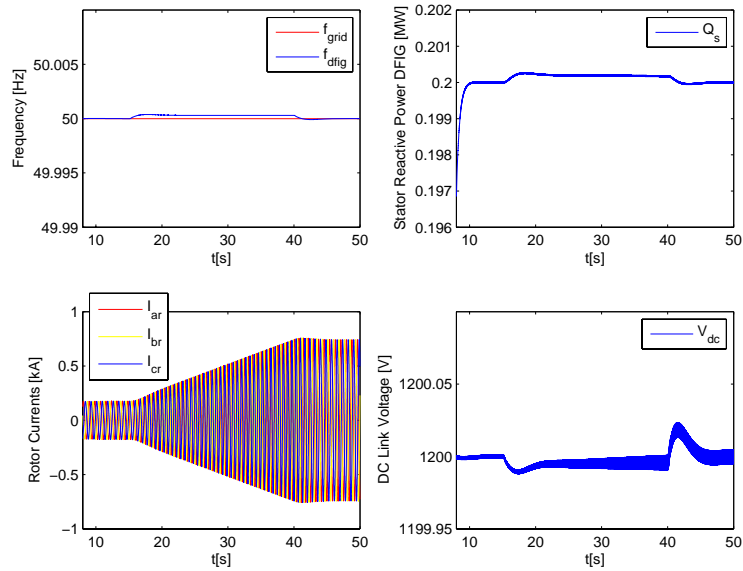
Figure A.6: *FSO response for a change in power demand from* 20% *to* 90%.

Appendix B

B.1 Choice of c for reference frame transformation

Clarke transformation in chapter 3 is given as:

$$
\begin{bmatrix} x_d \\ x_q \\ x_0 \end{bmatrix} = \begin{bmatrix} 1 & \frac{-1}{2} & \frac{-1}{2} \\ 0 & \frac{\sqrt{3}}{2} & \frac{-\sqrt{3}}{2} \end{bmatrix} \begin{bmatrix} x_a \\ x_b \\ x_c \end{bmatrix}
\tag{B.1}
$$

Then inverse Clarke transform is:

$$
\begin{bmatrix} x_a \\ x_b \\ x_c \end{bmatrix} = c \begin{bmatrix} 1 & 0 \\ \frac{-1}{2} & \frac{\sqrt{3}}{2} \\ \frac{-1}{2} & \frac{-\sqrt{3}}{2} \end{bmatrix} \begin{bmatrix} x_d \\ x_q \\ x_0 \end{bmatrix}
\tag{B.2}
$$

$$
\begin{bmatrix} x_a \\ x_b \\ x_c \end{bmatrix} = c \begin{bmatrix} 1 & 0 \\ \frac{-1}{2} & \frac{\sqrt{3}}{2} \\ \frac{-1}{2} & \frac{-\sqrt{3}}{2} \end{bmatrix} \begin{bmatrix} x_d \\ x_q \\ x_0 \end{bmatrix}
\tag{B.3}
$$

For a balanced system the last column can be neglected because the x_0 will be zero.

$$
x_a = \frac{1}{c}\frac{2}{3}x_d + x_q
\tag{B.4}
$$

$$
x_b = \frac{1}{c}(-\frac{1}{3}x_d + \frac{1}{\sqrt{3}}x_q)
\tag{B.5}
$$

$$
x_c = \frac{1}{c}(-\frac{1}{3}x_d - \frac{1}{\sqrt{3}}x_q)
\tag{B.6}
$$

Power in three phase is:

$$P_{abc} = v_a i_a + v_b i_b + v_c i_c \tag{B.7}$$

This power equation can also be written in term of derived components above as:

$$P_{abc} = \frac{1}{c}\frac{2}{3}v_d\frac{1}{c}\frac{2}{3}i_d + \frac{1}{c}(-\frac{1}{3}v_d + \frac{1}{\sqrt{3}}v_q)\frac{1}{c}(-\frac{1}{3}i_d + \frac{1}{\sqrt{3}}i_q) + \frac{1}{c}(-\frac{1}{3}v_d - \frac{1}{\sqrt{3}}v_q)\frac{1}{c}(-\frac{1}{3}i_d - \frac{1}{\sqrt{3}}i_q) \tag{B.8}$$

$$= \frac{1}{c^2}\frac{2}{3}(v_d i_d + v_q i_q) \tag{B.9}$$

First choose $c = \frac{2}{3}$

$$P_{abc} = \frac{3}{2}(v_d i_d + v_q i_q) = \frac{3}{2}P_{dq} \tag{B.10}$$

Now put $c = \sqrt{\frac{2}{3}}$

$$P_{abc} = v_d i_d + v_q i_q = P_{dq} \tag{B.11}$$

The above derivation shows that the power can be directly computed by multiplying with their respective d-q components if the value of c is chosen properly.

B.2 Solution to reference frame derivatives

The derivative of equations in chapter 3 can be solved as:

$$\frac{d}{dt}(\vec{\lambda}_s^k e^{j\theta_k}) = \frac{d}{dt}\vec{\lambda}_s^k.e^{j\theta_k} + \vec{\lambda}_s^k.je^{j\theta_k}.\frac{d}{dt}\theta_k \tag{B.12}$$

$$= \frac{d}{dt}\vec{\lambda}_s^k.e^{j\theta_k} + \vec{\lambda}_s^k.j\omega_k.je^{j\theta_k}; \tag{B.13}$$

Similarly transformation from rotor to arbitrary reference frame, derivative yields:

$$\frac{d}{dt}(\vec{\lambda}_r^k e^{j(\theta_k-\theta_m)}) = \frac{d}{dt}\vec{\lambda}_r^k.e^{j(\theta_k-\theta_m)} + \vec{\lambda}_r^k.je^{j(\theta_k-\theta_m)}.\frac{d}{dt}(\theta_k - \theta_m) \tag{B.14}$$

$$= \frac{d}{dt}\vec{\lambda}_r^k.e^{j(\theta_k-\theta_m)} + \vec{\lambda}_r^k.j(\omega_k - \omega_m).je^{j(\theta_k-\theta_m)}; \tag{B.15}$$

Where in above derivation $\frac{d}{dt}\theta_k = \omega_k$ and $\frac{d}{dt}\theta_m = \omega_m$.

Appendix C

C.1 DFIG Data (For Simulation)

$P_n = 1000[kW]$

$V_{s,rms} = 690Y[V]$

$I_{s,rms} = 836.74[A]$

$V_{r,rms} = 690Y[V]$

$n = 1500[rpm]$

$f = 50[Hz]$

$poles = 4$

$R_s = 5.24[m\Omega]$

$R_r = 5.24[m\Omega]$

$L_{ls} = 0.182[mH]$

$L_{lr} = 0.182[mH]$

$L_m = 5.23[mH]$

C.2 Motor Generator Set Data(For Lab Work)

This is the data for the Motor and DFIG used in the lab setup.

Generator Data

$P_n = 15[kW]$

$\Delta/Y = 220/380[V], \quad 55/32[A]$

$n = 1470[rpm], \quad 50[Hz]$

$Läufer\,Y\,280[V], \quad 33[A]$

$R_s = 0.12[\Omega]$

$R_r = 0.14[\Omega]$

$L_s = 13.74[mH]$

$L_r = 13.74[mH]$

$L_m = 13.52[mH]$

Motor Data

$P_n = 15[kW]$

$Volts = 380Y[V]$

$I_n = 31[A]$

$n = 1450[rpm], \quad 50[Hz]$

$P.F. = 0.82$

$Weight = 97[kg]$

$Duty = S1$

$Ins.Cl. = F$

$IP = 55$

ABB Motors, Made in Finland.

Appendix D

Appendix D

D.1   Connections Layout

Dspace board (CP1104)	DB15F	Flat cable
Slave I/O PWM	**DB15F**	**Flat cable 16 pin**
7	2	3
26	10	4
8	3	5
27	11	6
9	4	7
29	12	8
1	8	15
Digital I/O		
1	9	2
2	1	1
21	5	9
3	15	14
23	13	10
5	6	11
24	14	12
6	7	13
-	-	16

Dsapce board (CP1104)	PCB	Encoder
DB15M Incremental Encoder 1/2	**DB15F**	**DB15M/M-Conn.**
1	1	1/12
2	2	2/5
3	3	3/6
4	4	4/8
5	5	5/1
6	6	6/3
7	7	7/4
8	8	8/10
9	9	9/11
10	10	10/2

LEM
Transdcers

Op amp board

Dsapce board
(CP1104)

LEM Voltage
Transdcers DB15

CH1

11
12
4

+
M
-

+12V
-12V

RM

Op amp
circuit

BNC
BNC

CH2

10
5
3

+
M
-

+12V
-12V

RM

Op amp
circuit

BNC
BNC

CH3

9
1
2

+
M
-

+12V
-12V

RM

Op amp
circuit

BNC
BNC

CH4

13
7
6

+
M
-

+12V
-12V

RM

Op amp
circuit

BNC
BNC

CH5

15
14
8

+
M
-

+12V
-12V

RM

Op amp
circuit

BNC
BNC

LEM
Transdcers

Signal conditioning board

Dsapce board
(CP1104)

LEM Voltage
Transdcers DB15

CH1
11 + +12V
12 M
4 - -12V
RM Cf BNC BNC

CH2
10 + +12V
5 M
3 - -12V
RM Cf BNC BNC

CH3
9 + +12V
1 M
2 - -12V
RM Cf BNC BNC

CH4
13 + +12V
7 M
6 - -12V
RM Cf BNC BNC

CH5
15 + +12V
14 M
8 - -12V
RM Cf BNC BNC

LEM Transdcers	Op amp board	Dsapce board (CP1104)

LEM Current Transdcers DB9

CH1
- 8 — + — +12V
- 9 — M — RM — Op amp circuit — BNC — BNC
- 4 — − — -12V

CH2
- 7 — + — +12V
- 5 — M — RM — Op amp circuit — BNC — BNC
- 3 — − — -12V

CH3
- 6 — + — +12V
- 1 — M — RM — Op amp circuit — BNC — BNC
- 2 — − — -12V
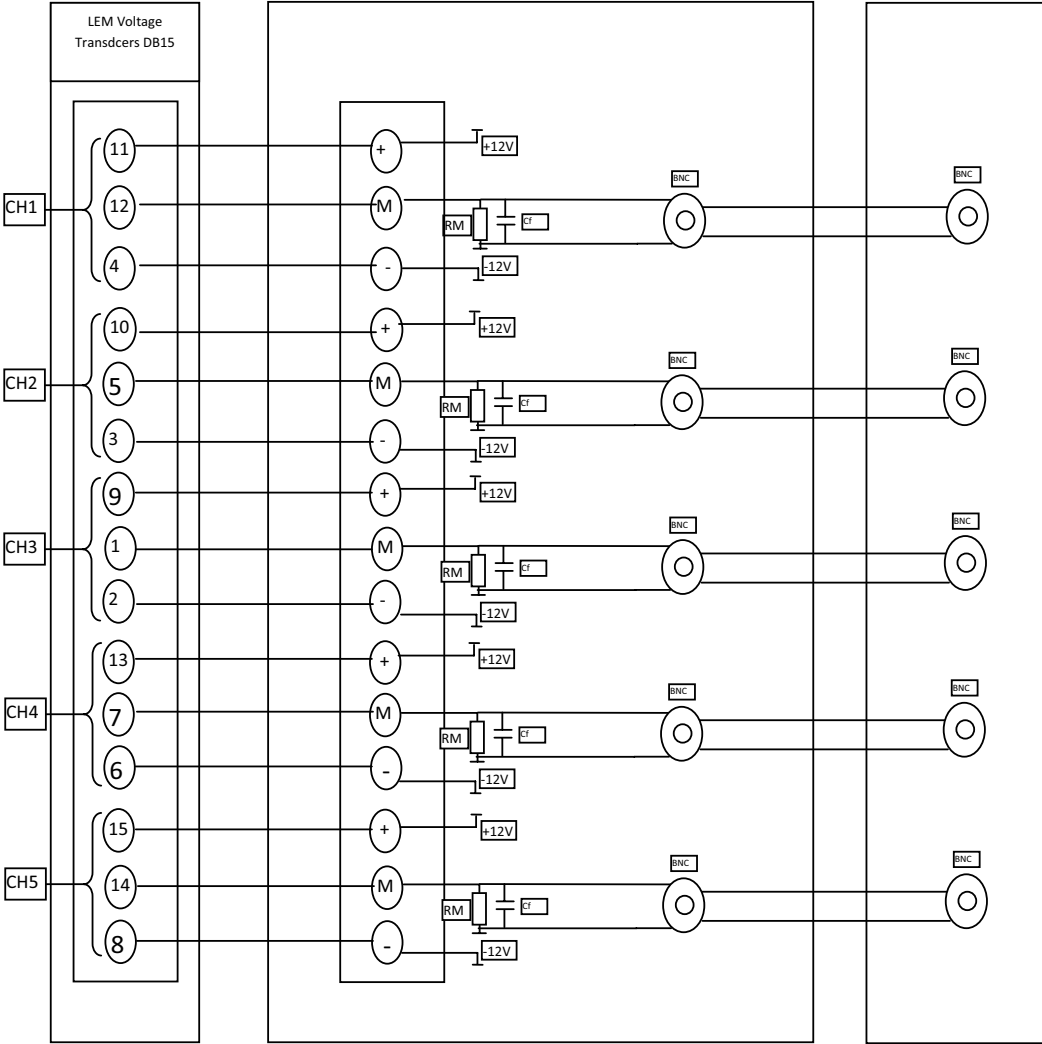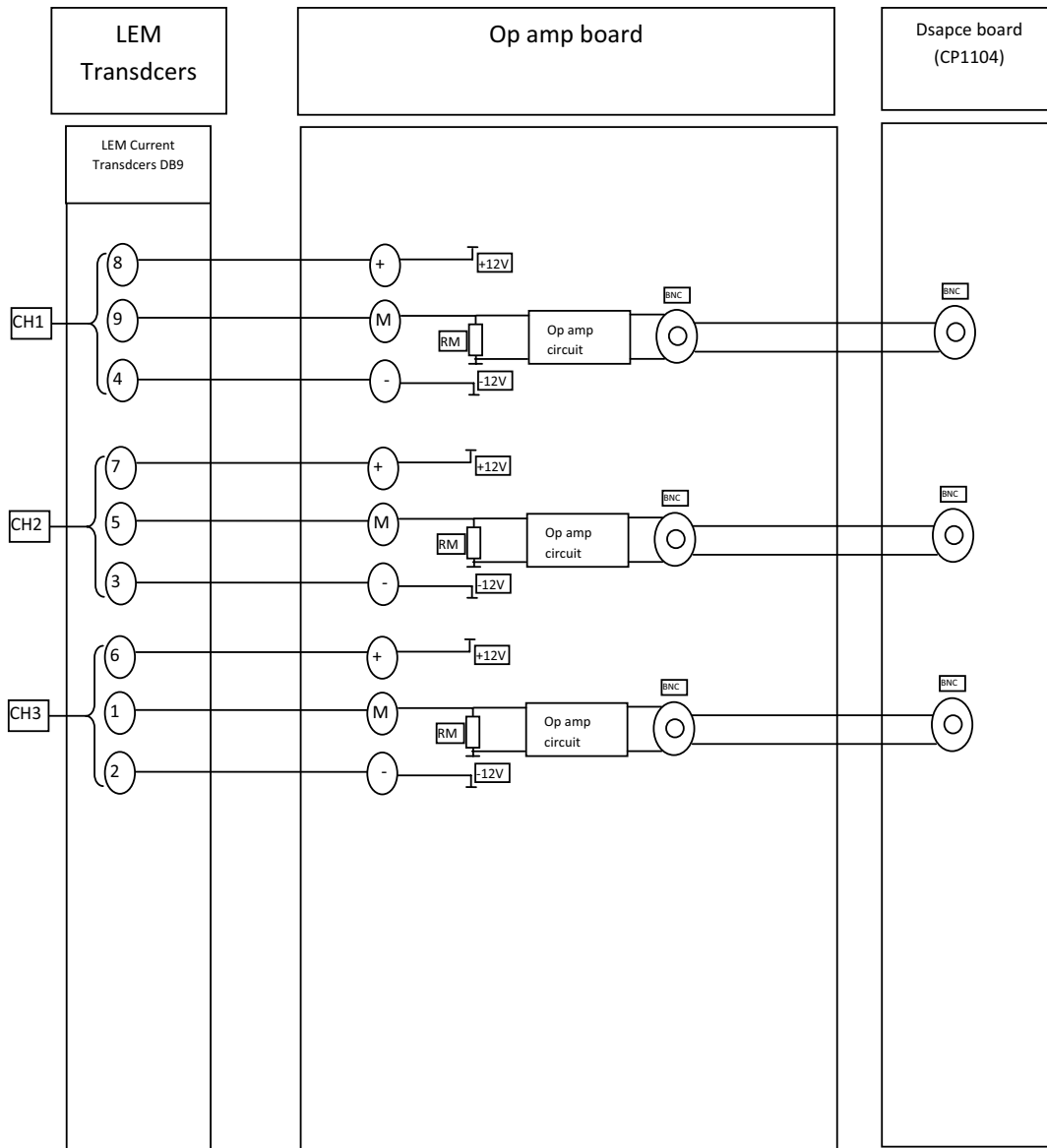
D.2   Data Sheets

Introduction to the DS1104

Objective	The dSPACE system based on the DS1104 R&D Controller Board comprises hardware and software.

Where to go from here

Information in this section

Hardware	13
Software	14

Hardware

Board description

The DS1104 R&D Controller Board is a standard board that can be plugged into a PCI slot of a PC. The DS1104 is specifically designed for the development of high-speed multivariable digital controllers and real-time simulations in various fields. It is a complete real-time control system based on a 603 PowerPC floating-point processor running at 250 MHz. For advanced I/O purposes, the board includes a slave-DSP subsystem based on the TMS320F240 DSP microcontroller.

For purposes of rapid control prototyping (RCP), specific interface connectors and connector panels (see below) provide easy access to all input and output signals of the board. Thus, the DS1104 R&D Controller Board is the ideal hardware for the dSPACE Prototyper development system for cost-sensitive RCP applications.

To demonstrate control design and implementation, demo equipment (VCFP Simulator) is available for the DS1104.

Easy access to input and output signals	Using an **adapter cable** you can link your external signals from the 100-pin I/O connector on the board to Sub-D connectors. So you can make a high-density connection between the board and the devices of your application via Sub-D connectors.
	Specific interface **connector panels** provide easy access to all the input and output signals of the DS1104 R&D Controller Board:
	■ The CP1104 **C**onnector **P**anel provides easy-to-use connections between the DS1104 R&D Controller Board and devices to be connected to it. Devices can be individually connected, disconnected or interchanged without soldering via BNC connectors and Sub-D connectors. This simplifies system construction, testing and troubleshooting.
	■ In addition to the CP1104, the CLP1104 **C**onnector/**L**ED Combi **P**anel provides an array of LEDs indicating the states of the digital signals.
Shipment	The DS1104 R&D Controller Board is a single-board system. The hardware package contains:
	■ One PCI-slot board with a bracket including a 100-pin I/O connector.
	■ One adapter cable with two 50-pin female Sub-D connectors. The adapter cable is optional.
	■ Only if ordered: CP1104 (or CLP1104) Connector Panel with adapter cable to the I/O connector of the board.

Software

Objective	The dSPACE software, such as the implementation and the experiment software, comes on DVD and has to be installed first.
Further information	For information on the software package, the installation and license handling, refer to *Introduction to dSPACE Software* (📖 *Software Installation and Management Guide*).

ROC/ROQ/ROD 400 Series with Clamping Flange

Rotary encoders for separate shaft coupling

ROC/ROQ/ROD 4xx
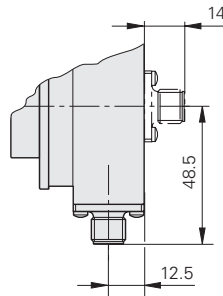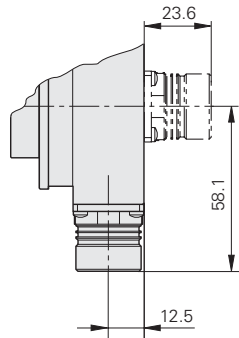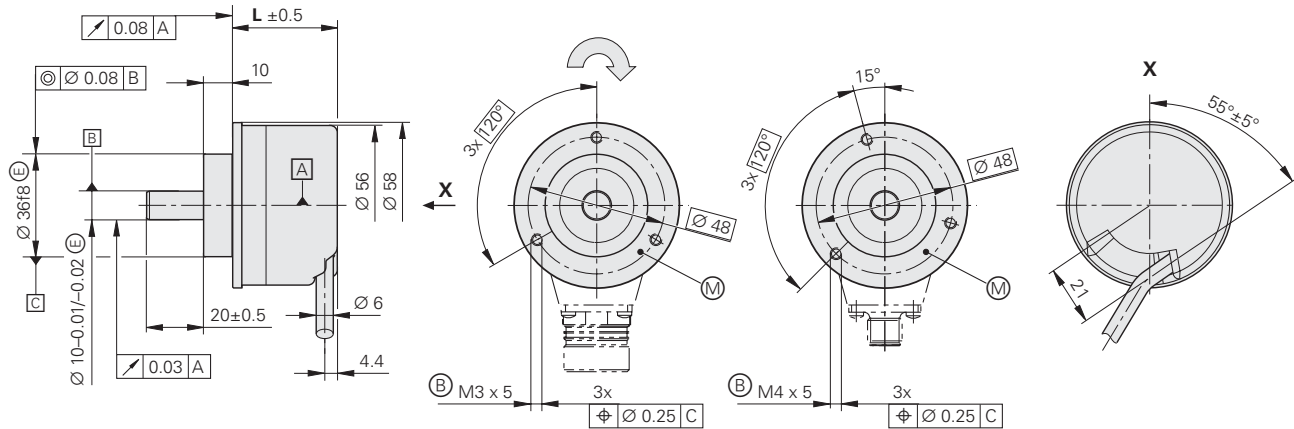
	L
ROD **ROC/ROQ 512 lines**	36.7
ROC/ROQ 2 048 lines **ROC 425/ROQ 437**	37.2

ROC 413/ROQ 425 with PROFIBUS DP
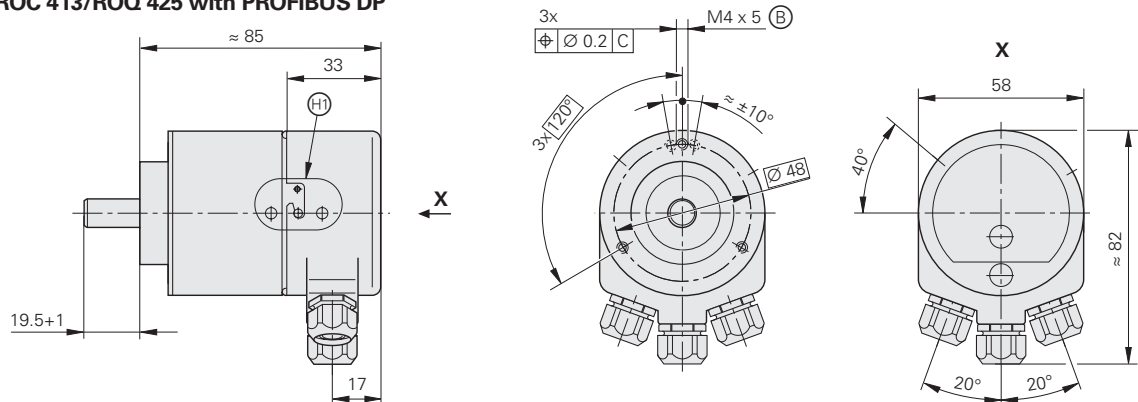
Dimensions in mm

Tolerancing ISO 8015
ISO 2768 - m H

Cable radial, also usable axially
Ⓐ = Ball bearing
Ⓑ = Threaded mounting hole
Ⓜ = Measuring point for operating temperature
Ⓗ = Shown rotated by 40°
↻ Direction of shaft rotation for output signals is described in interface description.

	Absolute								Incremental		
	Singleturn				**Multiturn**						
	ROC 425[1]	**ROC 413**[1]	**ROC 413**[1]	**ROC 413**	**ROQ 437**[1]	**ROQ 425**[1]	**ROQ 424**[1] **ROQ 425**[1]	**ROQ 425**	**ROD 420**	**ROD 430**	**ROD 480**
Absolute position values*	**EnDat 2.2;** Var. 22	**EnDat 2.2;** Var. 02	SSI	**PROFIBUS-DP**	**EnDat 2.2;** Var. 22	**EnDat 2.2;** Var. 02	SSI	**PROFIBUS-DP**	–		
Ordering information	EnDat 22	EnDat 02			EnDat 22	EnDat 02					
Positions per rev.	33554432 (25 bits)	8192 (13 bits)		8192 (13 bits)[3]	33554432 (25 bits)	8192 (13 bits)	4096 (12 bits) 8192 (13 bits)	8192 (13 bits)[3]	–		
Revolutions	–				4096			4096[3]	–		
Code	Pure binary		Gray	Pure binary	Pure binary		Gray	Pure binary	–		
Elec. permissible speed/Accuracy	≤ 12000 rpm for continuous position values	≤ 5000 rpm/± 1 LSB ≤ 12000 rpm/± 100 LSB			≤ 12000 rpm for continuous position values	≤ 5000 rpm/± 1 LSB ≤ 10000 rpm/± 100 LSB			–		
Calculation time t_{cal}	≤ 5 µs	≤ 0.25 µs	≤ 0.5 µs	–	≤ 5 µs	≤ 0.25 µs	≤ 0.5 µs	–	–		
Incremental signals	None	~ 1 V$_{PP}$[2]	–		None	~ 1 V$_{PP}$[2]	–		⊓⊔TTL	⊓⊔HTL	~ 1 V$_{PP}$[2]
Line counts*	–	**512**		512 (internal only)	–	**512**		512 (internal only)	50 100 150 200 250 360 500 512 720 1000 1024 1250 1500 1800 **2000 2048 2500 3600 4096 5000**		–
Cutoff freq. –3 dB Scanning frequency Edge separation a	– – –	≥ 100 kHz – –	– – –	– – –	– – –	≥ 100 kHz – –	– – –	– – –	– ≤ 300 kHz ≥ 0.43 µs		≥ 180 kHz – –
System accuracy	± 20″	± 60″			± 20″	± 60″			1/20 of grating period		
Power supply*	**3.6 to 5.25 V**	**5 V** ± 5 %	5 V ± 5 % or **10 to 30 V**	10 to 30 V	**3.6 to 5.25 V**	**5 V** ± 5 %	5 V ± 5 % or **10 to 30 V**	10 to 30 V	**5 V** ± 10 %	**10 to 30 V**	**5 V** ± 10 %
Current consumption without load	≤ 150 mA	≤ 160 mA	≤ 160 mA	≤ 125 mA at 24 V	≤ 180 mA	≤ 200 mA	≤ 200 mA	≤ 125 mA at 24 V	120 mA	150 mA	120 mA
Electrical connection*	• **Flange socket** M12, radial • **Cable 1 m**, with coupling M12	• **Flange socket** M23, axial or radial • Cable 1 m/5 m, with or without coupling M23		Screw terminals; radial cable exit	• Flange socket M12, radial • Cable 1 m, with coupling M12	• **Flange socket** M23, axial or radial • Cable 1 m/5 m, with or without coupling M23		Screw terminals; radial cable exit	• **Flange socket** M23, radial and axial • **Cable 1 m/**5 m, with or **without coupling** M23		
Shaft	Solid shaft D = 10 mm								Solid shaft D = 10 mm		
Mech. permissible speed	≤ 12000 rpm								≤ 12000 rpm		
Starting torque	≤ 0.01 Nm (at 20 °C)								≤ 0.01 Nm (at 20 °C)		
Moment of inertia of rotor	2.8 · 10⁻⁶ kgm²			3.6 · 10⁻⁶ kgm²	2.8 · 10⁻⁶ kgm²			3.6 · 10⁻⁶ kgm²	2.6 · 10⁻⁶ kgm²		
Shaft load[5]	Axial 10 N/radial 20 N at shaft end										
Vibration 55 to 2000 Hz **Shock** 6 ms/2 ms	≤ 300 m/s² (EN 60068-2-6) ≤ 1000 m/s²/≤ 2000 m/s² (EN 60068-2-27)								≤ 300 m/s² (EN 60068-2-6) ≤ 1000 m/s²/≤ 2000 m/s² (EN 60068-2-27)		
Max. operating temperature	U_P = 5 V: 100 °C U_P = 10 to 30 V: 85 °C			60 °C	U_P = 5 V: 100 °C U_P = 10 to 30 V: 85 °C			60 °C	100 °C		
Min. operating temperature	Flange socket or fixed cable: –40 °C Moving cable: –10 °C			–20 °C	Flange socket or fixed cable: –40 °C Moving cable: –10 °C			–20 °C	Flange socket or fixed cable: –40 °C Moving cable: –10 °C		
Protection EN 60529	IP 67 at housing; IP 64 at shaft end[4]								IP 67 at housing; IP 64 at shaft end[4]		
Weight	Approx. 0.35 kg								Approx. 0.3 kg		

Bold: These preferred versions are available on short notice
* Please indicate when ordering
[1] Available in 3rd quarter of 2005; for the previous version, see the *Rotary Encoders, January 2004* brochure

[2] Restricted tolerances: Signal amplitude 0.8 to 1.2 V$_{PP}$
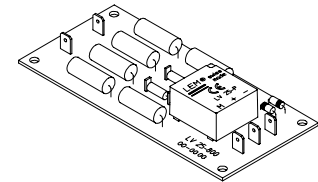[3] These functions are programmable

[4] IP 66 upon request
[5] Also see *Mechanical Design and Installation*

LEM

Voltage Transducer LV 25-800

V_{PN} = 800 V

For the electronic measurement of voltages : DC, AC, pulsed...,
with a galvanic isolation between the primary circuit (high voltage)
and the secondary circuit (electronic circuit).

LEM TRANSDUCERS 5 YEARS WARRANTY   CE

Electrical data

			$R_{M min}$	$R_{M max}$	
V_{PN}	Primary nominal r.m.s. voltage		800		V
V_P	Primary voltage, measuring range		0 .. ± 1200		V
I_{PN}	Primary nominal r.m.s. current		10		mA
R_M	Measuring resistance		$R_{M min}$	$R_{M max}$	
	with ± 12 V	@ ± 800 V_{max}	30	200	Ω
		@ ±1200 V_{max}	30	100	Ω
	with ± 15 V	@ ± 800 V_{max}	100	320	Ω
		@ ±1200 V_{max}	100	180	Ω
I_{SN}	Secondary nominal r.m.s. current		25		mA
K_N	Conversion ratio		800 V / 25 mA		
V_C	Supply voltage (± 5 %)		± 12 .. 15		V
I_C	Current consumption		10 (@±15V)+I_S		mA
V_d	R.m.s. voltage for AC isolation test [1], 50 Hz, 1 mn		4.1		kV

Features

- Closed loop (compensated) voltage transducer using the Hall effect
- Transducer with insulated plastic case recognized according to UL 94-V0
- Primary resistor R_1 and transducer mounted on printed circuit board 128 x 60 mm.

Accuracy - Dynamic performance data

			Typ	Max	
X_G	Overall Accuracy @ V_{PN} , T_A = 25°C			± 0.8	%
ε_L	Linearity			< 0.2	%
			Typ	Max	
I_O	Offset current @ I_P = 0, T_A = 25°C			± 0.15	mA
I_{OT}	Thermal drift of I_O	- 25°C .. + 25°C	± 0.10	± 0.60	mA
		+ 25°C .. + 70°C	± 0.10	± 0.60	mA
t_r	Response time @ 90 % of $V_{P max}$		25		µs

Advantages

- Excellent accuracy
- Very good linearity
- Low thermal drift
- High immunity to external interference.

Applications

- AC variable speed drives and servo motor drives
- Static converters for DC motor drives
- Uninterruptible Power Supplies (UPS)
- Power supplies for welding applications.

General data

T_A	Ambient operating temperature		- 25 .. + 70	°C
T_S	Ambient storage temperature		- 40 .. + 85	°C
N	Turns ratio		2500 : 1000	
P	Total primary power loss		8	W
R_1	Primary resistance @ T_A = 25°C		80	kΩ
R_S	Secondary coil resistance @ T_A = 70°C		110	Ω
m	Mass		60	g
	Standards [2]		EN 50178	

Notes : [1] Between primary and secondary
[2] A list of corresponding tests is available

980909/2

Dimensions LV 25-800 (in mm. 1 mm = 0.0394 inch)

Front view

5 faston 6,3x0,8

1.6
17.5
(19)

128
118 +/-0.2

R1	R5
R2	R7
R3	R8
R4	R6

LEM® swiss made LV 25-P/SP6

swiss made

D1
D2

+
M
-

20.32

+HT

–HT

2x10.16
50 +/-0.2
60

LV 25-800
00–00 00

Top view

4x⌀4.2

Standard 00   Year   Week
or N° SP..

Secondary terminals

Terminal + : supply voltage + 12 .. 15 V
Terminal M : measure
Terminal - : supply voltage - 12 .. 15 V

Connection

+HT

+HT   +   Is   RM   o +
LV 25-800   M   0V
–HT   -

–HT
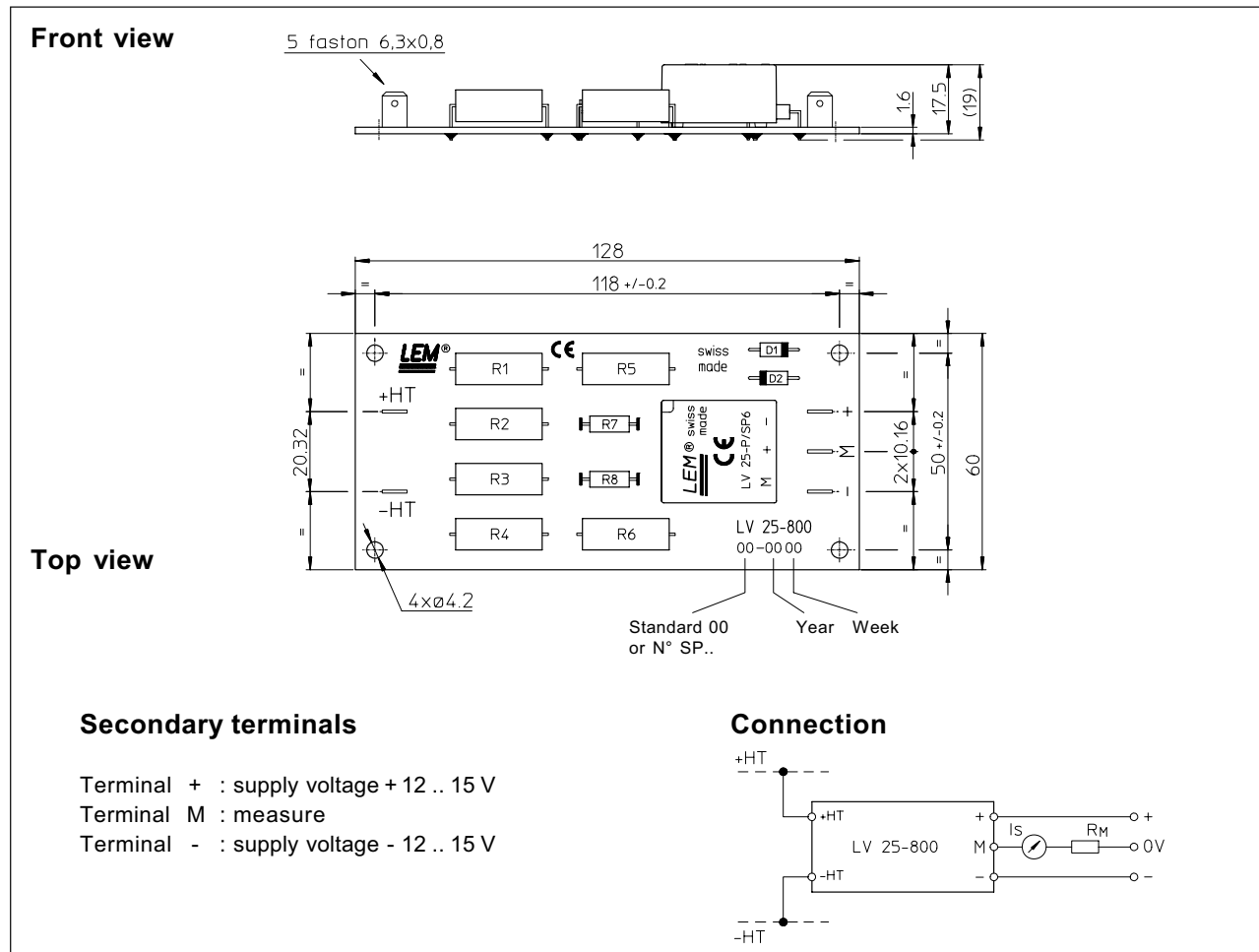
Mechanical characteristics

- General tolerance   ± 0.3 mm
- Fastening   4 holes ⌀ 4.2 mm
- Connection of primary   Faston 6.3 x 0.8 mm
- Connection of secondary   Faston 6.3 x 0.8 mm

Remarks

- I_S is positive when V_P is applied on terminal +HT.
- The primary circuit of the transducer must be linked to the connections where the voltage has to be measured.
- This is a standard model. For different versions (supply voltages, turns ratios, unidirectional measurements...), please contact us.

Current Transducer LA 205-S

For the electronic measurement of currents: DC, AC, pulsed..., with galvanic isolation between the primary circuit (high power) and the secondary circuit (electronic circuit).

I_{PN} = 200 A

16137
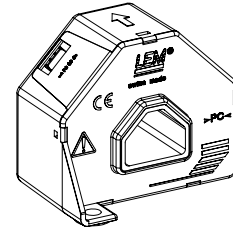
Electrical data

I_{PN}	Primary nominal current rms		200			A
I_{PM}	Primary current, measuring range		0 .. ± 300			A
$\hat{I}_{P\,max}$	Measuring overload [1]		600			A

				$T_A = 70°C$		$T_A = 85°C$	
R_M	Measuring resistance			$R_{M\,min}$	$R_{M\,max}$	$R_{M\,min}$	$R_{M\,max}$	
	with ± 12 V	@ ± 200 A $_{max}$	0	68	0	66	Ω
		@ ± 300 A $_{max}$	0	33	0	30	Ω
	with ± 15 V	@ ± 200 A $_{max}$	5	95	5	93	Ω
		@ ± 300 A $_{max}$	5	50	5	49	Ω
I_{SN}	Secondary nominal current rms		100			mA
K_N	Conversion ratio		1 : 2000			
V_C	Supply voltage (± 5 %)		± 12 .. 15			V
I_C	Current consumption		20 (@ ± 15 V) + I_S			mA

Accuracy - Dynamic performance data

		Typ	Max	
X_G	Overall accuracy @ I_{PN} , $T_A = 25°C$	± 0.8		%
ε_L	Linearity error	< 0.1		%
I_O	Offset current @ $I_P = 0$, $T_A = 25°C$		± 0.15	mA
I_{OM}	Magnetic offset current [2] @ $I_P = 0$ and specified R_M,			mA
	after an overload of 3 x I_{PN}		± 0.50	mA
I_{OT}	Temperature variation of I_O - 10°C .. + 85°C	± 0.15	± 0.30	mA
t_{ra}	Reaction time @ 10 % of I_{PN}	< 500		ns
t_r	Response time [3] @ 90 % of I_{PN} step	< 1		µs
di/dt	di/dt accurately followed	> 100		A/µs
BW	Frequency bandwidth (- 3 dB)	DC .. 100		kHz

General data

T_A	Ambient operating temperature		- 10 .. + 85	°C
T_S	Ambient storage temperature		- 40 .. + 90	°C
R_S	Secondary coil resistance	@ $T_A = 70°C$	35	Ω
		@ $T_A = 85°C$	37	Ω
m	Mass		110	g
	Standards		EN 50178: 1997	

Notes: [1] 3 mn/hour @ V_C = ± 15 V, R_M = 5 Ω
[2] The result of the coercive force (Hc) of the magnetic circuit
[3] With a di/dt of 100 A/µs.

Features

- Closed loop (compensated) current transducer using the Hall effect
- Isolated plastic case recognized according to UL 94-V0
- Patent pending.

Advantages

- Excellent accuracy
- Very good linearity
- Low temperature drift
- Optimized response time
- Wide frequency bandwidth
- No insertion losses
- High immunity to external interference
- Current overload capability.

Applications

- AC variable speed drives and servo motor drives
- Static converters for DC motor drives
- Battery supplied applications
- Uninterruptible Power Supplies (UPS)
- Switched Mode Power Supplies (SMPS)
- Power supplies for welding applications.

Application domain

- Industrial.

LEM reserves the right to carry out modifications on its transducers, in order to improve them, without prior notice.

Current Transducer LA 205-S

Isolation characteristics			
V_d	Rms voltage for AC isolation test, 50 Hz, 1 min	6	kV
$\hat{V}_w$	Impulse withstand voltage 1.2/50 µs	18	kV
		Min	
dCp	Creepage distance	25	mm
dCl	Clearance distance	23.25	mm
CTI	Comparative Tracking Index (group IIIa)	225	

Applications examples

According to EN 50178 and IEC 61010-1 standards and following conditions:

- Over voltage category OV 3
- Pollution degree PD2
- Non-uniform field

dCp, **dCl**, $\hat{V}_w$	EN 50178	IEC 61010-1
	Rated insulation voltage	Nominal voltage
Single insulation	2500 V	2500 V
Reinforced insulation	1250 V	1250 V

According VDE 0160 (1994):   single insulation 3250 V
                                 Reinforced insulation 1625 V

Safety

⚠

This transducer must be used in electric/electronic equipment with respect
to applicable standards and safety requirements in accordance with the
manufacturer's operating instructions.

⚡

Caution, risk of electrical shock

When operating the transducer, certain parts of the module can carry hazardous
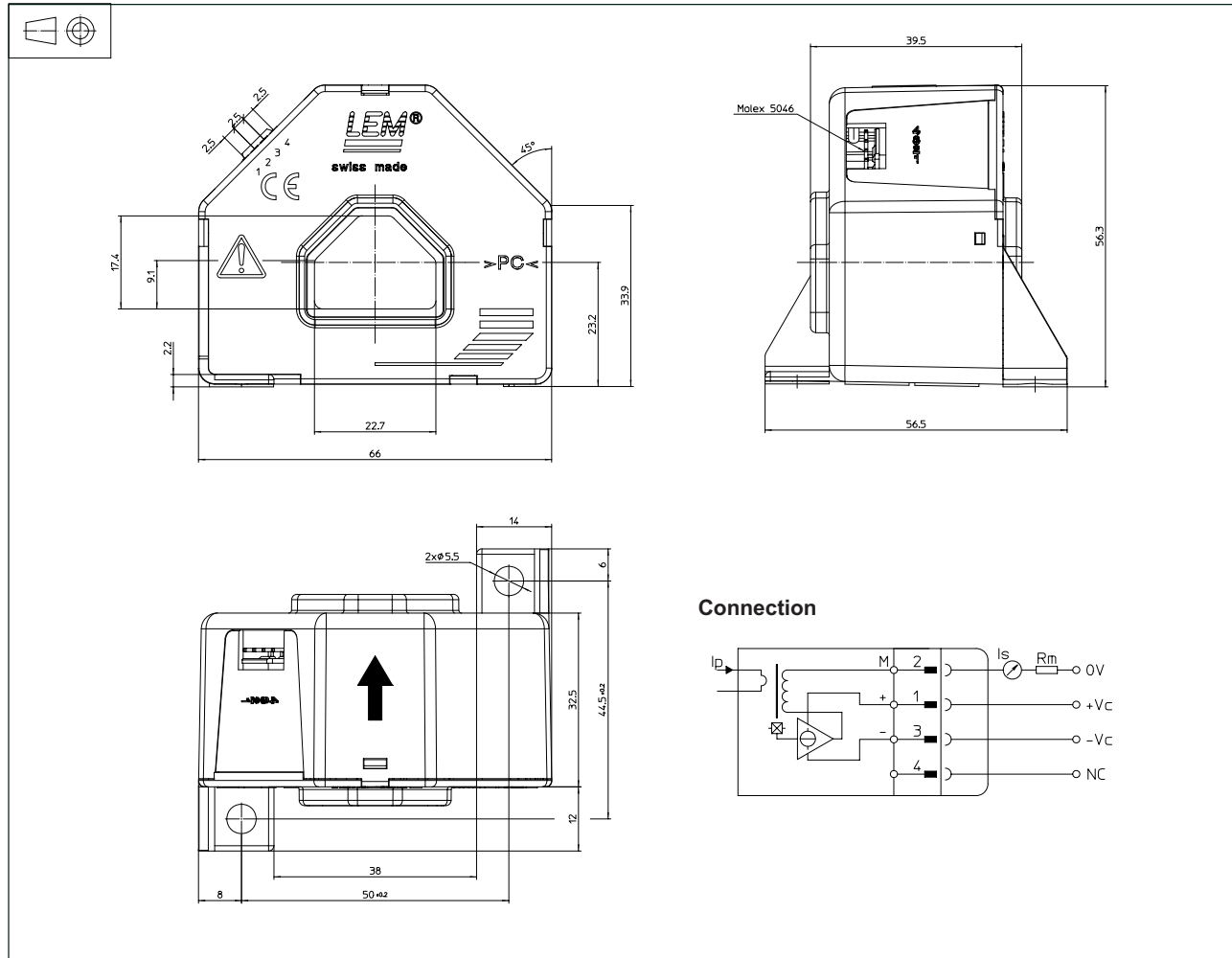voltage (eg. primary busbar, power supply).
Ignoring this warning can lead to injury and/or cause serious damage.
This transducer is a build-in device, whose conducting parts must be inaccessible
after installation.
A protective housing or additional shield could be used.
Main supply must be able to be disconnected.

Dimensions LA 205-S (in mm)

Connection

Mechanical characteristics

- General tolerance   ± 0.5 mm
- Transducer fastening   2 holes Ø 5.5 mm
       2 M5 steel screws
       Recommended fastening torque   1.2 Nm
- Primary through-hole   22.7 x 17.4 mm
- Connection of secondary   MOLEX 5046 4 pins
       tin plated

Remarks

- I_S is positive when I_P flows in the direction of the arrow.
- Temperature of the primary conductor should not exceed 100°C.
- Dynamic performances (di/dt and response time) are best with a single bar completely filling the primary hole.
- This is a standard model. For different versions (supply voltages, turns ratios, unidirectional measurements...), please contact us.

Page 3/3

110126/9   LEM reserves the right to carry out modifications on its transducers, in order to improve them, without prior notice.   www.lem.com